UNIVERSITÀ DEGLI STUDI DI TRIESTE

XXIV CICLO DEL DOTTORATO DI RICERCA IN

SCIENZE E TECNOLOGIE CHIMICHE E FARMACEUTICHE

SYNTHESIS AND EVALUATION OF NEW METAL-PORPHYRIN CONJUGATES FOR BIOMEDICAL APPLICATION

Settore scientifico disciplinare : CHIM/08

Ph D student:
Cinzia Spagnul

Supervisor:
Dr. Teresa Gianferrara

Ph D School Director:
Prof. Enzo Alessio

ANNO ACCADEMICO 2010/ 2011

And the end of our exploring

Will be to arrive when we started

*And know the place for the first time…**

T.S. ELIOT

Summary

This thesis reports the synthesis, the characterization and the biological evaluation of new classes of metal-porphyrin conjugates for potential bio-medical applications.
$[Ru([9]aneS3)(N\text{-}N)(L)][X]_n$ where N-N = nitrogen chelating ligand such as ethane-1,2-diamine (en) orbpy, L = S-dmso, Cl and X = CF_3SO_3 or PF_6, n = 2 or 1 respectively), $[Ru([9]aneN3)(dmso\text{-}S)_2Cl]Cl$, *fac*-$[^{99m}Tc\ (CO)_3(H_2O)_3]+$ and $[NEt_4]_2$ *fac*-$[ReBr_3(CO)_3]$ were chosen as metal fragments.

In the first section we describe different synthetic approaches to the preparation of porphyrin conjugates with Ru(II) coordination compounds.
Ru (II) fragments were chosen they have shown a promising anticancer activity both in vitro and in vivo, in murine models.
Water solubility in an important feature for biomedical application but usually porphyrins are fairly or not water soluble. The conjugation of a metal fragment to a porphyrin, beside increasing the solubility of the porphyrin macrocycle, is an intriguing alternative for making water soluble compounds that are expected to combine the cytotoxicity to the metal fragment to the phototoxicity of the porphyrins for an additive antitumor effect.
We varied the number and charge of the peripheral Ru fragments, and described conjugates whose total charge ranges from +4 to +8. We showed that the connection can occur through a single coordination bond (N(pyridyl)–Ru) or through multiple coordination bond (through a chelating bpy unit).
We demonstrated that *meso*-pyridylporphyrins (PyPs), besides being synthetically more affordable, allow to tune the geometry of the conjugates.
We showed that in the series of porphyrins with peripheral bpy units at *meso* positions, it is possible to vary the metal fragment and the length and the flexibility of the connectors between the bpyAc peripheral moieties and the *meso* C atoms to obtain compounds with different solubility
Finally some or those conjugates were evaluated as potential PDT agents.
Singlet oxygen quantum yield was evaluated for all of them as useful parameter.
The in vitro cell growth inhibition of some of such conjugates toward MDA-MB-231 human breast cancer cells and HBL-100 human non tumorigenic epithelial cells are reported, together with their phototoxic effects onMDAMB-231 cells. All conjugates have IC_{50} values in the low

micromolar range that decrease by 1 order of magnitude upon irradiation of cell cultures with visible light. This make them promising for PDT of cancer.

In the second section we describe the first example of ^{99m}Tc – porphyrins conjugates where the connection between the metal fragment and the porphyrins macrocycle occurred at the periphery of the cromophore, at *meso* position.

In radiopharmaceutical chemistry it is common to compare the retention time in the HPLC in the radiochromatogram of the ^{99m}Tc conjugate with the UV-vis trace of the corresponding non-radioactive Re congener to confirm the success of the labeling and to characterize unambiguously the ^{99m}Tc-conjugate.

By an accurate characterization of the water soluble porphyrinic precursors and of the Re(I) congeners, we were able to establish, for the first time, that only one $[^{99m}Tc\ (CO)_3]^+$ fragment is bounded at the periphery of the porphyrins.

Furthermore, all the ^{99m}Tc/Re-porphyrin conjugates were obtained with high purity level and reasonable to good yields. The total charge ranges from +1 to +3.

Stability studies performed by HPLC on the ^{99m}Tc-conjugates revealed an high stability under air at room temperature, in absence or presence of cells up to 30 minutes to 24 hours.

Since natural and synthetic porphyrins and metalloporphyrins are the most useful photosensitizers for PDT, we decided to evaluate the water soluble porphyrinic precursors and the Re(I)-porphyrins conjugates as potential photosensitizers for PDT.

The in vitro cell uptake, the cell growth inhibition toward HeLa cells are reported, together with their phototoxic effects on the same cell line.

All conjugates revealed a negligible cytotoxicity (IC_{50} values higher than 100 μM) after 24 h of exposure. Those value decrease by 1 order or magnitude upon irradiation with visible light (590-700 nm) at mild light doses (5 J/cm^2). We found that compounds uptake after 24h exposure is significantly different, and it does not affect appreciably their cytotoxicity. On the contrary, the phototoxicity is directly related to the ability of the compounds to penetrate cells. They proved to have from moderate to good singlet oxygen quantum yields and high photostability.

Taken together, those results make them promising for PDT of cancer.

List of abbreviations

bpyAc, 4-methyl-2,2-bipyridine-4'-carboxylic acid; CDMT = 2-chloro-4,6-dimethoxy-1,3,5-triazine; DAPI, 4',6-diamidino-2-phenylindolyl hydrochloride; DMA,9,10-dimethylanthracene; DMAP, dimethylaminopyridine; DMF, N,N-dimethylformamide; DMSO, dimethyl sulfoxide; DSS, 2,2-dimethyl-2,2-silapentane-5 - sulfonate; EDCI, N-(3-dimethylaminopropyl)-N'-ethylcarbodiimide hydrochloride; EDTA, ethylenediaminetetraacetic acid; en, ethane - 1,2-diamine; HOBt, 1-hydroxybenzotriazole; Hp, hematoporphyrin; LDL, low-density lipoprotein; MTT, thiazolyl blue tetrazolium bromide; NMM = *N*-methylmorpholine, PBS, phosphate-buffered saline; PDT, photodynamic therapy; ROS, reactive oxygen species; 4'TCMePP, *meso*-4'-tetracarboxymethylphenylporphyrin; TCPP, meso-4'-tetracarboxyphenylporphyrin; 4'-MPyTrMeP, 5- (4'-pyridyl) -10,15,20-tris (4'-carboxymethylphenyl) porphyrin; 4'-transDPyDMeP, 5,15 – bis (4'-pyridyl) -10,20-bis (4'-carboxymethylphenyl) porphyrins; 4'-cisDPyDMeP, 5,10-bis (4'-pyridyl) - 15,20 – bis (4'- carboxymethylphenyl) porphyrin; 4'-TrPyMMeP, 5,10,15-tris (4'-pyridyl) – 20 - (4'-carboxymethylphenyl) porphyrin; 4'-TPyP, tetra-4' - pyridylporphyrin; TFA, trifluoroacetic acid.

Table of Content

1. Introduction

1.1. Natural and sythetic water soluble porphyrins

Porphyrins are a very interesting class of molecules, especially for their chemical and biological properties. In fact they are currently under investigations in many research fields, such as catalysis, [1] conversion of solar energy [2] and spectroscopy. [3] In addition, these compounds play key roles in complex biological systems and, as photosynthetic models, [4] have been studied for their biological and biomedical applications.

From the structural point of view, all the porphyrins are characterized by an heterocyclic macrocycle composed of four modified pyrrole subunits interconnected at their α carbon atoms via methinebridges (=CH-) (Figure 1). The structure is completely aromatic with high conjugation and π electrons delocalization on the ring. The tetradentatemacrocycle defines a cavity of dimensions nearly perfect to coordinate strongly, after deprotonation of two protons inside, a large number of metal such as Fe(III) or (II), Zn(II), Cu(II) and Co(II).

Another important feature, for chemical application, is the stability of the porphyrin ring in strong acid and basic conditions. Strong bases such as alkoxides remove protons present on the inner nitrogen atoms (pK_a ~ 16) while pyrrolic nitrogen atoms have a pK_b ~ 9 and can be easily protonated with acids such as trifluoroacetic acid.[5]

The characteristic flatness, demonstrated by X-ray crystallography and the extensive electron delocalization in the macrocyclic core are decisive for the chemical activity and biological function of macromolecules.[6]

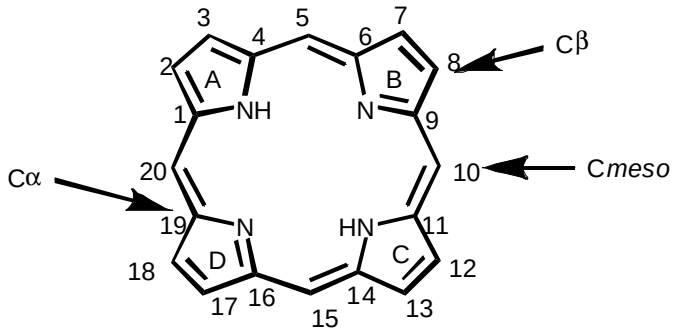

Figure 1. Schematic drawing of a porphyrins macrocycle.

As a consequence of the extensive electron delocalization, porphyrins typically have very intense absorption bands in the visible region and they are deeply colored; in fact the name porphyrin comes from a Greek word πορφυρος, *purple*.

In a typical visible absorption spectra, porphyrins usually show an intense Soret band at around 400 nm, which results from the delocalized cyclic electronic pathway, and several weaker absorption bands (Q bands) between 450 nm and 800 nm, which are responsible for the rich color (Figure 2).

Usually the insertion of peripheral substituent on the porphyrin ring induces relatively little changes in the intensity and wavelength of absorption while the protonation of the two inner nitrogen atoms or the insertion of a metal ion in the tetradentate cavity significantly change the absorption spectrum, with two typical Q-bands between 500 and 700 nm in addition to the Soret band. These changes are very useful to characterize metal porphyrins.[7]

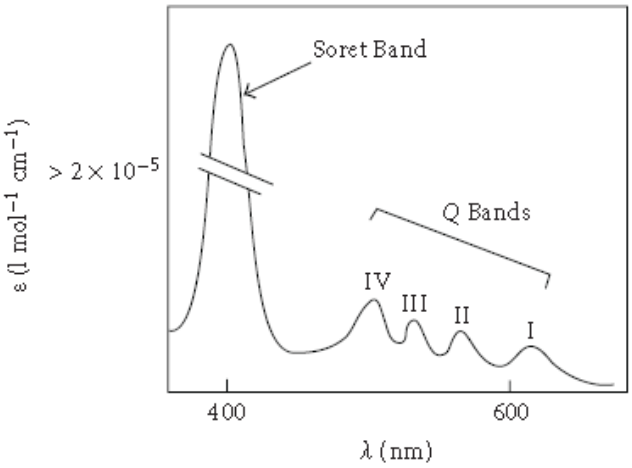

Figure 2.A typical UV-vis spectrum of a porphyrin

Since porphyrins are able to absorb in all the visible region at specific ranges of wavelengths, they are considered good chromophores and thus able to induce reversible or irreversible chemical changes on the surrounding biological substrates.

Furthermore, these macrocycles typically show preferential uptake and retention by tumor tissues, possibly via receptor-mediated endocytosis of low density lipoproteins (LDL). This suggestion is mainly supported by the observation that lipoproteins readily incorporate porphyrins, and that tumor cells have been found to exhibit elevated activity of LDL receptors.[8,9,10]

Since they are good chromophores with a good selectivity for tumor tissues, they are promising candidate for PDT.

1.2. Photodynamic Therapy in Cancer

1.2.1. General aspects

Photodynamic therapy (PDT) is an approved therapeutic procedure for the treatment of a variety of solid tumors and non-malignant lesions. It involves the local or systemic administration of a photosensitizer[11,12,13](porphyrin-like, chlorophyll-like, or dye compound) followed by irradiating the targeted disease site with non-thermal visible light of appropriate wavelength(s) (Figure 3).[14,15]

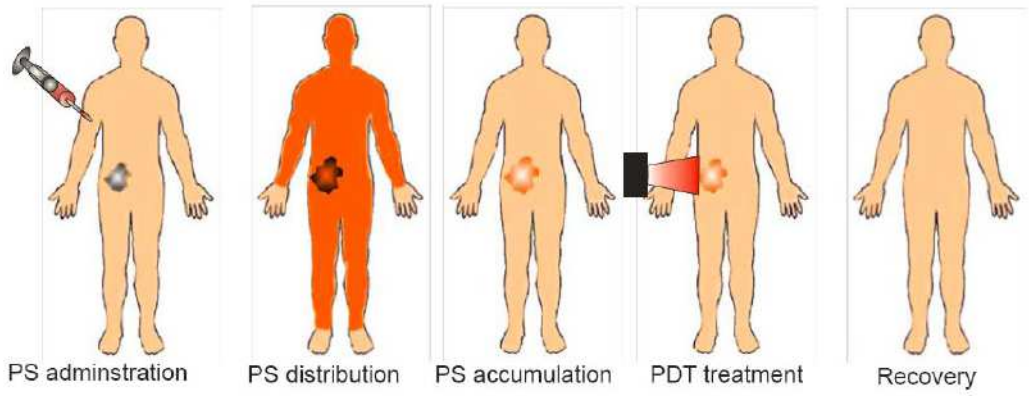

Figure 3. Schematic PDT treatment[16]

The anticancer effect of PDT is a consequence of a low-to-moderately selective degree of photosensitizer (PS) uptake by proliferating malignant cells, direct cytotoxicity of reactive oxygen species (ROS, mainly $^1O_2$) and a severe vascular damage that impairs blood supply to the treated area.[1718] Those biological effects of PDT are limited to the particular areas of tissues exposed to light.

Thanks to Thomas Dougherty's pioneering work, in 1975 it was demonstrated that the topical administration of a photosensitizer namely hematoporphyrin IX, and red light, successfully eradicated mammary and bladder tumor in mice. Nowadays PDT has been recognized as an experimental tool for treatment of tumors located in skin, lung, gall bladder, esophagous, head and neck.[19]

PDT as a treatment procedure has been accepted by the United States Food and Drug Administration for use in endo-bronchial and endo-esophageal cancer[20] and also as a treatment of premalignant and early malignant lesions of skin (actinic keratosis), bladder, breast, stomach and oral cavity.[21]

1.2.2. Photosensitizers

Photosensitizers (PS) are the key element in PDT. After the approval of Photofrin for the PDT treatment, researchers from all over the world got actively involved in developing efficient PSs.

Generally, a good photosensitizer must possess certain photophysical properties. For example, it should be able to produce singlet oxygen with high quantum yield (Φ_{Δ}).[22] In addition, a high molar extinction coefficient in the spectral region of the excitation light, a high triplet statequantum yield Φ_{T}, a relatively long triplet state lifetime (τ_{T}), and a high triplet-state energy are other important factors. The photobleaching of a PS is another important parameter. Aphotosensitizer that will photobleach slowly in tissues will be a better agent for PDT. Finally the amphiphilicity and water solubility are characteristic desiderable for a good PS.

From biological point of view, it should posses high selectivity in terms of target cells *versus* healthy cells, minimal skin photosensitivity and no dark toxicity.

Photosensitizers are generally classified as porphyrins or non-porphyrins. In fact, in the beginning, the attention has been focused on porphyrins and their analogues because their presence in natural systems makes them ideal candidates for use in biological singlet oxygen generation. As a result of their biological roles, these photosensitizers generally lack cytotoxicity in the absence of light, which proves important in certain applications .

The porphyrins and their derivatives have the ability to absorb several wavelengths in the UV-vis range. The long-lived triplet states of many porphyrins allow for high quantum yields. The introduction of different substituents on the macrocycle allows the tuning of the porphyrins properties. Some photosensitizers approved for clinical PDT treatments in humans are listed in Table 1.

Chemical classification	Photosensitizer tradename/company	Type of diseases	Country
Hematoporphyrin	Porfimer Na Photofrin	Barrett's displasia	U.S., Canada, EU, UK
		Cervical cancer	Japan
		Endobronchial cancer	Canada, Most EU Countries, Japan, U.S.
		Esophageal cancer	Canada, Most EU Countries, Japan, U.S.
		Gastric cancer	Japan
		Papillary bladder cancer	Canada
Protoporhyrin	Pro drug (5-aminolevulinic acid - ALA) converted tophotoactive protoporhyrinIX/ Levulan, Levulan Kerastick (for topical use)/Dusa Pharmaceuticals)	Actinic keratosis, Basal cell carcinoma	U.S., EU
Temoporfin	*m*THPC / Foscan Biolitec Pharma	Head and neckcancer	EU, Norway, Iceland
Verteporfin	Visudyne	Age-related Macular Degeneration	Canada, Most EU Countries, Japan, U.S.

Table 1. Photosensitizers approved in human diseases.

Commonly PSs are divided into three generations. First-generation PS are hematoporphyrin, its derivatives HpD, and the purified, commercially available and yet largely employed Photofrin (Figure 4).

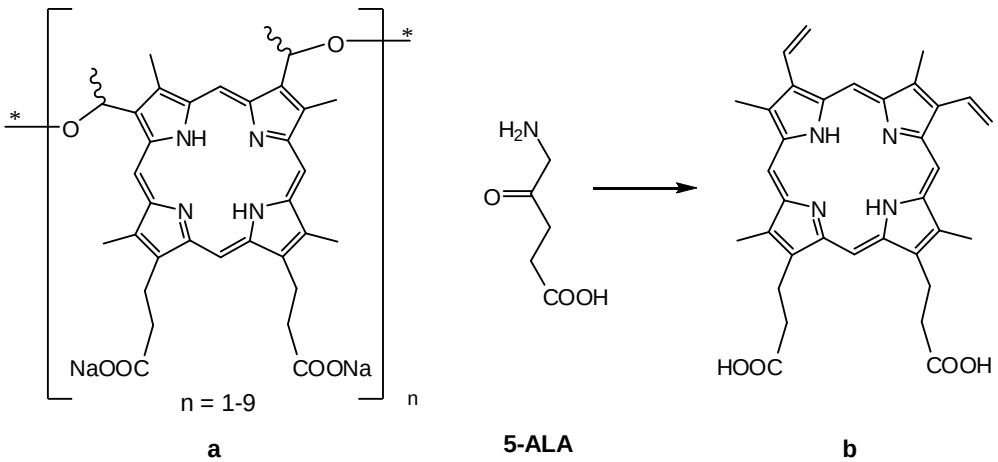

Figure 4. Examples of photosensitizers approved for clinical PDT. Photofrin **(a)** and 5-ALA, as a prodrug of Protoporhyrin (IX) (**b**).

Photofrin showed some advantages, such as the absence of intrinsic toxicity, the possibility of using small drug doses, the good clearance from normal tissue and the possibility of repeated administrations without serious consequences. But the complex composition, the prolonged photosensitivity (up to 3 months), the poor selectivity 0.1-3%,[23] the slow clearance rate and the relatively weak long-wavelength absorption moved the research for new photosensitizes.
Such photosensitizes belongs to the second generation. They include benzoporphyrin derivative, chlorins, phthalocyanines and texaphrins as well as naturally occurring compounds, such as hypericin, and 5-aminolevulinic acid (5-ALA) and some of its related esters[24] that promote the endogenous production of the protoporphyrin IX (PpIX) (Figure 4).
Now research is moving toward the synthesis of the third generation of photosensitizers, where dark toxicity, solubility and tumor selectivity are characteristic under optimization.
From this point of view, the design of new photosensitizers by using sugar moiety,[25] peptides,[26] and hormones [27]or fullerene [28] may afford excellent candidate PDT drugs.

1.2.3. Photochemistry

Upon absorption of a photon, the photosensitizer is activated to an exited single state (S1) and then, by intersystem crossing (4), it can converts to an exicited triplet state (T1) (Figure 5).

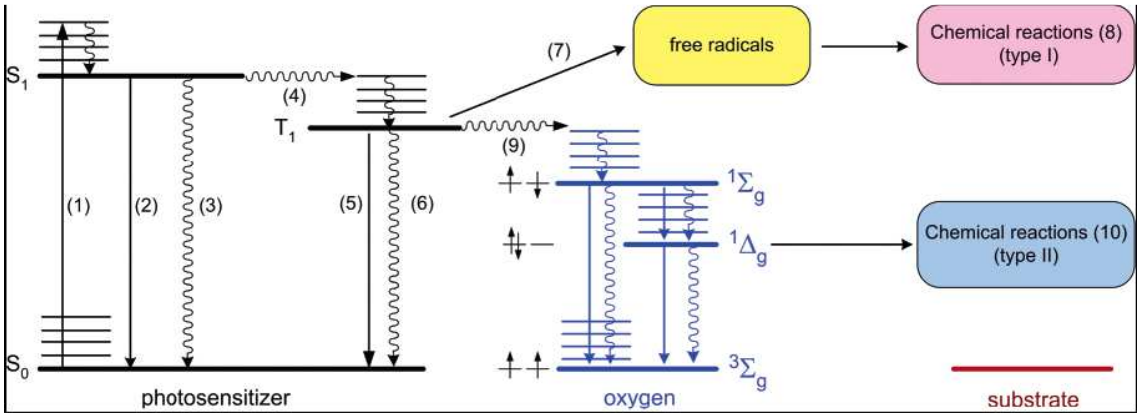

Figure 5. Jablonski diagramshowing the various modes of excitation and relaxation in a chromophore.
(1) = exited state, (2) = fluorescence emission (3) = internal conversion, (4) = intersystem crossing, (5) = fluorescence emission (6) = internal conversion, (7) = reaction of triplet state with surrounding molecules (8) = Type I reactions (9) = spin exchange with oxygen (10) = Type II reactions.

Since phosphorescence is a spin-forbidden decay, the lifetime of the T1 state is longer (from 10^{-3} to 10 µs) than that of the S1 state (from 10^{-9} to 10^{-6}ns). Consequently, the molecule in T1

excited state can react with the surrounding molecules, according two types of reactions, defined as Types I and II.

Firstly, in a Type I reaction, the photosensitizer can react directly with the biomolecules, such as the cell membrane constituents, and transfer a proton or an electron to form a radical anion or cation, respectively. These radicals may further react with oxygen to produce reactive oxygen species (ROS). Alternatively in a Type II reaction, the excited PS can transfer its energy directly to molecular oxygen to form excited state singlet oxygen that consequently induce apoptosis and necrosis of targeted cells and tissues (Type-II PDT).[29,30,31] It is highly probable that in the presence of molecular oxygen, and as a direct result of the photoirradiation of the PS molecule, both Type-I and II pathways play a pivotal role in disrupting cellular mechanisms and cellular structure.

Type I mechanism is favored at high concentration of photosensitizer, hypoxic environment or in the presence of others molecules that can be easily oxidized. Nevertheless, there is considerable evidence to suggest that the Type-II photo-oxygenation process predominates in the induction of cell damage, a consequence of the interaction between the irradiated photosensitiser and molecular oxygen.[32]

The energy required for the triplet to singlet transition in oxygen is 22 kcal mol^{-1}, which corresponds to a wavelength of 1274 nm (infrared light).[33] Thus relatively low energy is needed to produce singlet oxygen. The latter interaction usually involves energy transfer to yield chemically highly active singlet oxygen ($^1O_2$) which reacts with many biological molecules, including lipids, proteins, and nucleic acids, leading to cancer cell death.

Singlet oxygen ($^1O_2$) is so reactive that it has a lifetime that ranges from 10–100 µs in organic solvents. In an aqueous environment single oxygen's lifetime is reduced to approximately 2 µs because the energy of oxygen–hydrogen (O–H) stretching in water molecules nearly equals the excited-state energies of singlet oxygen. The energy is dissipated as heat by the stretching and vibrational motions of water molecules.

Because singlet oxygen reacts so rapidly, the oxidative damaged is highly localized to regions no larger in diameter than the thickness of a cell membrane. The sequence of reactions involved in the process is summarized in Figure 6.

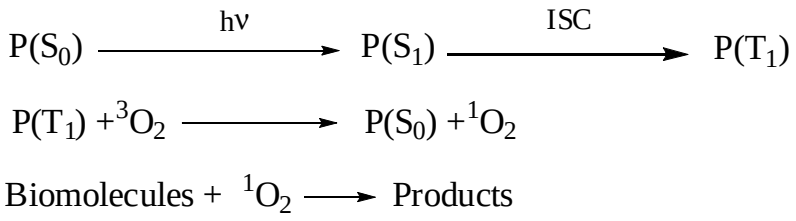

Figure 6. P = photosensitizer, $^3O_2$ = oxygen triplet ground state, $^1O_2$ =excited singlet oxygen, S0 and S1 = ground state and first excited singlet state, T1 = first triplet excited state, ISC = intersystem crossing.

When the photosensitizer returns from the triplet to the ground state, it can absorb another quantum of light and start again with a new cycle. Some photosensitizes undergo rapid decomposition in the presence of $^1O_2$ (*photobleaching*). This can be deleterious since the photosensitizer is no longer able to absorb light and thus to cause the phototoxic effect; however, it could be an advantage in biological systems where rapid breakdown of the photosensitizer after use is necessary.

The efficiency of production of singlet oxygen is an empirically determined quantity called the singlet-oxygen quantum yield (Φ_Δ). The singlet-oxygen quantum yield describes the number of singlet oxygen molecules that are formed per photon of energy absorbed and it correlates with triplet-state quantum yield Φ_T and with the efficiency of energy transfer .

1.2.4. Light

Selectivity in PDT can also be enhanced by selectively delivering the light to the tumor tissue and excluding it as fully as possible from the healthy tissues nearby. Nowadays different laser systems and incoherent light sources are used in PDT.[34]

A laser beam for its intrinsic characteristics differs from ordinary light, as it is collimated (parallel, with very low divergence), coherent (all waves are in phase), monochrome (line width 0.01 nmor less). The first feature allows to fix it at the end of a thin quartz fiber and to transmit it, by means of optical fibers in a beam of 0.4 to 1 mm diameter. This allows to irradiate tumors located internally and not just superficially.

The monochromatic wavelength allows to use the most appropriate wavelength for the absorption of light by the photosensitizer drug and to the maximize light transmission through tissues.

Light upon interaction with a tissue surface can be reflected, scattered, transmitted, or absorbed (Figure 7) depending on optical features of the tissue and on the light properties.

Light propagation in the tissue is affected by scattering occurring at inhomogenity sites, (e.g. membranes, nuclei), and by a number of factors such as the presence of absorbing dyes (hemoglobin, melanin) and water.[35] In general, light penetration depth is highly dependent on the tissue type and its intensity decreases with penetration depth through the tissue surface.

Since light penetration depth into most biological tissues increases upon increasing the wavelength, light of the spectral range called "phototherapeutic window" (620-850 nm) is predominantly used in phototherapy.

Compounds with aromatic systems and with extended conjugation, such as porphyrins, are able to absorb light with high efficiency. Although the absorption spectra of porphyrins show the Soret band, with higher absorption in the near UV and blue, the activation of the porphyrin is obtained with red light using the Q satellite bands. [36, 37] This is mainly due to the depth of penetration of light (from 3 to 8 mm) in the range from 630 to 800 nm (Figure 8).

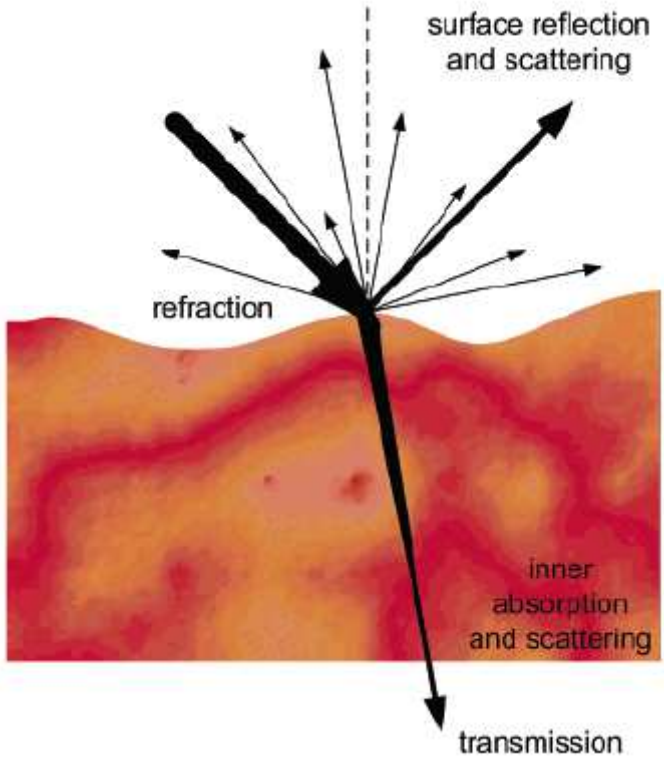

Figure 7. Interactions of light with a tissue. From ref. 35.

Since light penetration depth into most biological tissues increases upon increasing the wavelength, light of the spectral range called "phototherapeutic window" (620-850 nm) is predominantly used in phototherapy

Compounds with aromatic systems and with extended conjugation, such as porphyrins, are able to absorb light with high efficiency. Although the absorption spectra of porphyrins show the Soret band, with higher absorption in the near UV and blue, the activation of the

porphyrin is obtained with red light using the Q satellite bands.[1] This is mainly due to the depth of penetration of light (from 3 to 8 mm) in the range from 630 to 800 nm (Figure 7).

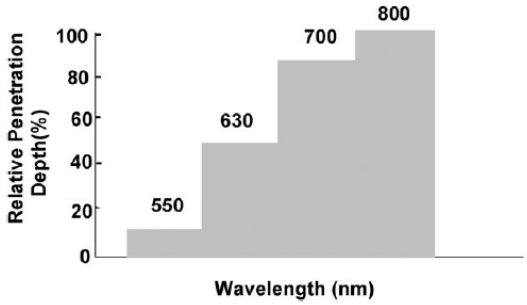

Figure 8. Relative diffusion depth of penetration with light at various wavelengths (assuming the depth of tissue penetration at 800 nm is 100%) [37]

The light dose administered is expressed in joules per unit of surface (J/cm^2). Typically fluencies of 10 J/cm^2 are applied in therapy for second-generation PSs (e.g. *m*THPC),[38] and this value depends to the extinction coefficient of the photosensitizer.

The tumors are illuminated with a dose-rate not exceeding 100 mW/cm^2 to avoid the appearance of thermal effects, being unspecific, that may overlap with those photodynamic. The total dose of light given usually depends on the type and size of the tumor. PDT induces necrosis of the treated tumors, which appears in two or three days.

1.2.5. Mechanism of Action/Damage and Subcellular Targets

Because of the limited migration of $^1O_2$ from the site of its formation [39], sites of initial cell and tissue damage of PDT are closely related to the localization of the sensitizer.[40]

The main damages induced by PDT occur where the photosensitizer localize within the cell.[42] Photosensitizers can accumulate almost everywhere within the cell; there they cause specific detrimental effects. Nevertheless, plasma and lysosomal membrane, mitochondria and endoplasmic reticulum (ER) represent the preferential targets.[41]

Due to its electrophilic nature, $^1O_2$ can give cycloaddition and oxidation reactions in various biomolecules, all of which are quite disruptive to biological processes.[42]

The ideal target includes unsaturated lipids, such as cholesterol, andα-amino acid residues of proteins (Scheme 1). Among these, tryptophan is the most reactive,[43] but also histidine and methionine can react.

[1]Potter W. R., in *Proceedings of SPIE* **1989**, *1065*, 88.

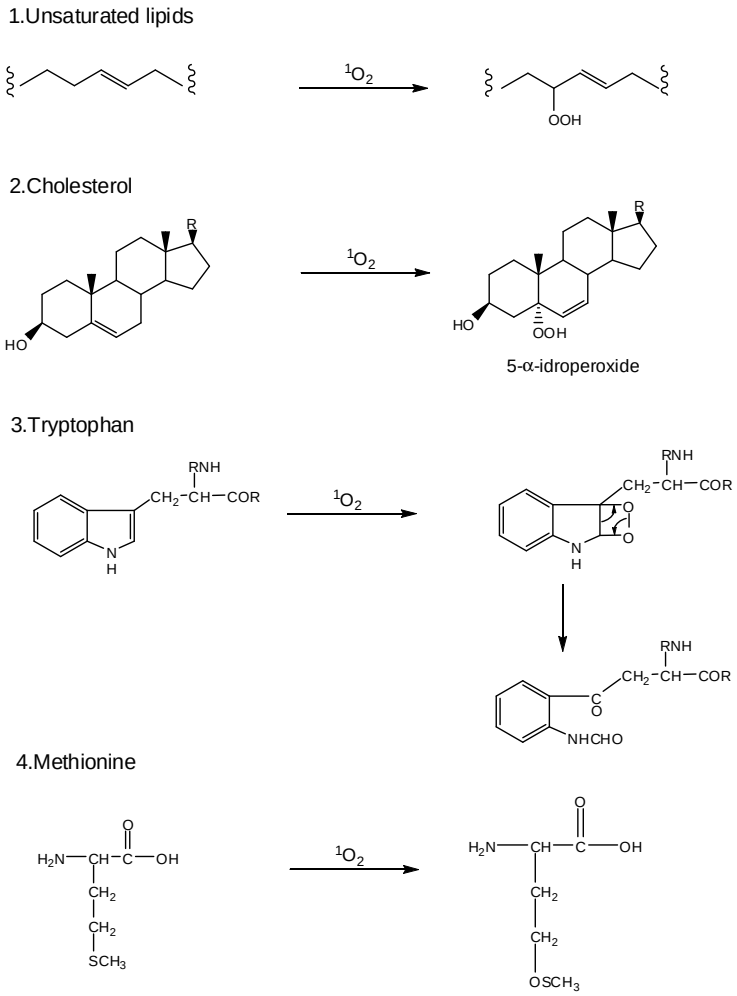

Scheme 1. Subcellular targets of $^1O_2$

Hydroperoxide (cholesterol) or endoperoxides (tryptophan) can be easily generated. The fate of these organic oxygenated compounds can be different. For example, cholesterol peroxide can trigger a massive immune response,[44] causing the destruction of the cell,[45] or it can be detoxified by using a membrane-based glutathione peroxidase to catalyze the two-electron reduction and detoxification of lipid hydroperoxides.[46]

Since the unsaturated lipids and proteins are essential constituents of biological membranes, reactions between singlet oxygen and the components of the membrane cause an alteration of the permeability of the membrane that leads to cytolysis, swelling, blistering on the cell membrane, release of vesicles containing enzymes, inhibition of enzymes of membrane such as Na^+, K^+-ATPase, destruction of the channels of the Ca^{2+}.[47]

For example, in mitochondria these events can lead the release of cytochrome C[48]and the subsequent rapid induction of apoptosis.[49,50] According to some authors the variations of

intracellular Ca^{2+} level are responsible for the increase in mitochondrial membrane permeabilization.
Regarding the ER, it has been reported that, after PDT, different heat shock proteins as well as the ER chaperones, GRP78/Bip, calreticulin, calnexin are induced in a time dependent manner.[51]

These photo-oxidated proteins can sustain the activation of unfolded protein response (UPR) that is involved in cell death both in vitroand in vivosystems. Therefore, a more accurate and critical evaluation is required.

Although the effects of cell damage are important for the destruction of tumor tissue, vascular damages are responsible of the complete death of tumor effects of PDT.
After irradiation, in fact, there is a cascade of biological responses, such as the accumulation of macrophages and platelets, the release of cytokines and prostaglandins, the platelet aggregation with the consequent thrombus formation. The result of these events is the total vascular stasis. This hypothesis is supported by some experimental observations. In particular, using the porfimer sodium (Photofrin) at 10 and 25 mg/kg in rat caused a dose-related constriction of arteriolein the site of application of light.[52]

In the PDT vascular stasis is generally irreversible and it is followed by necrosis of the tumor tissue.[53]The apoptotic response may contribute to antitumor effect of PDT, especially if the photosensitizer is localized preferentially in the mitochondria, because these organelles are capable to induce and control nuclear apoptosis.

Moreover, since most PDT sensitizers do not accumulate in cell nuclei, PDT has generally a low potential of causing DNA damage, mutations, and carcinogenesis [54] thus allowing the frequent repetition of phototherapeutic treatments.
Additionally, PDT leads to activation of tumor directed, systemic immune responses.[55,56, 57]
For example it has been demonstrated that PDT causes invasion and leukocyte infiltration of the tumor, events that are typical of acute inflammation and immunity. In addition, PDT appears to increase the presentation of tumor-derived antigen to T cells. At the same time, PDT stimulates the recruitment of host leukocytes, lymphocytes, neutrophils and macrophages into tumor tissue, by up-regulating the inflammatory cytokines interleukin IL-6 and IL-1.[58] Once generated by PDT, these cells cause an immune reaction that may be important for the eradication of disseminated tumor cells and/or located in metastatic sites.

2. Ru-Porphyrins conjugates

2.1. Approaches toward the synthesis of water soluble porphyrins

Synthetic porphyrins are of considerable interest in biology, especially for properties such as the structural similarity with heme and vitamin B_{12}. Natural porphyrins are present in the prosthetic group of hemoglobin and myoglobin which are responsible for oxygen transportation in red blood cells and oxygen storage in living tissue, and of some proteins with enzymatic activity such as cytochromes, catalases and peroxidases, involved especially in the cellular respiration.

Unfortunately most porphyrins do not have an appreciable solubility in water, at pH close to neutrality, to permit biological and biomedical applications. An important goal is therefore to increase the water solubility of these structures. Several approaches have been developed to synthesize water-soluble porphyrins. A well established strategy involves the attachment of either hydrophilic or easily ionisable (or altogether charged) functional groups to the periphery of the chromophore, mainly at the *meso* positions.

Thus, it is possible to obtain either cationic or anionic water soluble derivatives. Cationic porphyrins are commonly derived from *meso*-tetra(aminophenyl)porphyrin or from *meso*-tetrapyridylporphyrin by protonation or alkylation of the pyridyl groups, respectively. Anionic porphyrins are prepared by attachment of -OH, -COOH, or -SO_3Na functions to the aryl groups in *meso*-tetra-arylporphyrins .

Other strategies involve the introduction of water-soluble biocompatible polymers such as poly(ethyleneglycol) monomethyl ether [59] or sugar units.[60]

Some of these water soluble compounds, are of utmost interest for biomedical applications, and they have been extensively investigated in several bio-related fields, such as: *i*.specific binding of DNA as intra/extra intercalating agents,[61] *ii*. interactions with quadruplex DNA and telomerase inhibition,[62] *iii*. chemical or photochemical induced DNA cleavage,[63] *iv*. antiviral activity, including HIV-1,[64] *v*. boron neutron capture therapy (BNCT) of tumors,[65] *vi*. selective interaction with potassium channels,[66] *vii*. acetylcholinesterase inhibition,[67] *viii*. antibacterial activity,[68] and *ix*. photodynamic therapy for the treatment of cancer (PDT).[69] As previously discussed PDT represents a successful application of porphyrins for the treatment of cancer for the tumor-targeting properties of the porphyrins and the absorption in the red regionof the electromagnetic spectrum.

The coordination of water-soluble (e.g. charged) metal complexes to peripheral sites of the porphyrins is an intriguing alternative to the synthetic strategies described above for making water-soluble compounds. Such conjugates might have improved characteristics for

biomedical applications: *i*. if the metal complex possess anantiproliferative activity, they might combine the phototoxicity of the porphyrins chromophore and the cytotoxicity of the metal fragment for additive antitumour effect; *ii*. they might behave as carrier ligands for the active transport of anticancer metal fragments into cancer cells. Porphyrins show preferential uptake and retention by tumor tissues (tumor-localization properties); [70]*iii*.provided that the conjugates are sufficiently stable, the fluorescence emission of the chromophore might be exploited for tracking the biodistribution of the metal in the extra- and intra-cellular environment of malignant cells through fluorescence microscopy.

2.2. Metal-based anticancer agents

Platinum complexes

Metal complexes became very attractive as anticancer agents since 1965 when Rosenberg observed for the first time the anti-proliferative effects of some chloro-ammino platinum complexes. Cisplatin (*cis*-$[PtCl_2(NH_3)_2]$) is the parent compound of this class of agents and it is still one of the most effective chemotherapeutic agents in clinical use.[71] Its ability to inhibit tumor growth is related to its efficient binding to nuclear DNA after release of the two chloride ions: in other words, cisplatin is a pro-drug that is activated by hydrolysis.

In over three decades of dedicated efforts to develop cisplatin analogues and Pt complexes that break the cisplatin paradigm, only two Pt compounds, namely carboplatin ($[Pt(cbdc)(NH_3)_2]$ where cbdc = 1,1-cyclobutane dicarboxylate) [72] and oxaliplatin ([Pt(ox)(DACH)] where ox = oxalate and DACH = diamino cyclohexane), have been approved for worldwide clinical use. Platinum compounds have been the treatment of choice for ovarian, testicular, head and neck, and small cell lung cancer for the past 20 years. Despite its clinical success, cisplatin has several drawbacks: *i.* severe toxicity, in particular nephrotoxicity, neurotoxicity and emetogenesis; *ii.* applicability to a relative narrow range of tumors; *iii.* limited solubility in aqueous solution; *iv.*spontaneous or acquired resistance to some tumors.

Ruthenium complexes

The development of drug resistance, the toxic side-effects of cisplatin, and the lack of activity of platinum compounds against several types of cancer [73] have prompted the search for new metal-based antitumor drugs. Since complexes of transition metals other than platinum may exhibit antitumor activity markedly different from that of cisplatin and its analogues, several metals have been investigated. Among many transition metal compounds, ruthenium complexes have attracted great interest for their potential use as anti-cancer agents and have been widely investigated in the past 30 years.

While Pt(II) complexes are characterized by a the square-planar geometry, Ru(III) and Ru(II) (the more common oxidation states in aqueous solution) are usually esacoordinate and with octahedrical structure and are often fairly inert to ligand substitution.

The two most representative compounds of this class are KP1019 and NAMI-A, developed in the 1990s by Keppler [74] and Alessio [75] respectively (Figure 9).

They both have completed phase I clinical trials with promising results.[76] NAMI-A has started already a phase II combination study, whereas the sodium salt of KP1019, KP1339, was selected for further development because it is about 35-times more water soluble than its parent compound.

Both compounds are moderately cytotoxic in vitro and, in animal models, have activities different from established Pt drugs: KP1019 showed excellent activity against platinum resistant colorectal tumors,[77] whereas NAMI-A was found to be particularly active against the development and growth of metastases of solid tumors,[78] even in advanced stage.[79]

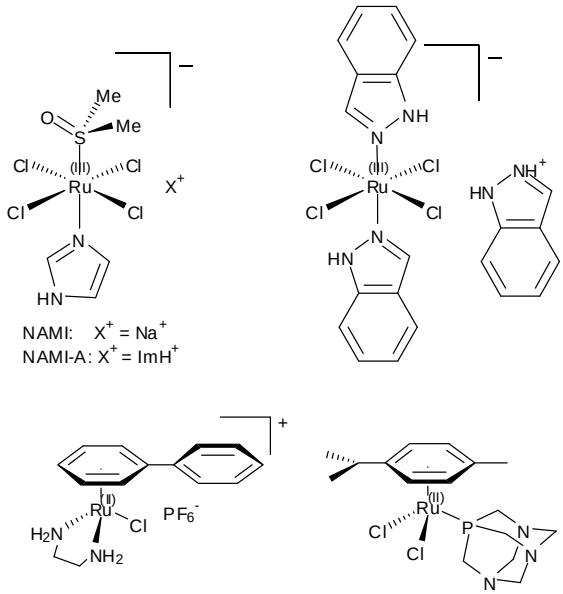

Figure 9. Schematic structures of NAMI-A (top, left), KP1019 and KP1339 (top, right), RM175 (down, left), RAPTA-C (down, right).

In recent years, entirely new classes of organometallic Ru(II)-arene compounds, developed by the groups of Sadler, [80] Dyson, [81] Keppler [82] and others, [83] were found to have promising anticancer activity both in vitro and, in some cases, also in vivo in murine models. [84] Interestingly, some of them proved to be active also against cisplatin-resistant xenografts.[85]

Representative examples of these organometallic compounds (also called *piano-stool* compounds) are $[Ru(\eta^6\text{-arene})Cl(L\text{-}L)]^{n+}$ (L-L = azotate chelating ligand, n = 1; L-L = oxygen anionic chelating ligand, n = 0).

Among them, active compounds are $[Ru(\eta^6\text{-arene})Cl(en)](PF_6)$ (en = etilendiammine, arene = benzene, *p*-cymene (Cym), tetrahydroanthracene (THA), dihydroanthracene (DHA), biphenyl (Bip). Representative examples are $[(\eta^6\text{-biphenyl})Ru(en)Cl][PF_6]$ (RM175) and $[(\eta^6\text{-p-cymene})\text{- }RuCl_2(pta)]$ (RAPTA-C) (Figure 9).

Since cytotoxicity of the metal fragment increases with the lipophilicity,[86] Prof. Alessio's research group started a structure-activity relationship investigation aimed to establish whether the η^6–arene fragment of these organometallic half sandwich compounds might be effectively replaced with a neutral face-capping ligand while maintaining the other ligands unchanged.

Thus, they developed series of new half sandwich Ru(II) coordination compounds of the general formula $[Ru([9]aneS_3)(chel)L][X]_n$, [87,88] (where chel = neutral *N–N* chelating ligand such as en, 2,2'-bipyridine (bipy) or substituted bipy, L = Cl n = 1, L = dmso n = 2, [X] = $CF_3SO_3^-$, PF_6^-), were the aromatic ligand has been replaced by the sulfur macrocyle 1,4,7-trithiacyclononane ([9]aneS3)or by the corresponding nitrogen macrocycle 1,4,7-triazacyclononane ([9]aneN3, also known astacn) [89] (Figure 10).

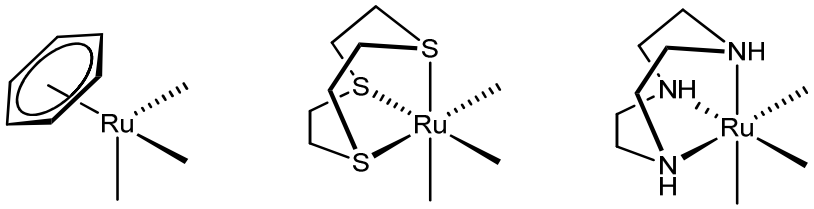

Figure 10. Schematic structures of Ru(II) compounds with aromatic ligands (left) and Ru(II) compounds with 1,4,7-trithiacyclononane(center), and 1,4,7-triazacyclononane (right) .

In general, they demonstrated that Ru-[9]aneS3 compounds have a cytotoxicity comparable to that of the corresponding organometallic analogs. The most cytotoxic complex among this class was $[Ru([9]aneS_3)(en)Cl][OTf]$, that was found to be ca. 10 times less cytotoxic than the corresponding *piano-stool* organometallic compound RM175 against human breast cancer MDA-MB-231 cells.

Those data suggest that the aromatic fragment of the piano-stool Ru (II) compounds is not an essential feature for the in vitro anticancer activity and it might be effectively replaced by another face-capping ligand with a low steric demand such as [9]aneS3.

2.3. Metal-porphyrin conjugates

The coordination of metal complexes to porphyrin systems for biomedical applications has been investigated over the past decade, but only few examples are reported in literature.

Song et al. reported an increase of the antitumor activity of anionic and cationic porphyrin-platinum conjugates (Figure 11) compared to the platinum complexes against murine leukemia L1210 cell line. [90] They found that the coordination of a Pt(II) fragment in peripheral position did not affect the tumor-targeting properties of the porphyrins.

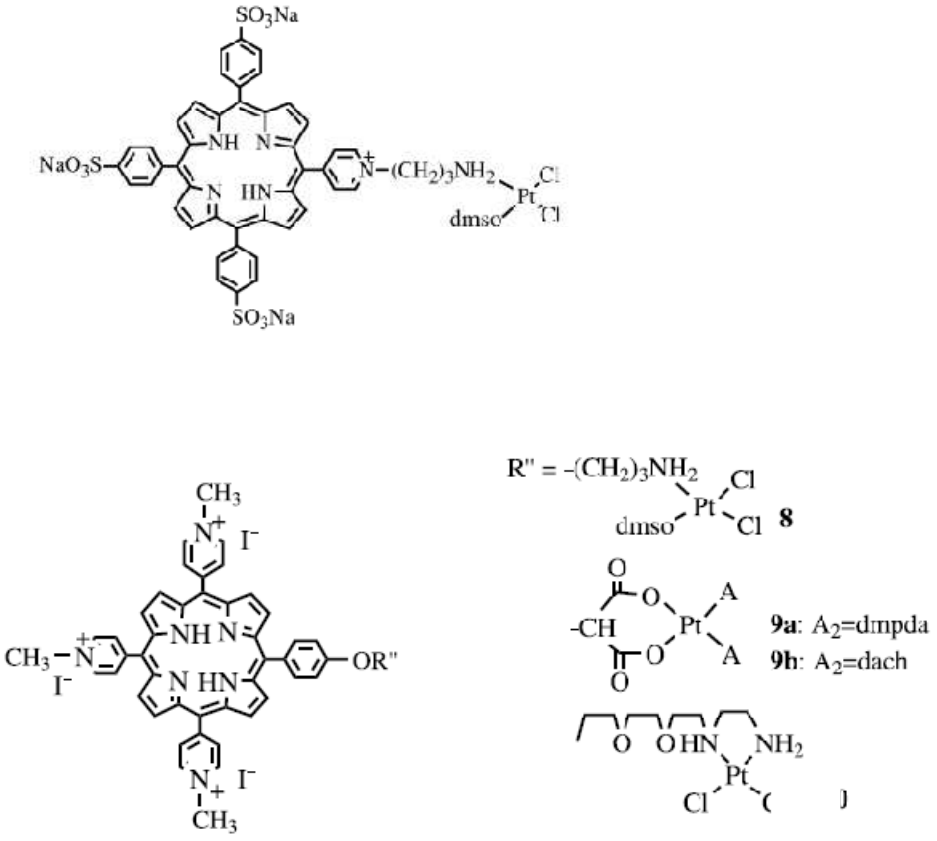

Figure 11. Schematic structure of cationic porphyrin–platinum(II) conjugates.Adapted from ref. 90.

Brunner et al. derivatized asymmetric tetraarylporphyrins [60] and hematoporphyrin [91]with a platinum(II) fragment (Figure 12). Their aim was to combine the cytostatic activity of cisplatin or oxaliplatin and thephotodynamic effect of hematoporphyrin and or asymmetric tetraarylporphyrins in the same molecule after irradiation with red light.[90, 91]

This study demonstrated an increase of the antitumor activity of the platinum moiety by an additional light-induced toxicity. Some of the most active conjugates of the two series of compounds are shown in Figure 12.

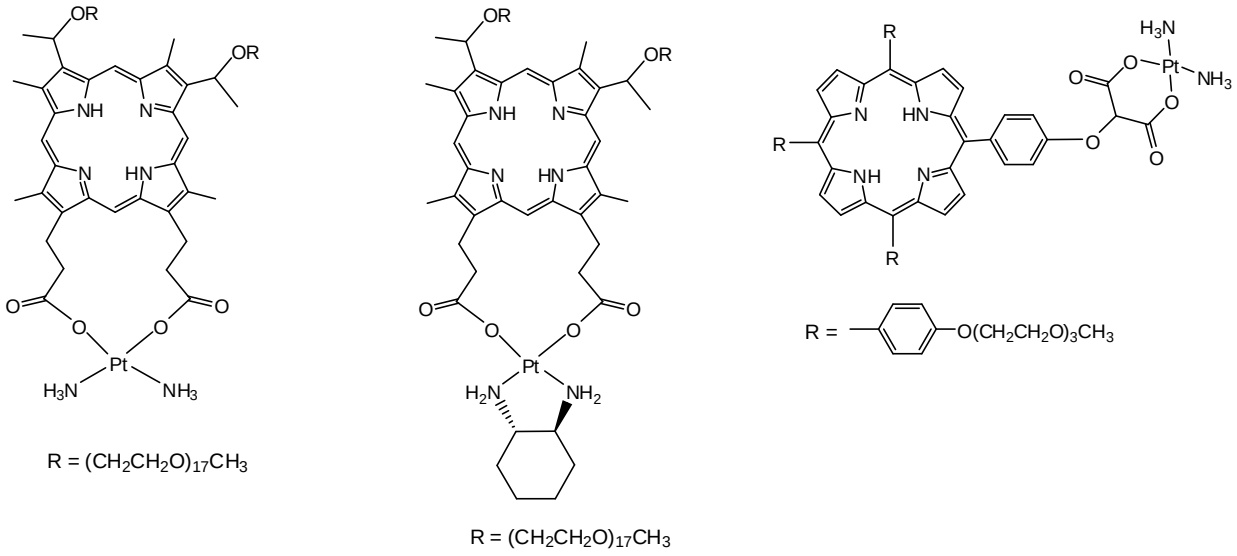

Figure 12. Schematic drawing of some Pt-porphyrin conjugates,[59, 91]

More recently, Guo and co-workers described a dinuclear cisplatin-phthalocyanine conjugate that showed a remarkable enhancement of cytotoxicity against tumor cell lines when irradiated with red light.[92]

Porphyrin units decorated at the periphery with ruthenium complexes have been already reported in literature and promising preliminary results were obtained in specific biologic assay.

Therrien and co-workers recently reported that neutral conjugates of *meso*-3'- and 4'-pyridylporphyrins with organometallic *piano stool* [Ru(η^6-arene)Cl_2] fragments (Figure 13) are moderately cytotoxic in the dark against Me300 human melanoma cells, and become cytotoxic upon irradiation with visible light. [93] Interestingly, photodynamic studies revealed that, 3'-pyridyl photosensitizers were better photosensitizers than 4'-pyridyl photosensitizers. However, due to the very low solubility of the complexes in water, the biological application seems to be rather limited. Furthermore, the possible dissociation of the arene moiety in vivo leads a substantial risk of toxicity of these compounds.

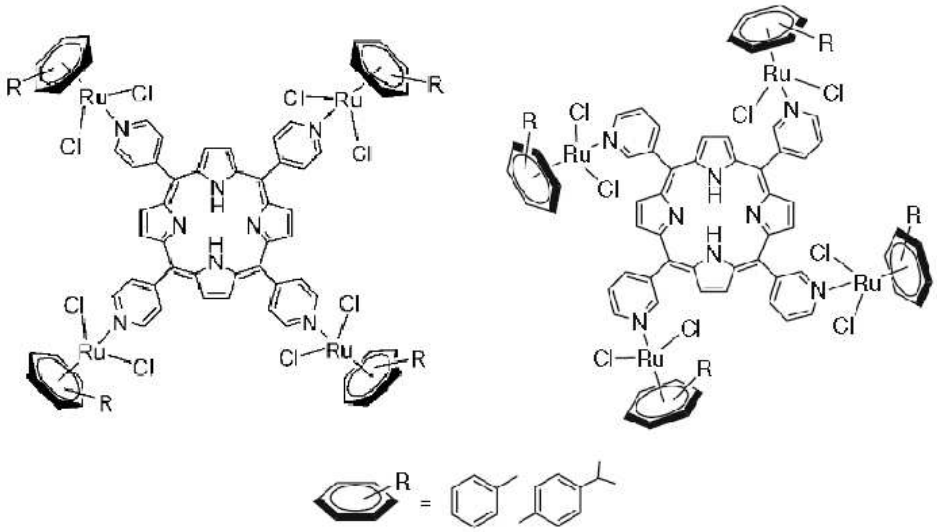

Figure 13. Schematic structure of Ru(η^6-arene)-porphyrins. Adapted from ref. 93a.

Swavey and co-workers reported the synthesis and the characterization of new cationic fluorinated porphyrins bearing one or two [Ru(bpy)$_2$Cl] fragments (Figure 14).[94 95] The ruthenium porphyrin conjugates were able to bind DNA and photocleave supercoiled DNA when irradiated with low-energy light. In addition, this complexes showed low dark toxicity but initiates apoptosis in melanoma cells upon irradiation in the visible range.

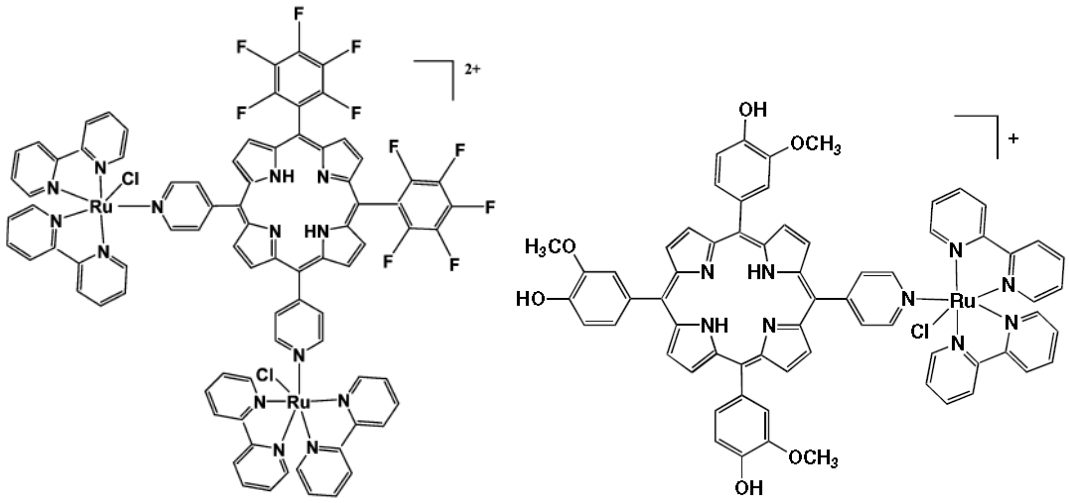

Figure 14. Schematic structure of fluorinated Ru-porphyrinsAdapted from refs. 94 and 95 respectively.

2.4.Synthesis and Characterization of Ru(II)-porphyrin conjugates

The aim of this work was to synthesize water soluble compounds that are expected to combine the cytotoxicity to the metal fragment to the phototoxicity of the porphyrins for an additive antitumor effect.

Conjugation strategies

The coordination of a porphyrin to peripheral metal fragments can occur either through a single bond or through multiple bonds (*i.e.* through a chelating moiety). Typically, pyridyl rings are used as peripheral ligands for the coordination of late transition metal ions. [96,97,98] The former synthetic approach has an indubitable advantage: the commercially available, or otherwise easily prepared, *meso*-pyridylporphyrins (PyPs) can be exploited.

In PyPs, the pyridyl N atoms can be either in 3'(3'PyP) or, more commonly, in 4' position (4'PyP). Even though synthetically more demanding, also PyPs in which the pyridyl rings are not directly bound at the *meso* positions, but are connected thorough a spacer, have been used occasionally.[99] In the case of ruthenium, the vast majority of the conjugates reported in the literature involve the symmetrical coordination of four equal Ru fragments to a *meso*-tetrapyridylporphyrin (TPyP).[100,101] In general, relatively few TPyP-$(Ru)_4$ conjugates were explicitly prepared for biomedical investigations. In such context, the peripheral Ru fragments were typically of the type $Ru(chel)_2X$, where chel is a polypyridyl ligand. [102, 103] The choice of rutheniumpolypyridyl complexes was motivated by two main reasons: *i*. they have a good affinity for DNA.[104] Thus, similarly to Pt(II) fragments, they might behave as chaperones and help localizing the porphyrins photosensitizer close to DNA where the photoinduced generation of ROS would be more effective for inducing cell damage. *ii*. They are potential photosensitizers, and some of them were found capable of DNA photooxidation and photocleavage. [105 , 106 , 107] Examples of mono- and di-pyridylporphyrins conjugated to Ru polypyridyl fragments were also recently reported and their DNA binding properties and photocleavage capability described.[94, 95,108]The residual *meso*-phenyl groups may be exploited for increasingwater solubility (*e.g.* through appropriate substituents) or forenhancing the photophysical properties (*e.g.* by fluorination).

Besides the already mentioned compounds by Therrien and coworkers,[93] recently, we described the preparation and characterization of several new Ru-porphyrin conjugates that

bear either negatively charged NAMI-A-type Ru(III) fragments or negatively charged ruthenium(II)nitrosyl complexes.[109]

Nevertheless, the single-bond conjugates might be insufficiently stable towards aquation under in vivo conditions, with consequent loss of the peripheral Ru fragments. Conjugation through multiple bonds increases the stability of the adducts but poses the necessity of developing affordable synthetic strategies towards porphyrins with peripheral chelating moieties. Even though a few examples of such Ru-porphyrin conjugates are known in the literature, we are unaware that any of them was explicitly prepared and investigated for biomedical purposes so far.

Herein, both coniugation strategies were applied to synthesize Ru–porphyrin conjugates.

4'PyPs and 3'PyPs were used for the coordination of Ru fragments through a single coordination bond (Figure 15a).

Furthermore we describe the preparation in acceptable yields of a series of porphyrins that bear 4 peripheral bipyridinemoieties connected through an amide bond or through a flexible linkers of variable length and hydrophilicity. Lately these porphyrins were used for the coordination of Ru fragments through a double coordination bonds (Figure 15b).

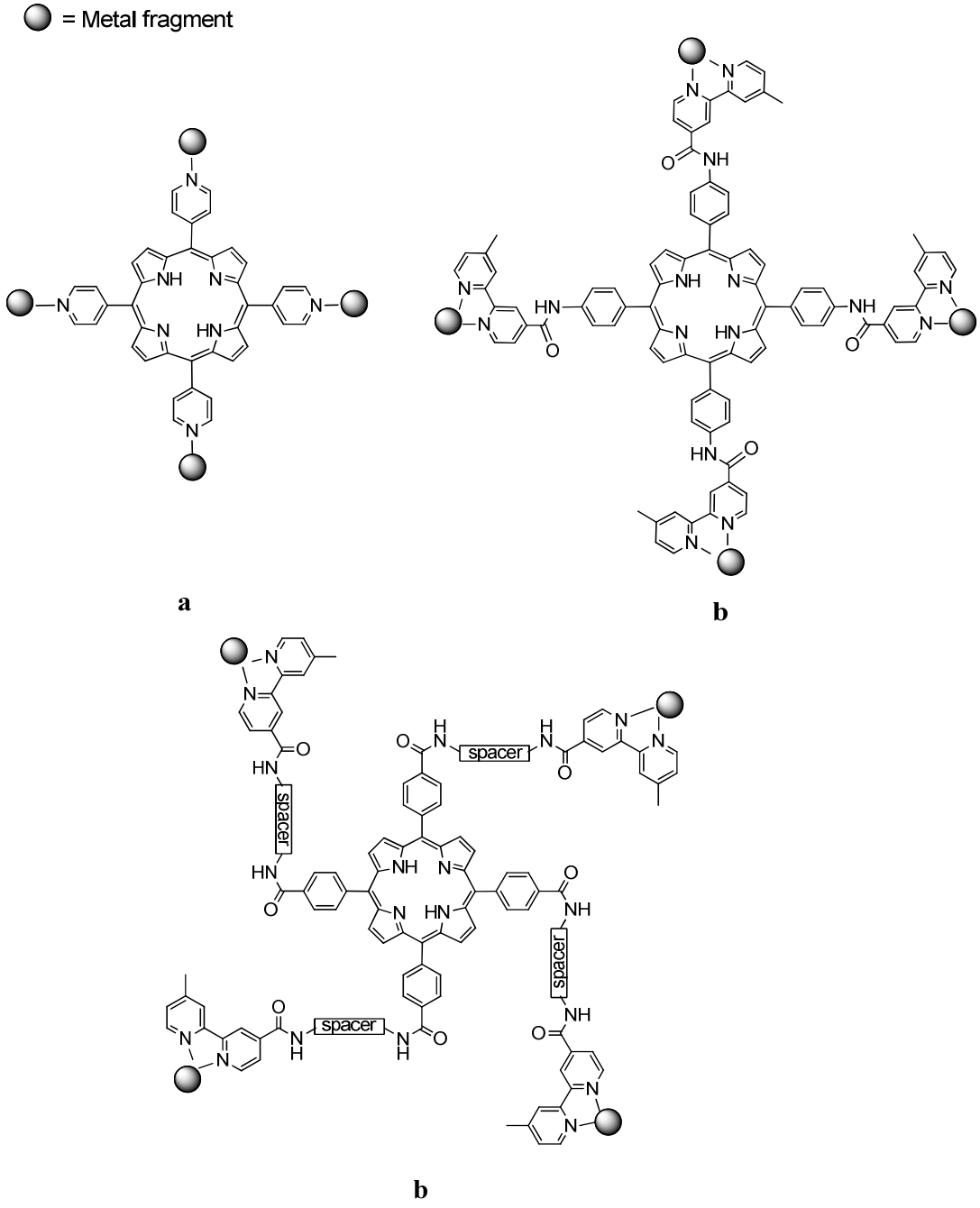

Figure 15. Metal-porphyrins conjugates through single bond (**a**) or multiple bonds (**b**).

2.4.1. Conjugates with meso 4'-tetrapyridylporphyrin (4'-TPyP).

We performed the coordination of 4'TPyP to half-sandwich Ru(II) fragments.

Treatment of 4'TPyP with a slight excess of [Ru([9]aneS3)(en)Cl][CF_3SO_3] in the presence of Ag(CF_3SO_3) for removing the chlorido ligand) affords the octacationic conjugate [4'TPyP{Ru([9]aneS3)(en)}$_4$][CF_3SO_3]$_8$ (**2**) in excellent yield (Scheme 2).

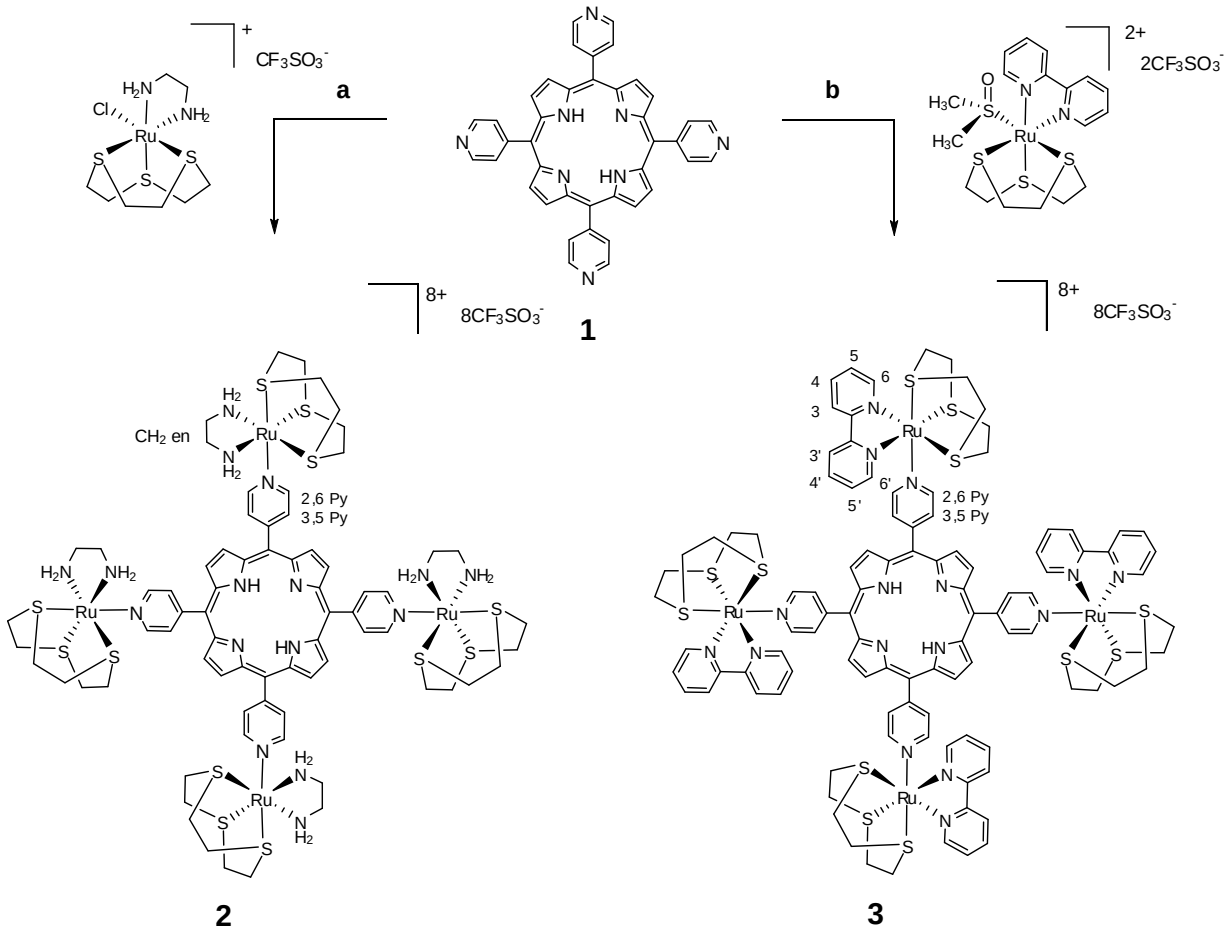

Scheme 2. Synthesis of [4'TPyP{Ru([9]aneS3)(en)}$_4$][CF_3SO_3]$_8$ (**2**) [a]and [4'TPyP{Ru([9]aneS3)(bpy)}$_4$][CF_3SO_3]$_4$ (**3**).[b]

[a]Reactions and conditions: (a) methanol/chloroform, 4h, reflux (92%). (b) methanol/chloroform, 8h, reflux (71%)

Compound **2**, besides being soluble in organic solvents such as methanol and nitromethane, is also well soluble in aqueous solution and in PBS (pH=7.4).

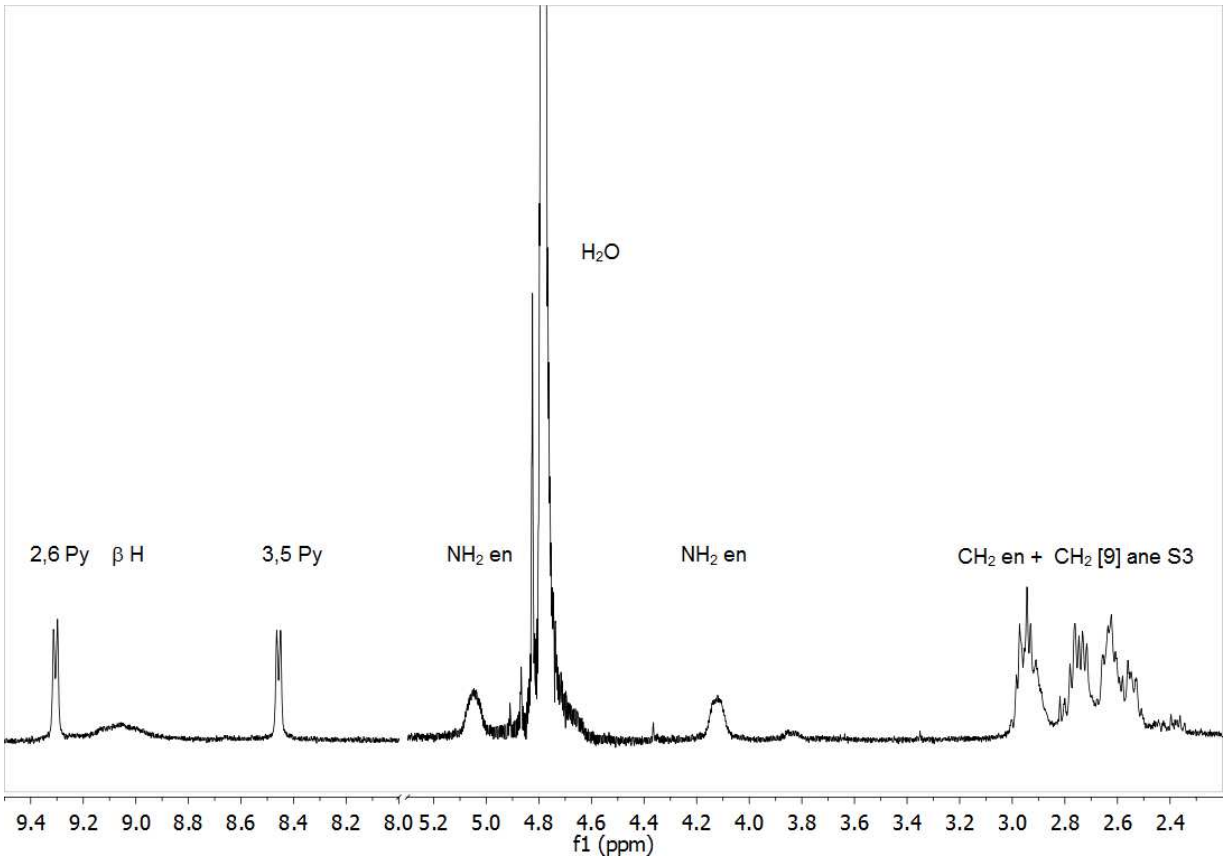

Figure 16.[1]H NMR spectrum (500 MHz) of **2** in D_2O. See Scheme 2 for numbering scheme.

Overall, the [1]H NMR spectrum of **2** is consistent with the symmetry of the compound: all peripheral Ru fragments are equivalent. All proton resonances are sharp at 20 °C, with the exception of the βH signal that is remarkably broad (Figure 16). The four equivalent pyridyl rings give two well resolved doublets in the aromatic region of the spectrum. The upfield region is similar to that of the precursor Ru complex: in D_2O the two pairs of diastereotopic protons on the equivalent NH_2 groups give two well resolved resonances at δ = 4.17 and 5.09 (coupled in the H-H COSY spectrum), whereas the CH_2 protons of en and of [9]aneS3 resonate as a series of partially overlapping multiplets between δ = 2.6 and 3.1 (Figure 16). Only four aliphatic [13]C resonances are observed in the HSQC spectrum (one for the en carbons and three for the [9]aneS3 carbons), consistent with a C_S symmetry in solution for each equivalent Ru fragment, as was found in the precursor.[87]

The corresponding conjugate [4'TPyP{Ru([9]aneS3)(bpy)}$_4$][CF_3SO_3]$_8$, (**3**) with bpy in the place of en, was obtained by treatment of 4'TPyP with[Ru([9]aneS3)(bpy)(dmso-S)][CF_3SO_3]$_2$ upon replacement of dmso by the pyridyl groups (Scheme 2). Compound **3** was also characterized in the solid state by X-ray crystallography: the tetranuclear cation is

composed of four $[[Ru([9]aneS3)(bpy)]^{2+}$ units bound to the *meso* pyridyl moieties in a centro-symmetric arrangement (Figure 17).

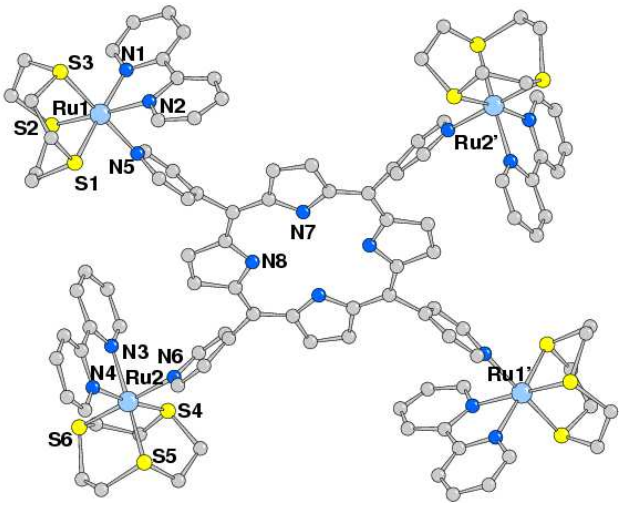

Figure 17. Molecular structure of the centro-symmetric complex cation of $[4'TPyP\{Ru([9]aneS3)(bpy)\}_4][CF_3SO_3]_8$ (**3**).

The cation presents a pseudo four fold axis normal to the porphyrin mean plane: the four Ru fragments are iso-oriented, with intermetallic side distances of 14.303(4) Å (Ru1···Ru2) and 14.213(3) Å (Ru1···Ru2'). The Ru centers have a distorted octahedral coordination sphere, with Ru–S and Ru–N(bpy) coordination distances that average to 2.17(1) Å 2.373(5) Å, respectively (*i.e.* they are longer by ca. 0.05 and 0.03 Å, respectively, than those found in the Ru(II) precursor).[88] The two independent *meso* pyridyl rings N5 and N6 form a dihedral angle with the porphyrin mean plane of ca. 68° and deviate slightly from a linear coordination, with Ru–N(py)···C(*meso*) angles significantly narrower than 180° (168.3 and 172.9°, respectively). As a consequence, the bpy ligands are considerably canted towards the adjacent *meso* pyridyl rings (dihedral angles between the mean planes of 62.4(4) and 72.8(4)°, Figure 18). A pyridine ring of each bpy is located approximately in the porphyrin plane (Figure 18), at a distance of ca. 4.45 Å from a pyrrole hydrogen atom. This feature, probably dictated by packing effects, might be compatible with weak CH···π interactions.

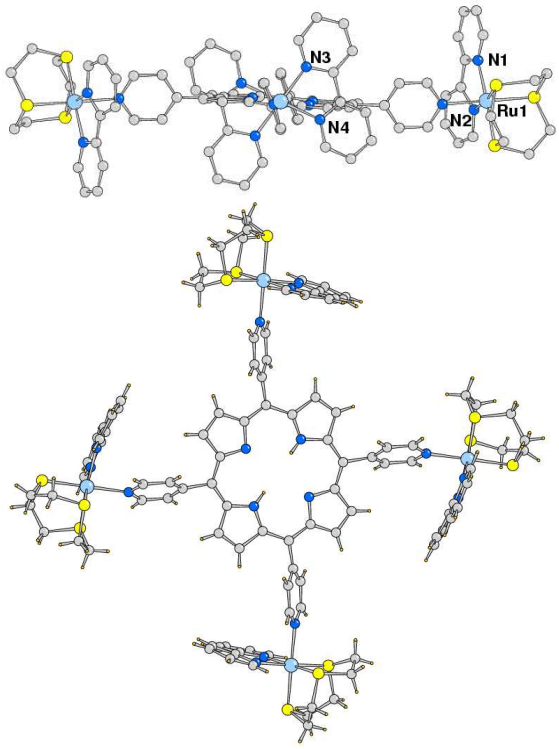

Figure 18. Top: side view of the complex cation of **3** along the Ru2···Ru2' direction ([9]aneS3 ligands and Ru2 ions omitted for clarity). Bottom: top view showing the canting of the bpy ligands towards the pyrrole rings.

Compound **3** is mildly soluble in water and in phosphate buffer at pH 7.4.

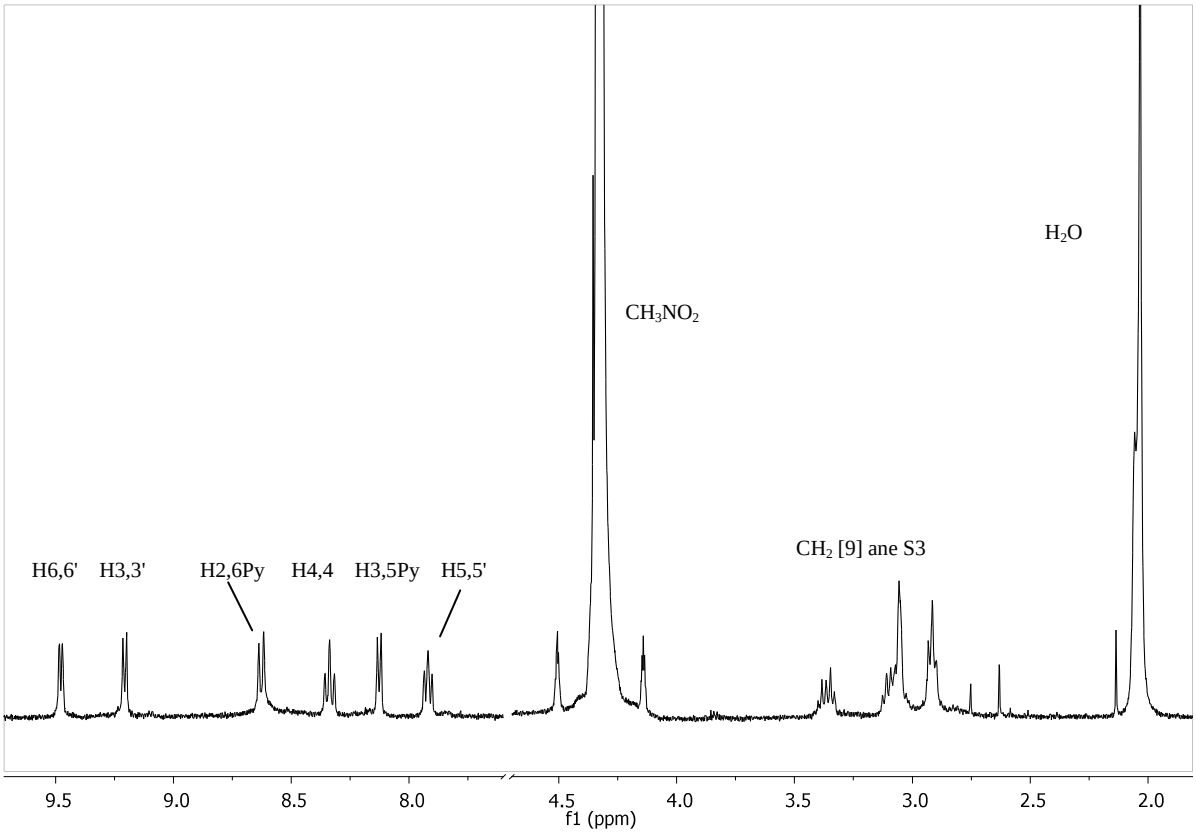

Figure 19. ^{1}H NMR spectrum (500 MHz) of **3** in CD_3NO_2. See Scheme 2 for numbering scheme.

As for **2**, the ^{1}H NMR spectrum of **3** in CD_3NO_2(Figure 19) shows sharp signals at 20 °C (with the exception of the βH resonance) and is consistent with the symmetry of the molecule (Scheme 2). The single set of bpy and pyridyl signals (four and two, respectively) implies that all four metal fragments are equivalent and that each of them has a C_S symmetry. The anisotropic shielding of the bpy rings, that are perpendicular to the plane of the porphyrin, more than counteracts the deshielding typically observed upon coordination of 4'PyPs to Ru(II) fragments;[110]as a consequence, the resonances of 4'TPyP are shifted slightly upfield compared to **2** (δ H2,6 = 8.63 in **3***vs* 9.31 in **2**;δ H3,5 = 8.14 in **3** *vs* 8.41 in **2**).

As already mentioned, both **2** and **3** have very broad βH resonances at 20 °C, suggesting the occurrence of conformational equilibria. Variable temperature (VT) NMR experiments showed that for **2**, in CD_3NO_2 solution, the resonance of the eight pyrrole protons becomes a sharp singlet at 65 °C, whereas at -30 °C in CD_3OD solution it splits into two equally intense sharp singlets (δ= 9.30 and 8.97) that are not correlated in the H-H COSY spectrum. (Figure 20).

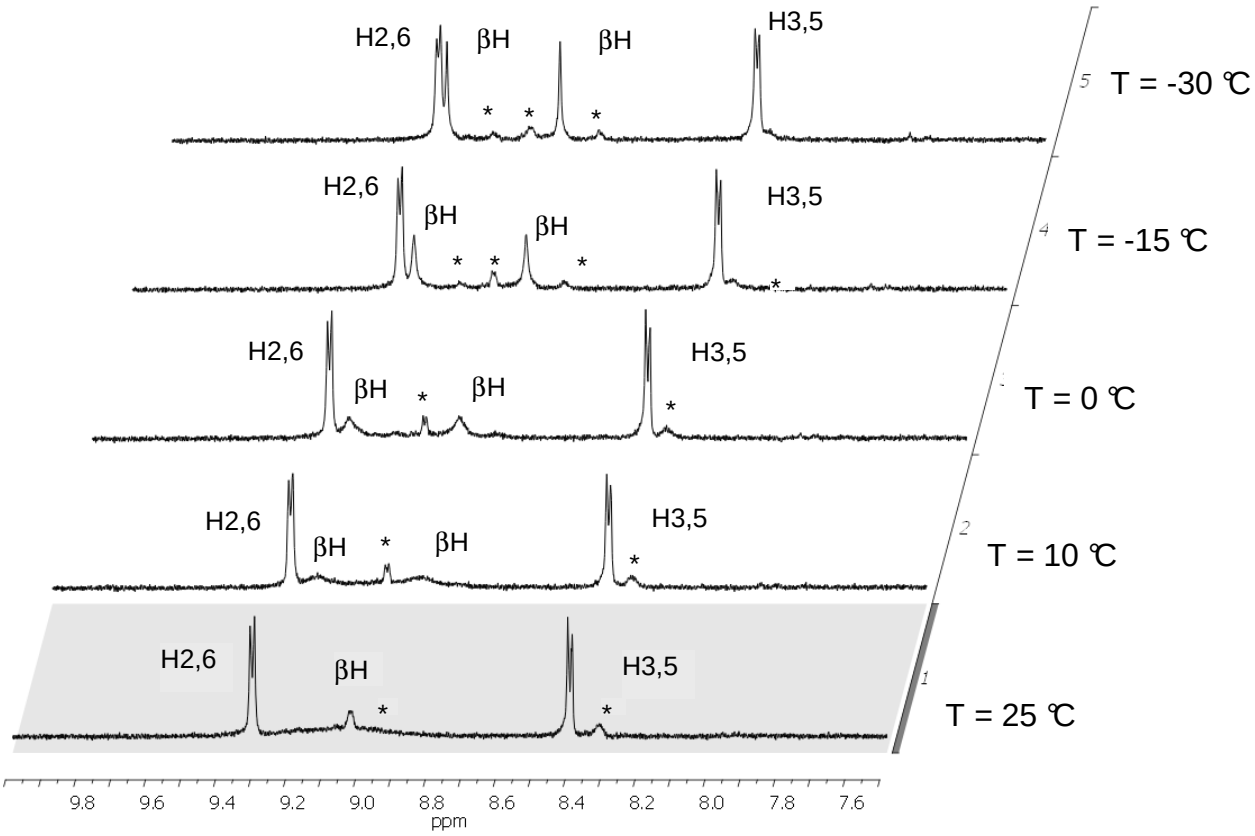

Figure 20. Temperature dependence of the ^{1}H NMR spectrum (downfield region) of [4'TPyP{Ru([9]aneS3)(en)}$_4$][CF_3SO_3]$_8$ (**2**) in CD_3OD. *: impurity.

The βH resonance of the bpy derivative **3** has a very similar temperature dependence in CD_3OD/CD_3NO_2 (99:1) solution and splits into two equally intense sharp singlets at -40 °C (δ = 8.89 and 8.51, Figure 21)

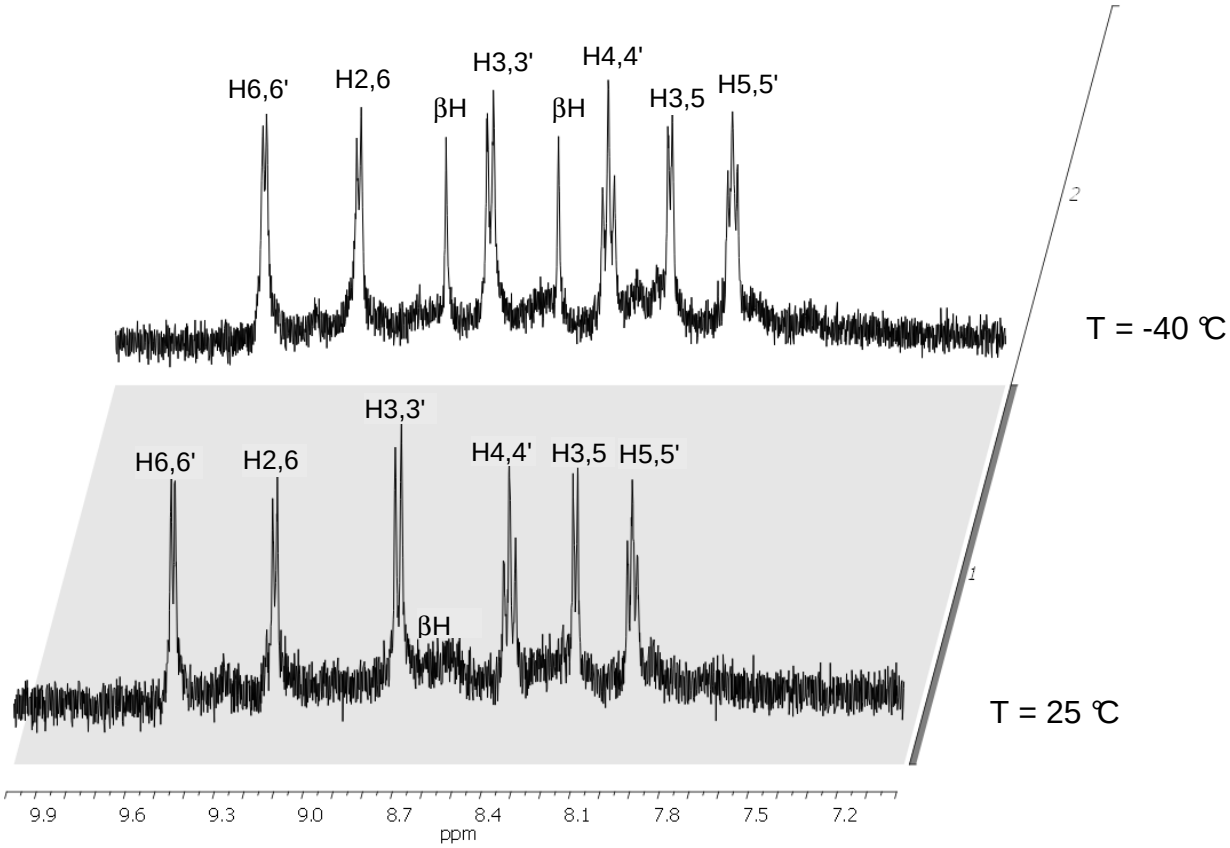

Figure 21. Temperature dependence of the ^1H NMR spectrum (downfield region) of $[4'TPyP\{Ru([9]aneS3)(bpy)\}_4][CF_3SO_3]_8$ (**3**) in CD_3OD/CD_3NO_2 (99:1) solution.

The upfield singlet was assigned to the four pyrrole protons that are directly shielded by the bpy rings. The βH NMR pattern found for both **2** and **3** at low T is compatible with the presence in solution of a frozen conformer with a D_{2h} symmetry, with adjacent Ru fragments arranged in a pairwise fashion: en (or bpy) ligands on Ru units at *meso* positions 5, 10 (and 15, 20) face each other, while those on the *meso* positions 5, 20 (and 10, 15) are far apart (Figure 20 and Figure 21). The two types of βH protons, a and b, are exchanged by the concerted rotation of the four Ru complexes. This geometry is different from that found in the solid state for **3**(Figure 22), where all Ru fragments are iso-oriented, but is similar to that found by us for the Re(I) conjugate $[4'TPyP\{Re(CO)_3(bpy)\}_4][CF_3SO_3]_4$.[111]

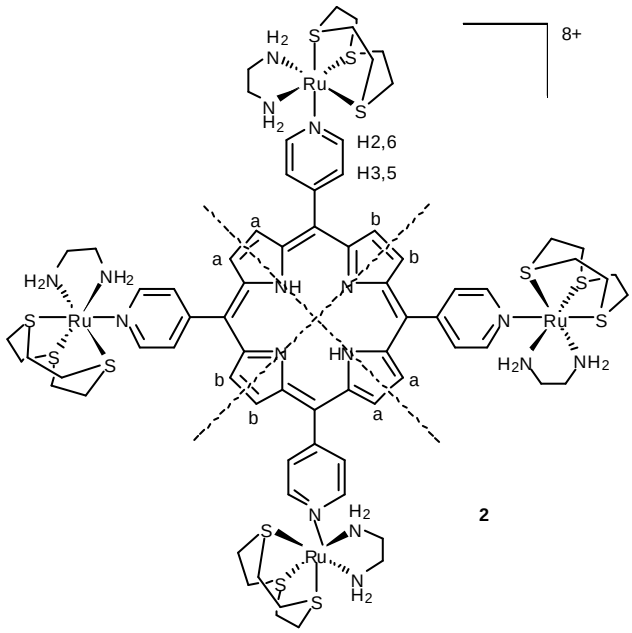

Figure 22. Schematic structure of the prevailing conformer of **2** at low T. Dotted lines indicate the two symmetry planes. The two sets of equivalent βH protons, responsible for the two singlets in the low t NMR spectrum, are labeled a and b.

Both porphyrin conjugates **2** and **3** are very stable in aqueous solution and in phosphate buffer at physiological pH: their NMR and visible spectra remain unchanged for hours. This behavior is consistent with the substitutionally inert coordination sphere of the Ru(II) fragments.

2.4.2. Conjugates with meso 3'-tetrapyridylporphyrin (3'-TPyP).

Photodynamic studies by Therrien et al. revealed that 3'-pyridylporphyin photosensitizers are more efficient than 4'-pyridylporphyrinanalogs. [93] Starting from these observation, we synthesized the 3'-pyridylporphyrin conjugates bearing in peripheral positions the same Ru(II) fragments, $[Ru([9]aneS3)(en)]^{2+}$ and $[Ru([9]aneS3)(bpy)]^{2+}$, of Ru-4'TPyPs previously described.

The synthesis of 3'TPyP was performed following asynthetic procedure reported in literature.[112]

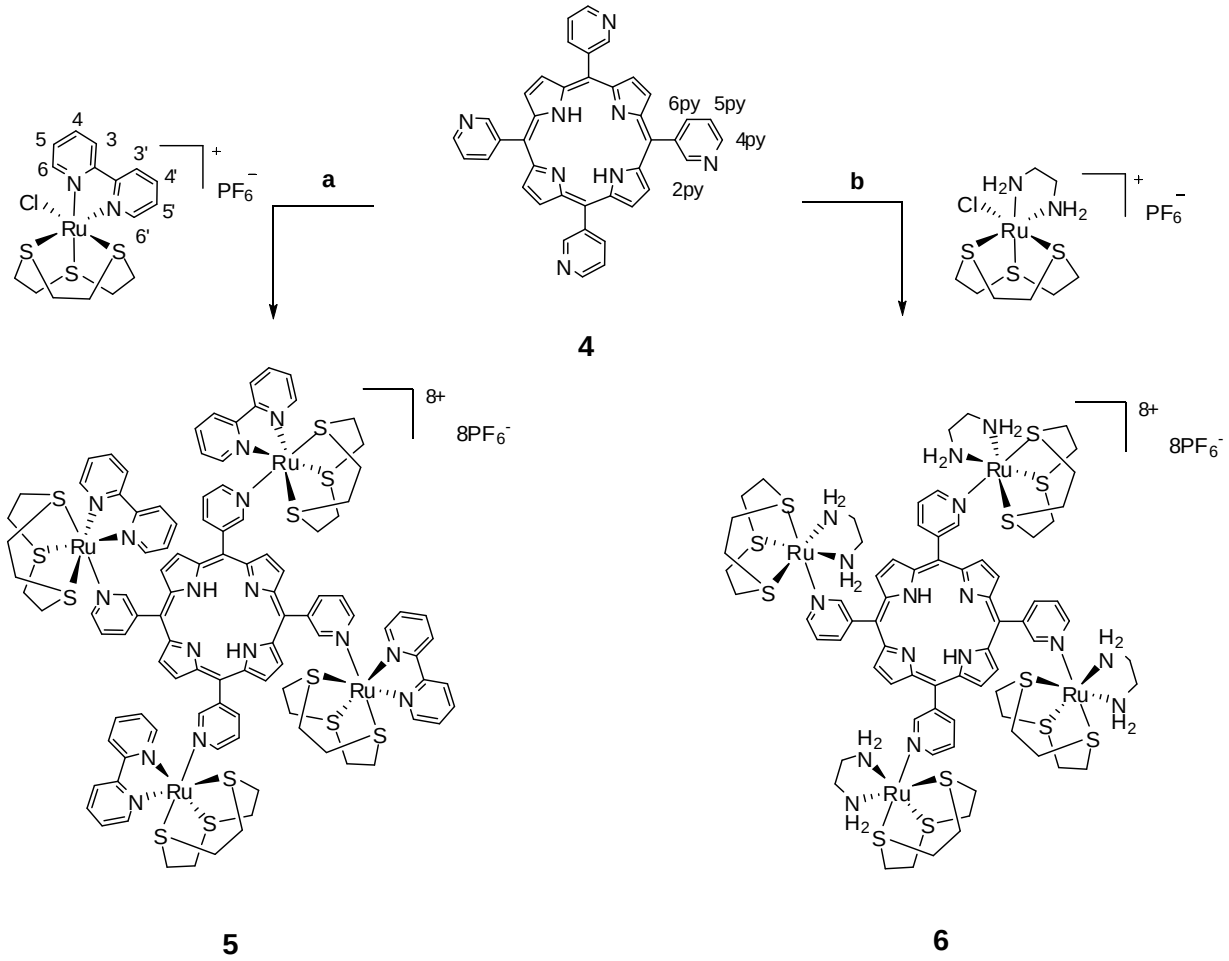

Scheme 3. Synthetic strategy towards the synthesis of $[3'TPyP\{Ru([9]aneS3)(bpy)\}_4][PF_6]_8$ (**5**)[a] and $[3'TPyP\{Ru([9]aneS3)(en)\}_4][PF_6]_8$ (**6**)[b].
[a]Reactions and conditions: (a) methanol/chloroform, 48h, reflux (86%)[b] methanol/chloroform, 48h, reflux (76%).

Treatment of 3'TPyP with a slight excess of either $[Ru([9]aneS3)(bpy)Cl][PF_6]$ or $[Ru([9]aneS3)(en)(Cl)][PF_6]$ (in the presence of $AgPF_6$ for removing the chlorido ligand)

afforded the octacationic conjugates [3'TPyP{Ru([9]aneS3)(bpy)}$_4$][PF_6]$_8$ (**5**) or [3'TPyP{Ru([9]aneS3)(en)}$_4$][PF_6]$_8$ (**6**), respectively, in excellent yield (Scheme 4).
While compound **6** is soluble in water and in PBS, **5** is only mildly soluble in water but it is soluble in organic solvents such as methanol and nitromethane.

Compound **5** was characterized in solid state by single crystal X-ray analysis. The structural determination evidenced in the crystal the tetranuclear complex beside the PF_6^- anions and two nitromethane molecules per complex unit.
The complex, composed of four [Ru([9]aneS3)(bpy)]$^{2+}$ units bound to the *meso* pyridyl moieties, has a fourfold symmetry being located about a crystallographic $\bar{4}$ axis (Figure 23), so that the metals are alternatively displaced above and below the porphyrin mean plane.

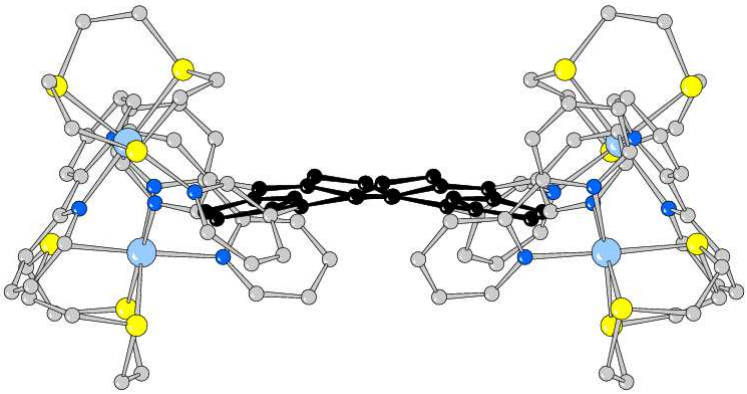

Figure 23. Side view of the complex cation [3'TPyP{Ru([9]aneS3)(bpy)}$_4$][PF_6]$_8$ (**5**) (porphirine moiety in black)

The crystallographically independent metal unit is chelated by the nitrogens of bipyridine, by the sulfur atoms of the tripodal ligand and complete the distorted octahedral coordination sphere through the nitrogen donor of the pyridine unit bound to the meso position of the porphyrin. The metals are separated by 12.357 Å, while diagonal distance is 17.034 Å (Figure 24).

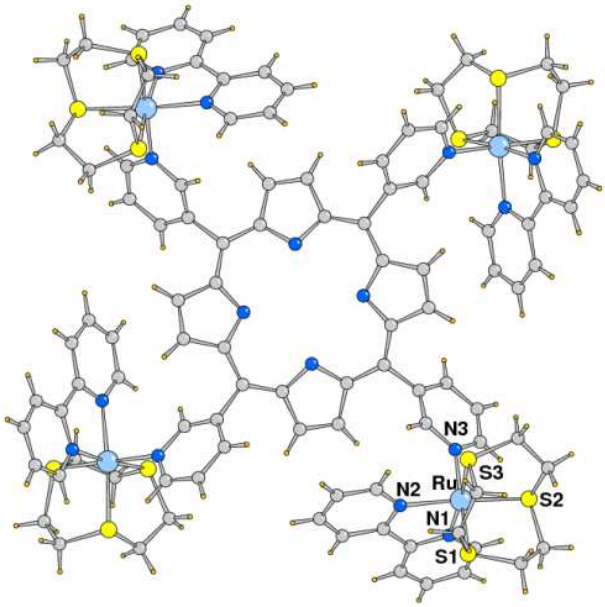

Figure 24. Molecular structure of the complex cation of [3'TPyP{Ru([9]aneS3)(bpy)}$_4$][PF_6]$_8$ (**5**) viewed down the fourfold symmetry axis. (**5**).

The Ru-N(bpy) bond distances (of 2.084(8) and 2.080(8) Å) are slightly shorter than those relative of Ru-N(pyridine) (2.118(7) Å), while the Ru-S are similar within their esd's (range 2.299(3)–2.316(2) Å). The coordination angles provide indication of the distortions in the coordination sphere of the metal (coordination *cis* angles between 78.3 (4) and 97.5 (3)°). The geometrical parameters of the coordination sphere are comparable to those measured in the corresponding complex [4'-TpyP{Ru([9]aneS3)(bipy)}$_4$]$^{8+}$. The ^{1}H NMR spectrum of **5** in CD_3NO_2 at room temperature is reported in Figure 25. The downfield region is quite complex: it shows a manifold of relatively broad and overlapping multiplets suggesting the coexistence of several conformers, owing to hindered rotation about the C(*meso*)–C(pyridyl) bond (and perhaps also the N-Ru bond) (Figures 23-24). Thus, no assignment was attempted. This behavior has been already observed in the spectrum of the rhenium-3'tetrapyridylporphyrin derivative [111]

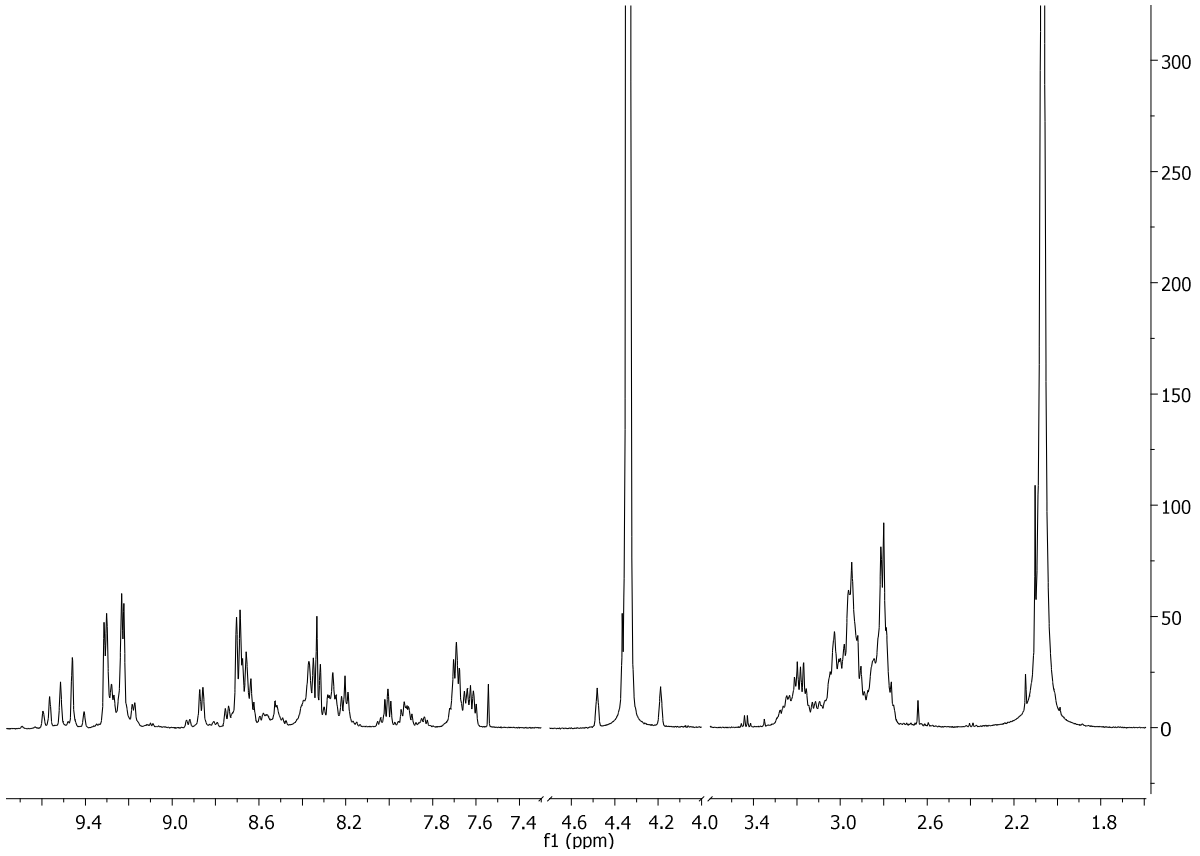

Figure 25. ^{1}H NMR spectrum of **5** in CD_3NO_2.

The ^{1}H NMR spectrum of **5** in CD_3NO_2 at room temperature is reported in Figure 25. The downfield region is quite complex: it shows a manifold of relatively broad and overlapping multiplets suggesting the coexistence of several conformers, owing to hindered rotation about the C(*meso*)–C(pyridyl) bond (and perhaps also about the N–Ru bond). The conformational equilibria must be slow on the NMR time scale. This behavior has been already observed for similar conjugates of 3'TPyP with rhenium(I) complexes. Even though full assignment was not attempted, the most downfield manifold of (at least 5) singlets can be assigned to H2 on the pyridyl ring. The number of H2 singlets is not necessarily coincident with the number of conformers: this would be the case only if in each conformer the four bpy ligands are made equivalent by the symmetry.

The ^{1}H NMR spectrum of **6** in CD_3NO_2 (Figure 26) is similar to that of **5**, even though obviously less crowded in the aromatic region. The resonances were assigned by means of a conventional H-H COSY spectrum.

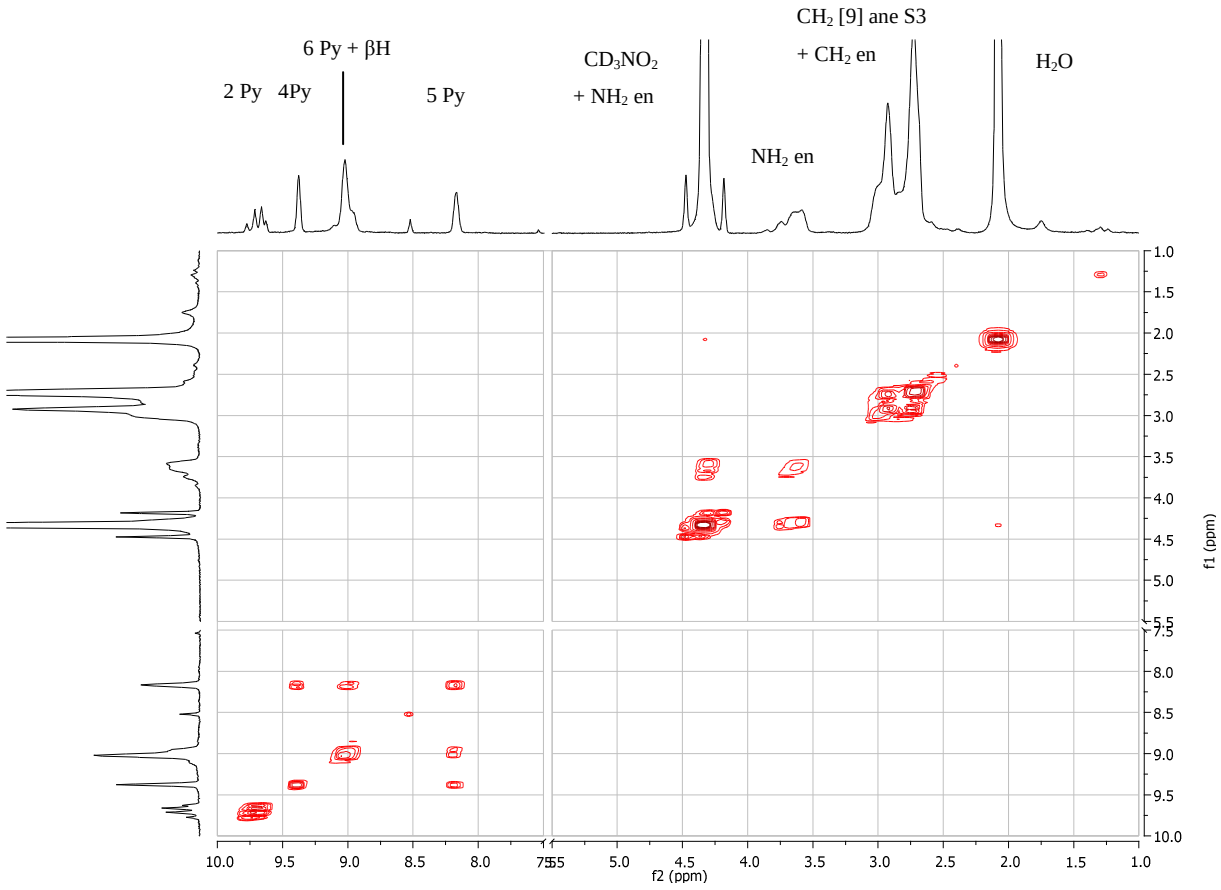

Figure 26.H-H COSY spectrum of **6** in CD_3NO_2. See Scheme 3 for numbering scheme.

All the aromatic resonances are very broad and only the signal at δ 9.70 shows a multiplicity. The most upfield signal at δ 8.17, was assigned to the pyridyl proton 5 py, as H-H COSY spectrum (Figure 26) displays two strong cross peaks between this resonance and vicinal protons 4py (δ 9.37) and 6py (δ 9.01). The resonances of protons 2py and 4py closest to the coordinated N atom are the most downfield (δ 9.70 and 9.37 respectively).

βH and the pyridyl proton 6py (δ 9.02) overlap and are quite broad. The pyridyl proton 2py which should resonate as a singlet consists of a multiplet that may reflect the presence of the four conformers in solution.

In the upfield region the spectrum shows, beside the multiplets of [9]aneS3 and the multiplets of the CH_2 en that resonate together (δ 2.73 –3.02, 64 H), a broad multiplet at (δ 2.73 –3.02) for the NH_2en that integrates for 8 protons. The resonance of the remaining 8 NH_2 en protons overlaps with the resonance of residual CH_3NO_2, as shown in Figure 26.

2.4.3. Conjugates with *meso*-tetra(bpy-phenyl)porphyrin (Bpy_4-PP)

We report here the preparation and characterization of a porphyrin that bears 4 peripheral bpy moieties at *meso* positions, *meso*-tetra(bpy-phenyl)porphyrin (Bpy_4-PP) (Figure 13) and its conjugates with half-sandwich Ru(II) fragments. Bpy_4-PP was obtained in excellent yield by direct coupling of *meso*-(*p*-aminophenyl)porphyrin, $p(NH_2)_4PP$ with 4-methyl- 2,2'-bipyridine-4'-carboxylic acid (bpyAc), obtained in 32% yield starting from 4,4'-dimethyl-[2,2']-bipyridine by consecutive SeO_2 and Ag_2O oxidation without isolation of the intermediates.

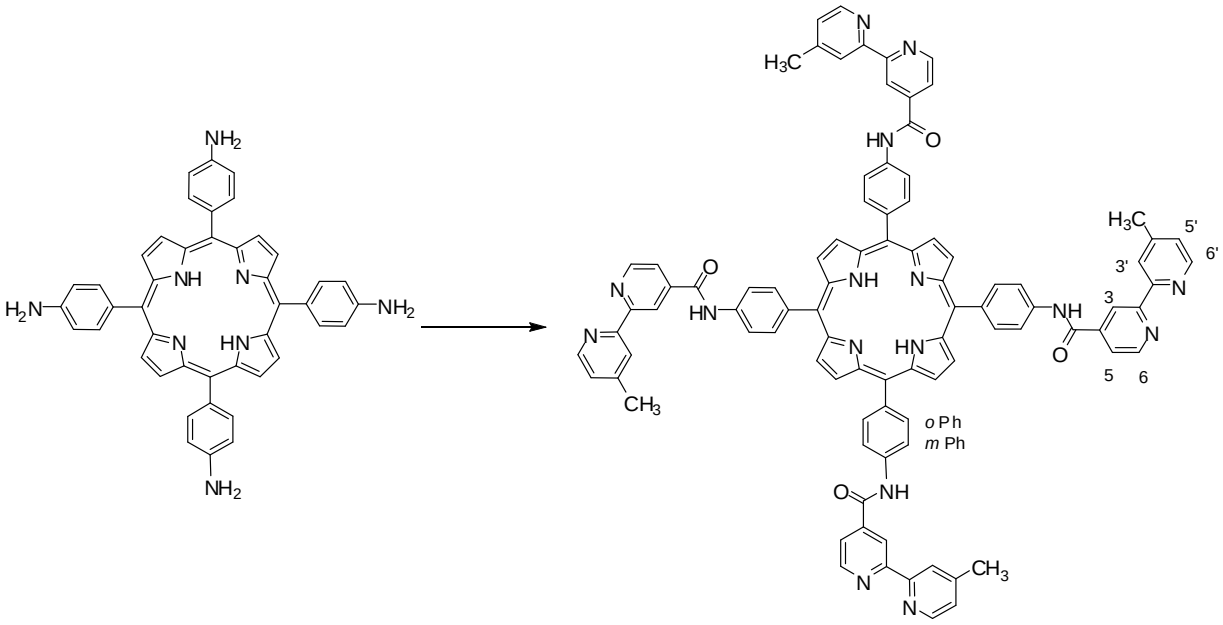

7

Scheme 4.Synthesis of Bpy_4-PP (**7**)[a]

[a]Reactions and conditions: (a) EDCI, BpyAc, pyridine, 2h, rt (91%).

The coupling reaction was carried out in pyridine, using, *N*-(3-dimethylaminopropyl)-*N*'-ethylcarbodiimide hydrochloride (EDCI) as coupling reagent. The ^1H NMR spectrum of Bpy_4-PP is show in Figure 27. Assignments, performed through conventional 2D correlation spectra, were consistent with those already reported in the literature for Bpy-PP and Bpy_2-*cis*PP.[113],[114]

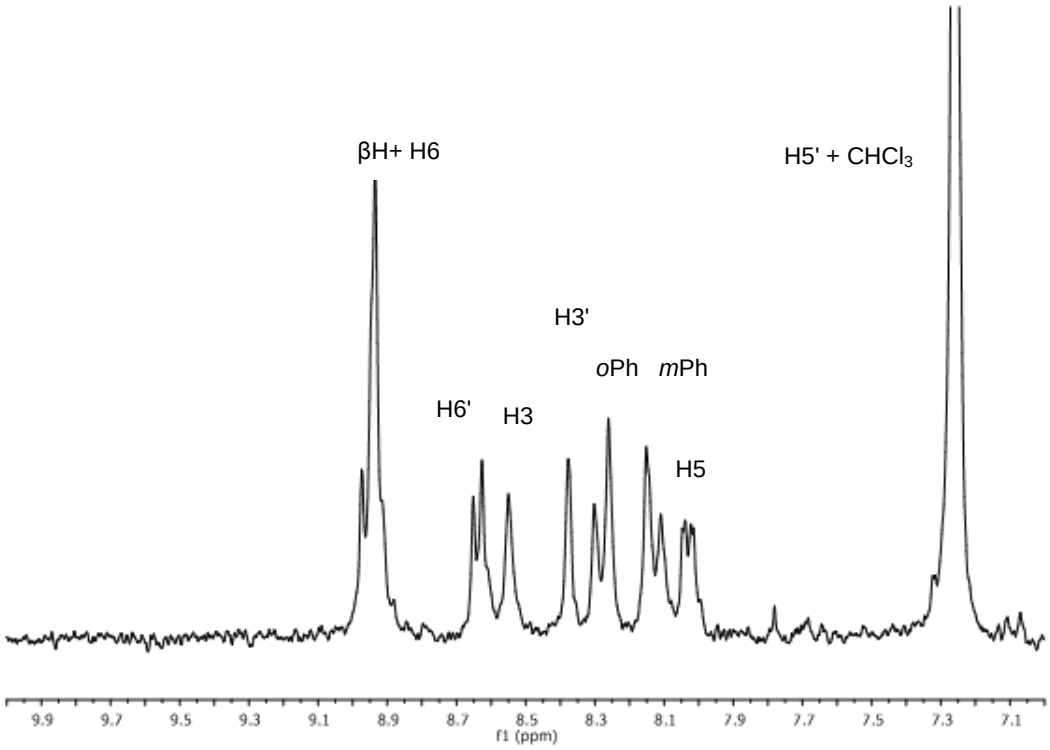

Figure 27:Downfield region of ^{1}H NMR spectrum of **7**in $CDCl_3$.See Scheme 4 for numbering scheme.

The six inequivalent bpyAc protons give six resolved resonances (four doublets and two singlets). The most downfield of them is typically the H6 doublet, partially overlapped with the βH resonance. The chemical shifts of all the aromatic resonances, and that of H3 in particular, were found to depend on the concentration probably because of aggregation mediated by π-π stacking. The singlet of the methyl group in 4' position, that falls at *ca.* δ 2.5, is correlated in a NOESY spectrum to the resonances of the adjacent H3' and H5' protons.

This feature, in conjunction with the H-H COSY spectrum, allowed us to distinguish the two inequivalent halves of bpyAc. The amidic NH resonance typically falls in the range δ 10– 11 and rapidly decreases in time due to H/D exchange with the solvent. In Bpy_4-PP the eight equivalent pyrrole protons resonate as a singlet.

The Bpy_4-PP was treated with a 4.4 amount of the half-sandwich Ru(II) precursor $[Ru([9]aneS3)(dmso)_3][CF_3SO_3]_2$ in $CHCl_3$-acetone mixture: replacement of two adjacent dmso ligands by the bpy moieties afforded the corresponding conjugate $[Bpy_4\text{-}PP\{Ru([9]aneS3)(dmso\text{-}S)\}_4][CF_3SO_3]_8$ (**8**) in good yield.

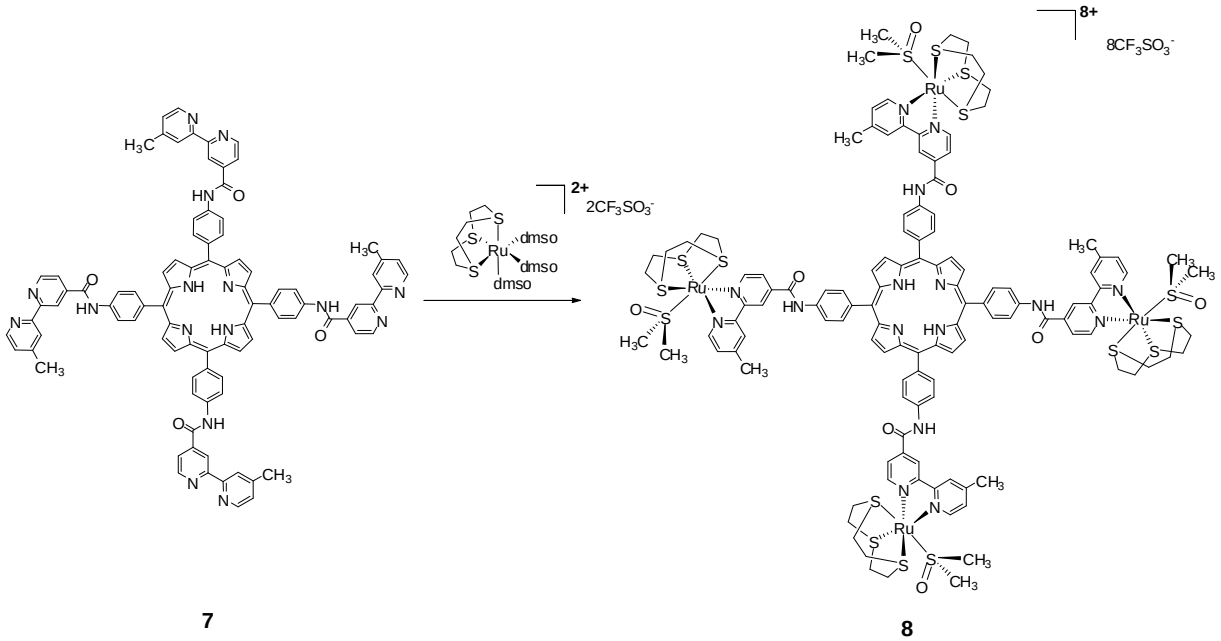

Scheme 5. Synthesis of [bpy$_4$-PP{Ru([9]aneS3)(dmso- S)}$_4$][CF_3SO_3]$_8$(**8**)

The conjugate has been characterized by mono- and bidimensional NMR spectroscopy (it is soluble in $CDCl_3$, CD_2Cl_2, CD_3NO_2, dmso but scarcely soluble in water. The model complex [Ru([9]aneS3)(bpyAc)(dmso-*S*)][CF_3SO_3]$_2$ [88] was characterized by NMR spectroscopy and X-ray crystallography and it was used as reference for NMR assignments.

In general, all proton NMR resonances of conjugate **8** are slightly broader than those in the free porphyrin orin the model complex. [88] The ^{1}H NMR spectrum of [Bpy$_4$-PP{Ru([9]aneS3)(dmso-*S*)}$_4$][CF_3SO_3]$_8$ (**8**) (Figure 28) shows in the upfield region, beside the multiplets of [9]aneS3 (δ2.9– 3.4), three singlets of equal intensities between δ 2.7 and 2.9. By analogy with the spectrum of the model complex, [88] the upfield singlet was attributed to the methyl on bpyAc (attribution confirmed by the NOESY experiment) and the other two to the diastereotopic methyls of dmso-*S*. In the downfield region, the six resonances of the bpyAc protons are shifted downfield of 0.3-0.5 ppm.

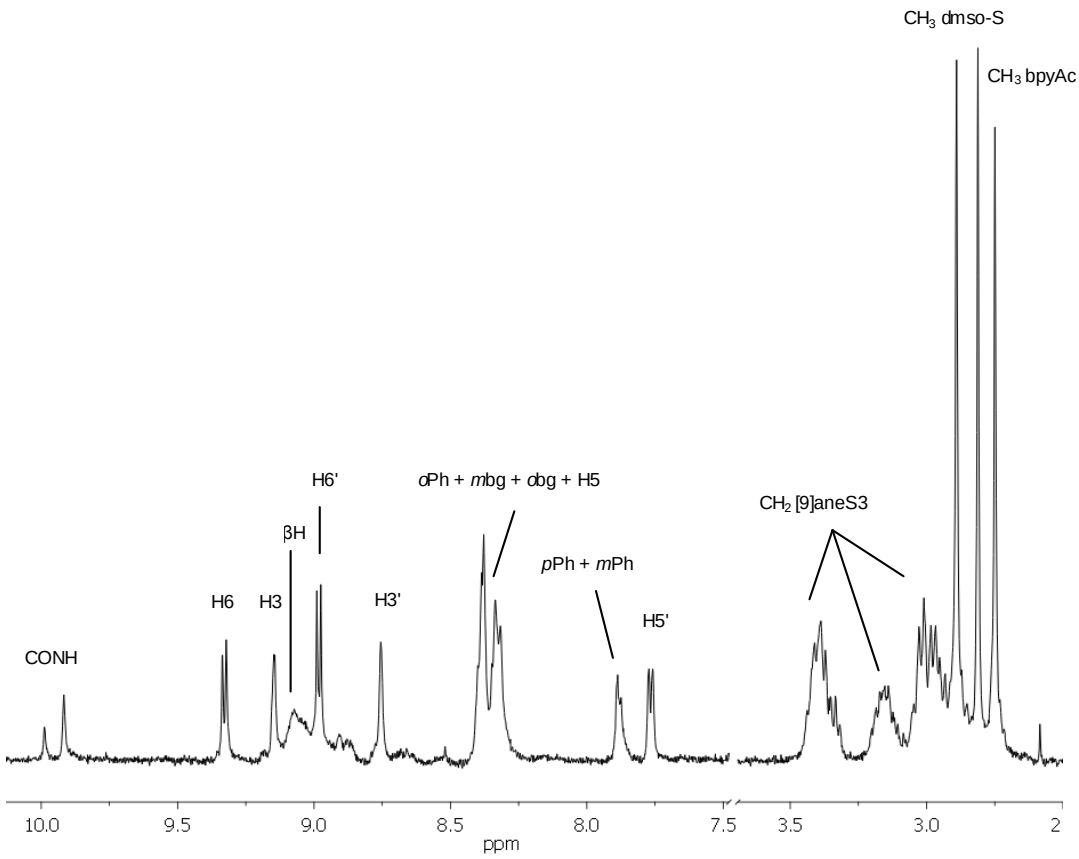

Figure 28. ^{1}H NMR spectrum (500 MHz) of [Bpy$_4$-PP{Ru([9]aneS3)(dmso-*S*)}$_4$][CF_3SO_3]$_8$(**12**). See Scheme 4 for numbering scheme.

Optically matched dmso solutions of Bpy$_4$-PP **7** and conjugate **8** showed very similar fluorescence spectra upon selective excitation at the Soret band (λex = 425 nm, λem = 656 nm). The emission intensity of **8** is *ca.* 20% lower than that of the parent porphyrins as expected because of the peripheral heavy atoms.[96]

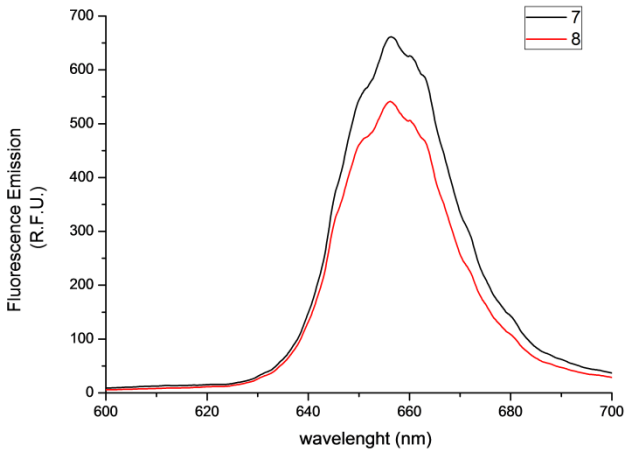

Figure 29. Fluorescence spectra (λex = 425 nm, λem = 656 nm) of optically matched dmsosolutions of Bpy$_4$-PP (**7**) (black) and [{Bpy$_4$-PP}{Ru([9]aneS3)(dmso-S)}$_4$][CF_3SO_3]$_8$ (**8**) (red)

2.4.4. Conjugates with (TetbpyPP) and (TedabpyPP)

Basically the same multi-step synthetic route was followed to obtain the two new extended-arms porphyrins, TetbpyPP (**9**) and TedabpyPP (**10**) (Scheme 6), that bear four peripheral bpy fragments at the *meso* positions.

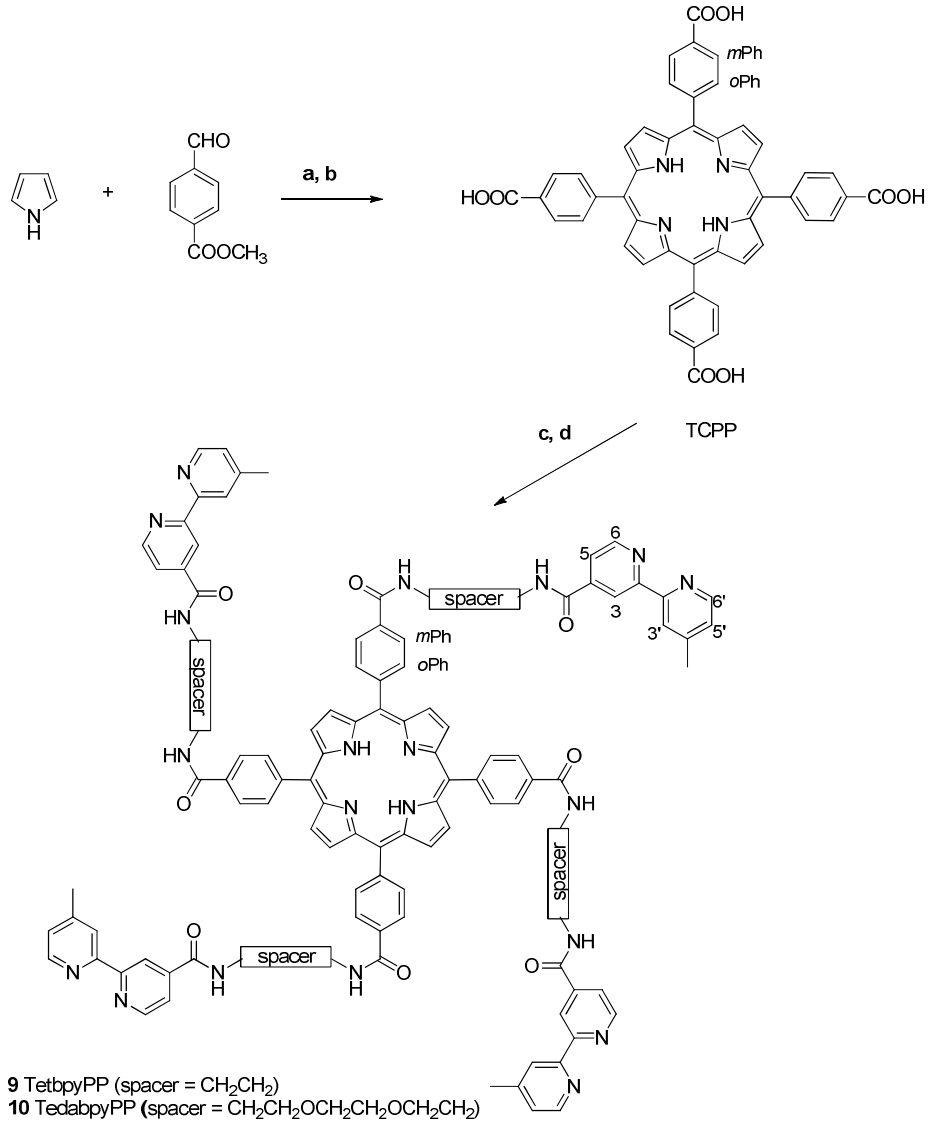

Scheme 6. Synthetic route to **9** and **10**.[a]

a Reactions and conditions: (a) propionic acid, reflux, 1.5 h (21%); (b) KOH aq 40%, THF/CH_3OH 2:1, 40 °C, 1 h (93%); (c) EDCI/HOBt/DMAP, $NH_2CH_2CH_2OCH_2CH_2OCH_2CH_2NHBoc$ (72%) DMF, rt, 24 h or EDCI/HOBt, $NH_2CH_2CH_2NHBoc$, DMF, rt, 2.5 h; then TFA, rt, 2 h (100%); (d) EDCI/HOBt/DMAP, bpyAc, DMF, rt, 24 h (96% and 74%).

First, the condensation of pyrrole and methyl 4-formyl benzoate [115] followed by hydrolysis in basic conditions in THF/MeOH, gave the *meso*-4'-tetracarboxyphenylporphyrin, TCPP. The hydroxybenzotriazole (HOBt) ester of TCPP was then coupled with either *N*-Boc-2,2′-

diethylamine (yield 60%) or *N*-Boc-2,2′-(ethylenedioxy) diethylamine (yield 72%) in DMF. These intermediates (TetNHBocPP and TedaNHBocPP, respectively) were quantitatively deprotected using TFA in CH_2Cl_2 and then coupled with bpyAc in the same experimental conditions, giving **9** (74%) or **10** (96%), respectively. The extended-arms bpy-porphyrins were characterized by UV–vis and ^{1}H NMR spectroscopy (Figures 30 and 31), and by electrospray mass spectrometry (Figure 32).

Both porphyrins are well soluble in dmso, but totally unsoluble in water, so that comparative biological tests could not be performed.

The ^{1}H NMR spectra of **9** and **10** in dmso-d_6 and CD_2Cl_2 show complex pattern of resonances. The chemical shifts of all the resonances were assigned by means of conventional H-H COSY spectra (Figure 30 and 31) and by comparison with the bpy-porphyrins previously prepared.

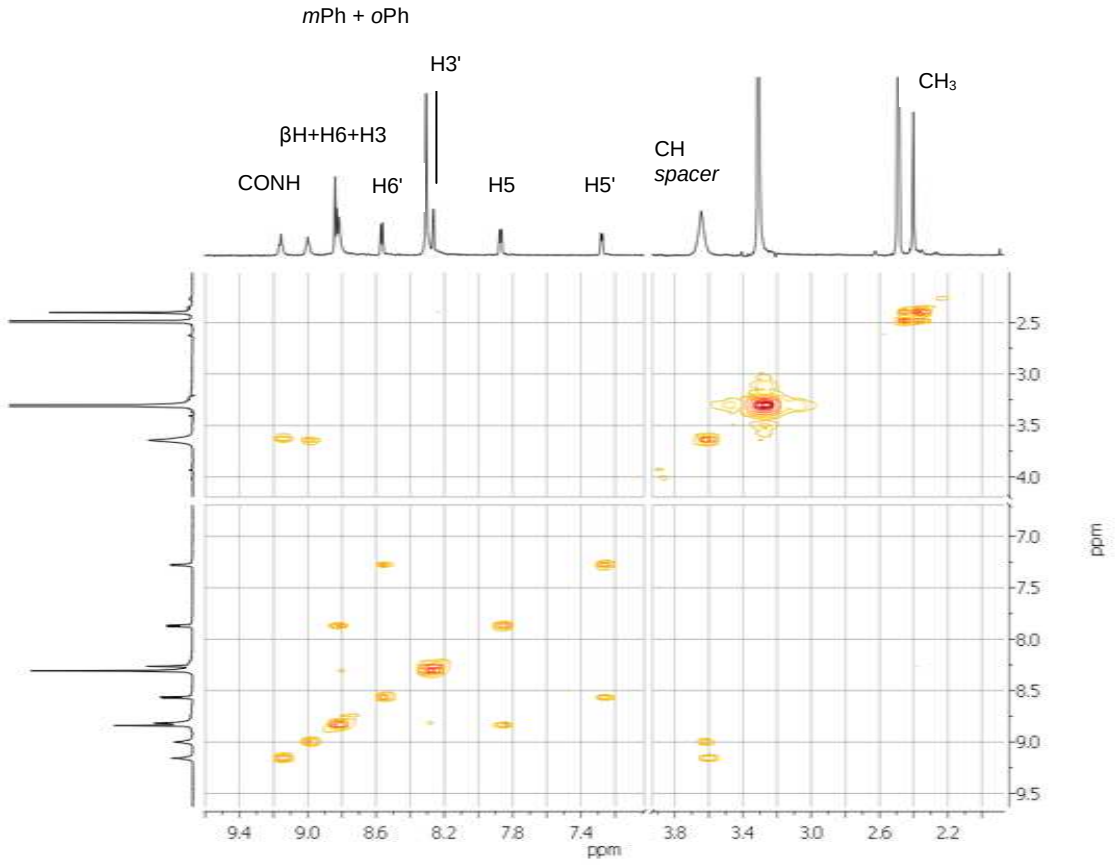

Figure 30. H-H COSY NMR spectrum of TetbpyPP **9** in dmso-d_6.

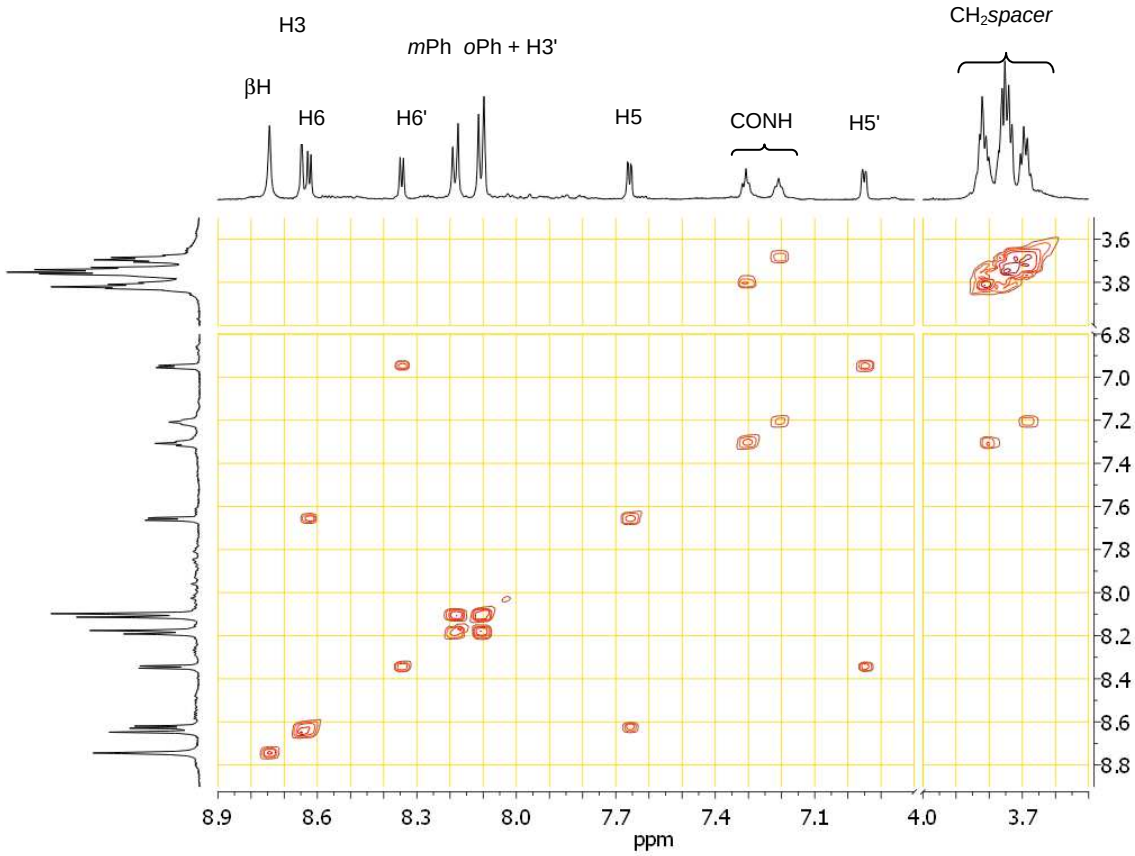

Figure 31. H-H COSY NMR spectrum of TedabpyPP **10** in CD_2Cl_2.

For each porphyrin the six inequivalent bpyAc protons give six resolved resonances (four doublets and two singlets) equally spaced in both spectra. Herin the NMR and ESI-MS characterization of **10** is described (Figure 31).

The H-HCOSY spectrum of **10** shows a strong cross peak between the doublet of the H6 (δ 8.62) and the doublet of the H5 (δ 7.66). The proton H5' resonates as a doublet at δ 6.96 and it is coupled with the doublet at δ 8.35, attributed to the adjacent proton H6'. The singlet at δ 8.74 integrating for 8H refers to βH pyrrolic protons. The two doublets at δ 8.11 and 8.18 are related to the *o/m* Ph protons. In the H-H COSY spectrum of **10** this resonance at higher fields overlaps with the resonance of the proton H3' and integrates for 12H. The two broadened triplets at δ 7.21 and 7.31 were attributed to the resonances of the amide protons by HSQC experiments.

In the upfield region the methyl protons of the bpy resonate as a singlet at δ 2.21 (12H). The aliphatic CH_2 protons resonate as multiplets of low intensity between δ 3.65 and 3.88. They both display a strong cross peak with the amide protons in the H-HCOSY spectrum. Finally, the pyrrole NH protons resonate at δ -3.00 as a broad singlet.

Compound **10** was also characterized by spectrometry ESI-MS. The spectrum reported in Figure 32 displays the molecular peak MH^+ at *m*/*z* 2096.7 together with the peaks $M+Na^+$ (*m*/*z* 2118.6), $M+K^+$ (*m*/*z* 2134.5) and $M+Na^++K^+$ (*m*/*z* 2158.5).

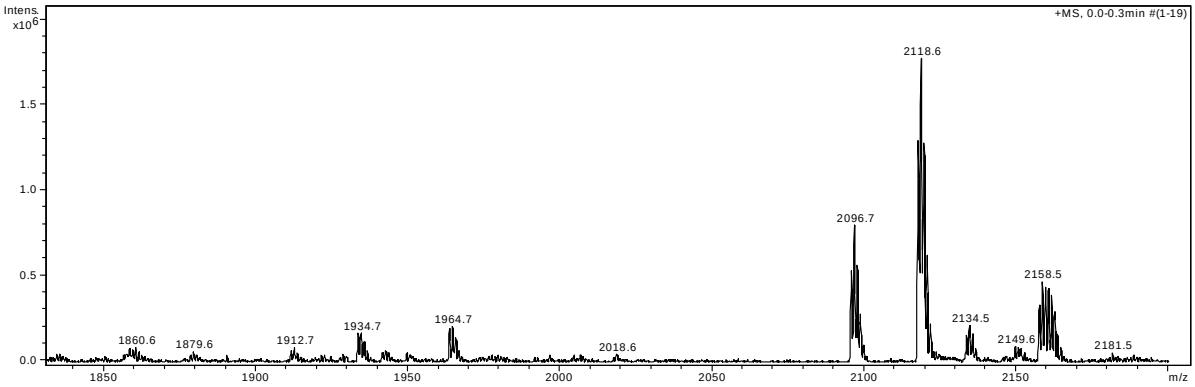

Figure 32.ESI-MS spectrum of **10**.

Treatment of either porphyrins **9** and **10** with four equivalents of the neutral Ru (II) precursor [Ru([9]aneS3)(dmso)Cl_2] in refluxing CH_2Cl_2/MeOH mixtures afforded – upon replacement of the dmso and a chloride ligand by the bpy moieties –the corresponding tetraruthenated compounds in excellent yield: [TedabpyPP{Ru([9]aneS3)Cl}$_4$]Cl_4 (**11**) (Scheme 7) or [TetbpyPP{Ru([9]aneS3)Cl}$_4$]Cl_4 (**12**), respectively.

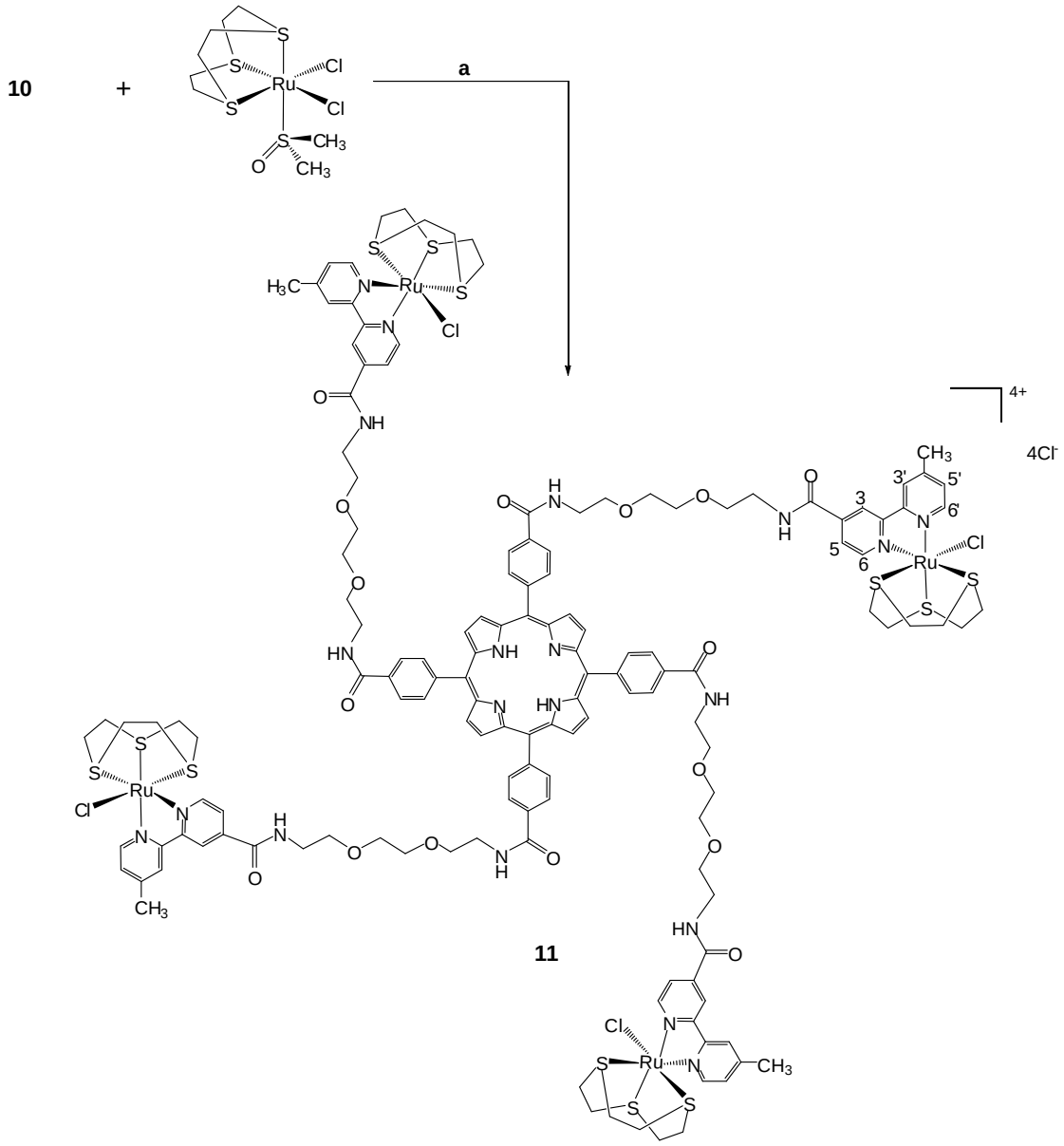

Scheme 7.Schematic structure of the ruthenium-porphyrin conjugate **11**[a]**.**
[a]Reactions and conditions: (a) methanol/diclometane, 24h, reflux (92%)

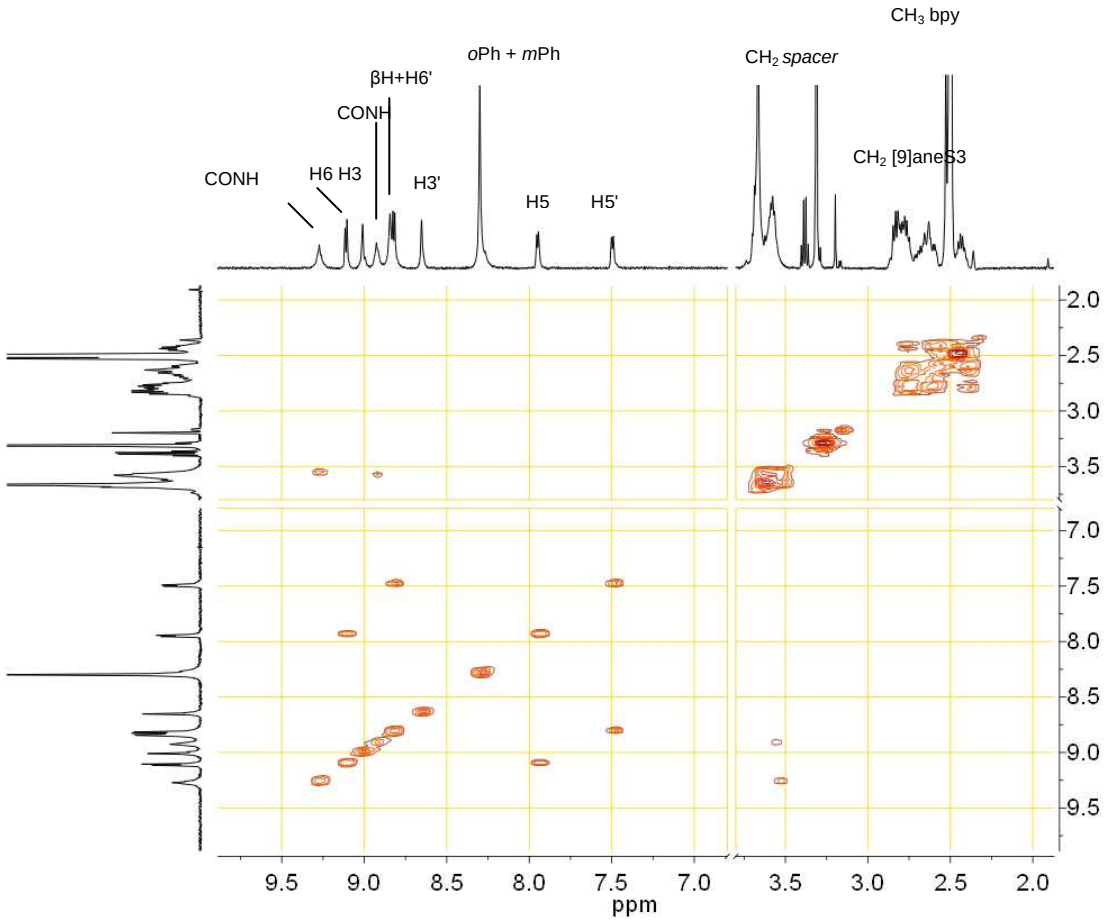

Figure 33. H-H COSY NMR spectrum of **11** in dmso-d_6.

Herein the more polar conjugate **11** is described (Figure 33). Even though compound **11** has a good solubility in water, its proton NMR spectrum in D_2O presents only broad peaks, possibly due to aggregation occurring at NMR concentrations as previously observed with other Ru-porphyrin conjugates.[116] For this reason the NMR spectra of both compounds were recorded in dmso-d_6, where only sharp resonances are observed. In general, the NMR spectra of both conjugates are consistent with their expected four-fold symmetry, *i.e.* all peripheral Ru fragments are equivalent. The ^{1}H NMR spectrum of **11** in the upfield region shows, beside the multiplets of [9]aneS3 (δ 2.40 – 2.85), a singlet at δ 2.53 for the methyl on bpyAc, and the multiplets of the aliphatic spacer (δ 3.55 – 3.70). The two internal NH pyrrole protons appear as a broad singlet at δ ≈ -2.9. In the downfield region, the six resonances of the bpyAc protons maintain the same relative pattern as in the free TedabpyPP except for H3 and H6 (even though, as typical for these compounds, they are slightly broader than those in the free porphyrins). While the resonances of H5,5' (see Scheme 7 for numbering scheme) are scarcely affected by coordination to Ru, those of H6,6' and H3,3' are shifted downfield by ca. 0.5 ppm. Also the two triplets of the amide NH protons are remarkably shifted downfield (ca. 2 ppm compared to free TedabpyPP), but this effect is most likely due to the change of

solvent (dmso-d_6*vs* CD_2Cl_2). The correlation H-H COSY spectrum of **11** displays two strong cross peaks between vicinal bipyridyl protons (H5 and H6, H5' and H6'), and two weaker peaks between the multiplets for the CH_2 protons of the spacer and the NH amide protons (Figure 33). We attributed the most downfield NH resonance to the amide group close to the bpy moiety. The ^{1}H NMR spectrum of **12** displays several overlapping resonances of the bpyAc protons, and only those of H5,5' are well resolved (Figure 34). Owing to its very low solubility in water, compound 1**2** was not investigated further.

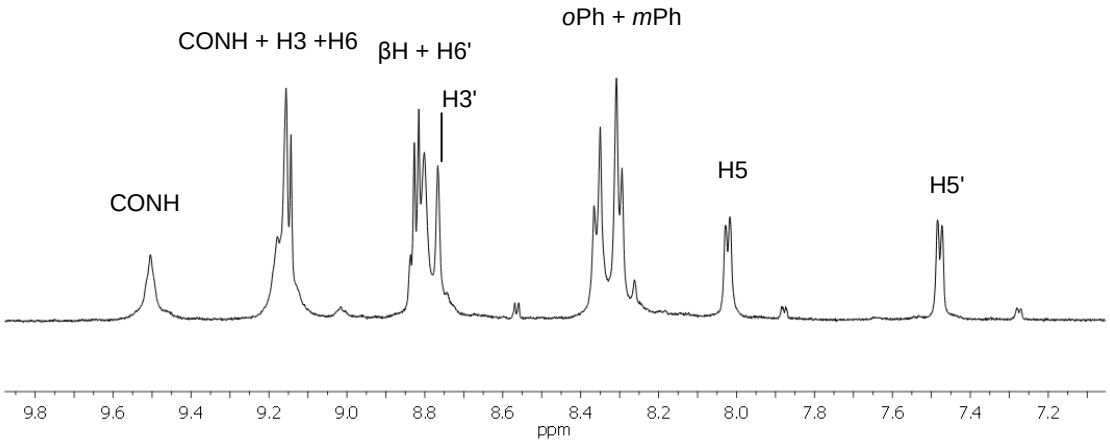

Figure 34. ^{1}H NMR spectrum of **12** in dmso-$d_6$in the aromatic region.

Consistent with what observed already for compound **8**, the fluorescence spectrum of **11** is very similar to that of the parent porphyrin **10** except for the ca. 25% quenching of the emission intensity attributed to the peripheral heavy atoms (Figure 35).

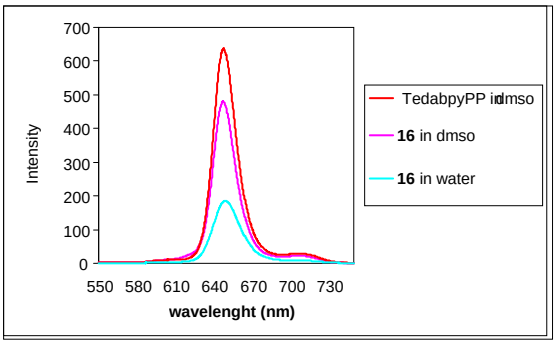

Figure 35: Emission spectra of 0.2 A solutions of **10**indmso (red), **11** in dmso (pink) and in water (cyan). λ_{ex} 421 nm, λ_{em} 648 nm.

The fluorescence properties of porphyrins are useful to study their aggregation behavior in solution. In fact porphyrins in their monomeric form usually show intense fluorescence emissions, which are partially or completely quenched upon aggregation in solution.[61] The fluorescence spectra of 0.2 A solutions of **11** in dmso and in water upon excitation of the Soret band showed an emission band at 648 nm; the significant reduction in emission intensity on going from dmso to H_2O (≈ 60 %) suggests that the ruthenium-porphyrin conjugate aggregates in water (Figure 35). This finding is consistent with the very low resolution of the ^{1}H NMR spectrum in D_2O. The time course of UV-vis absorbance spectrum of **11** in aqueous solution was recorded at 25 °C. The Soret band absorbance gradually increased (≈ 14 %) until an almost constant value was reached after 3 h (Figure 36**a** and **b**).

ab

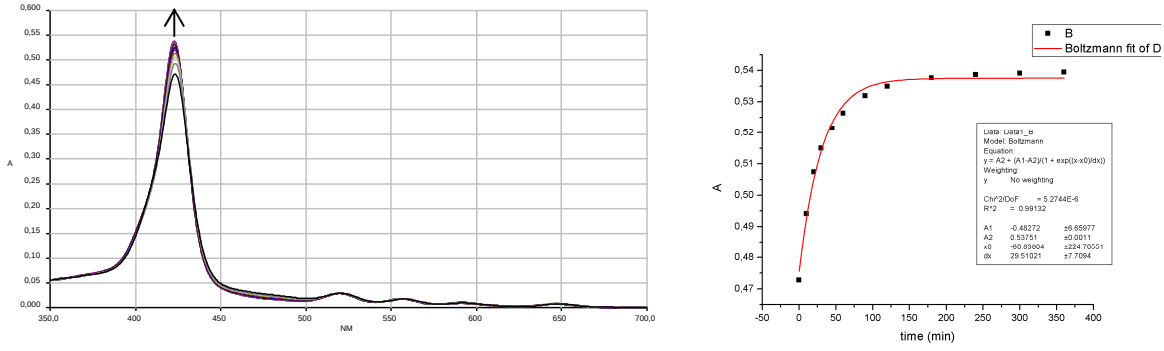

Figure 36: (a) UV-vis spectra of **11** (0.2 A solution in water) recorded at 10 min (0 – 40 min), 20 min (40 min - 60 min), 30 min (1 h – 2 h), 60 min (2 h – 6 h) intervals. (b) Boltzmann fitting of absorbance data.

No shape modification or shift of the Soret band were observed, suggesting that no major chemical modification of the porphyrin structure is occurring and that the minor absorbance increase might be due to chloride hydrolysis and formation of the Ru-aquo species (Figure 36).[87]

[TedabpyPP{Ru([9]anoN3)(dmso-S)}$_4$](Cl)$_8$ (13)

We showed before that TedabpyPP is a good precursor for the efficient preparation of the octacationic porphyrin conjugate **11** bearing the sulphur macrocycle 1,4,7-tritiocyclononane ([9]aneS_3).

To extend the structure-relationship investigations we synthesized a new Ru-porphyrin conjugate in which tritiocyclononane is replaced by the nitrogen macrocycle 1,4,7-triazacyclononane ([9]aneN3, tacn).

With this aim we used the complex [Ru([9]aneN3)(dmso-*S*)$_2$Cl]Cl as metal precursor to obtain the conjugate[TedabpyPP{Ru([9]aneN3)(dmso-*S*)}$_4$](Cl)$_8$(**13**) (Scheme 8). For the synthesis of **13** it was necessary to vary the reaction conditions previously described to synthesize **11**, increasing the reaction time from 24 to 48h and using a 1:5 ratioporphyrin / Ru in dichloromethane/methanol 1:3.

At reaction completion, the solution was concentrated and treated with diethyl ether to precipitate the product. After filtering and washing with diethyl ether and diclorometane, the porphyrins conjugate **13** was obtained in 79% yield.

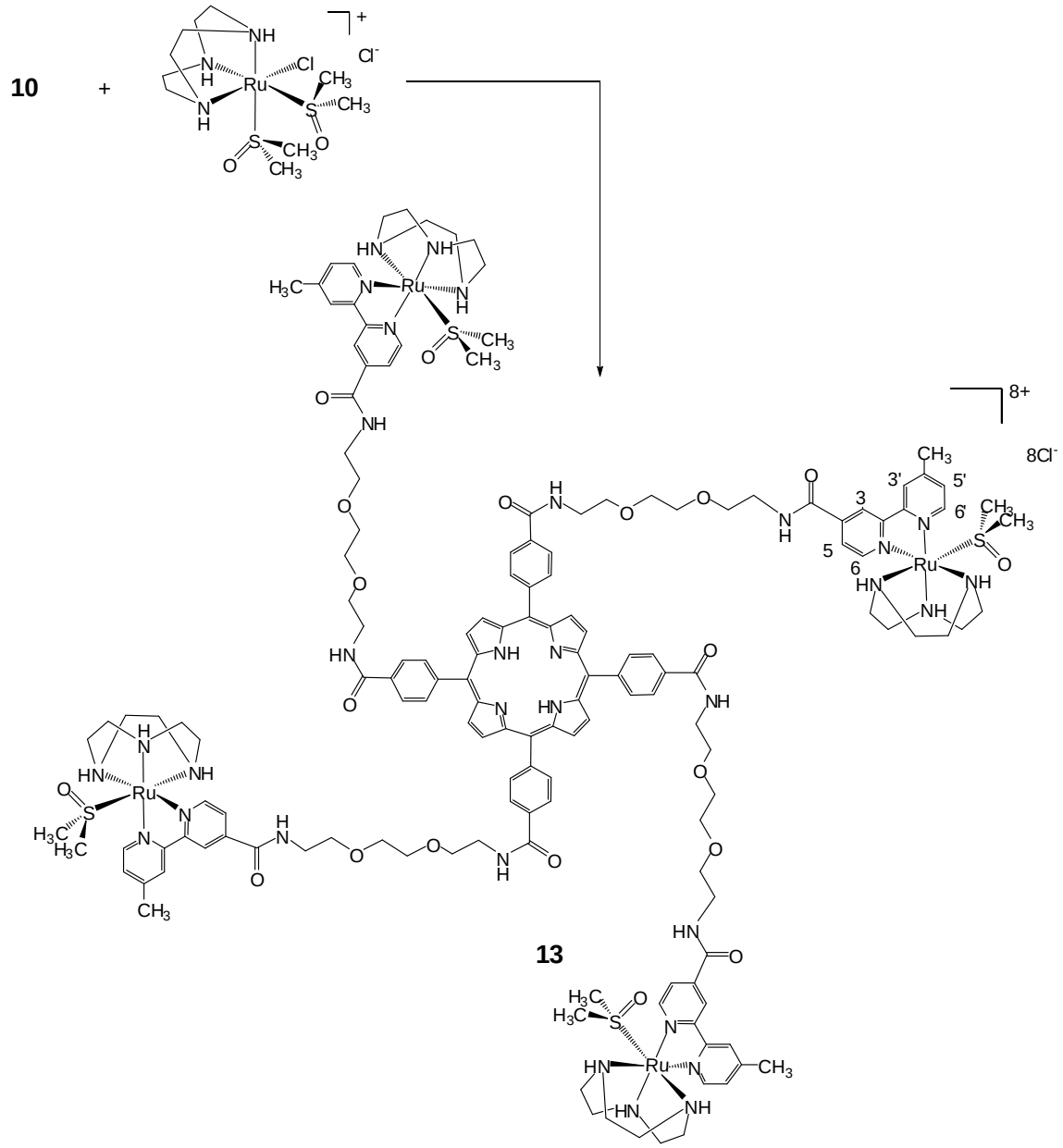

Scheme 8. Synthetic route to [TedabpyPP{Ru([9]aneN3)(dmso-*S*)}$_4$](Cl)$_8$ (**13**).[a]
[a]Reactions and conditions: (a) methanol/diclometane, 48h, reflux (79%)

The ottacationic ruthenium conjugate **13** was characterized by mono- and bidimensional ^{1}H NMR spectroscopy.

All the resonances were assigned by means of conventional H-H COSY spectra and by comparison with the bpy-porphyrins previously prepared.

The H-H COSY spectrum of **13** recorded in dmso-d_6 at room temperature shows in the downfield region (Figure 37) a cross peak between the two well resolved doublets at δ 7.62 and 8.10 attributed to the bipyridil protons H5' and H6'and between protons H5 and H6 at δ 7.62 and 9.16 respectively. The protons of [9]aneN3, resonate as two boad multiplets at δ 6.06

(4H) and 7.22 (8H), respectively. Those assignations were confirmed by HSQC experiments (Figure 38a). The *o/m*Ph (16H) protons resonate in a multiplet at δ 8.31.

The two broad triplets at δ 8.99 and 9.49 were attributed to the resonances of the amide protons by HSQC experiments (Figure 38a). The βH and H3' (δ 8.85), and the bipyridyl protons H6' and H3 (δ 9.16) overlap and are quite broad.

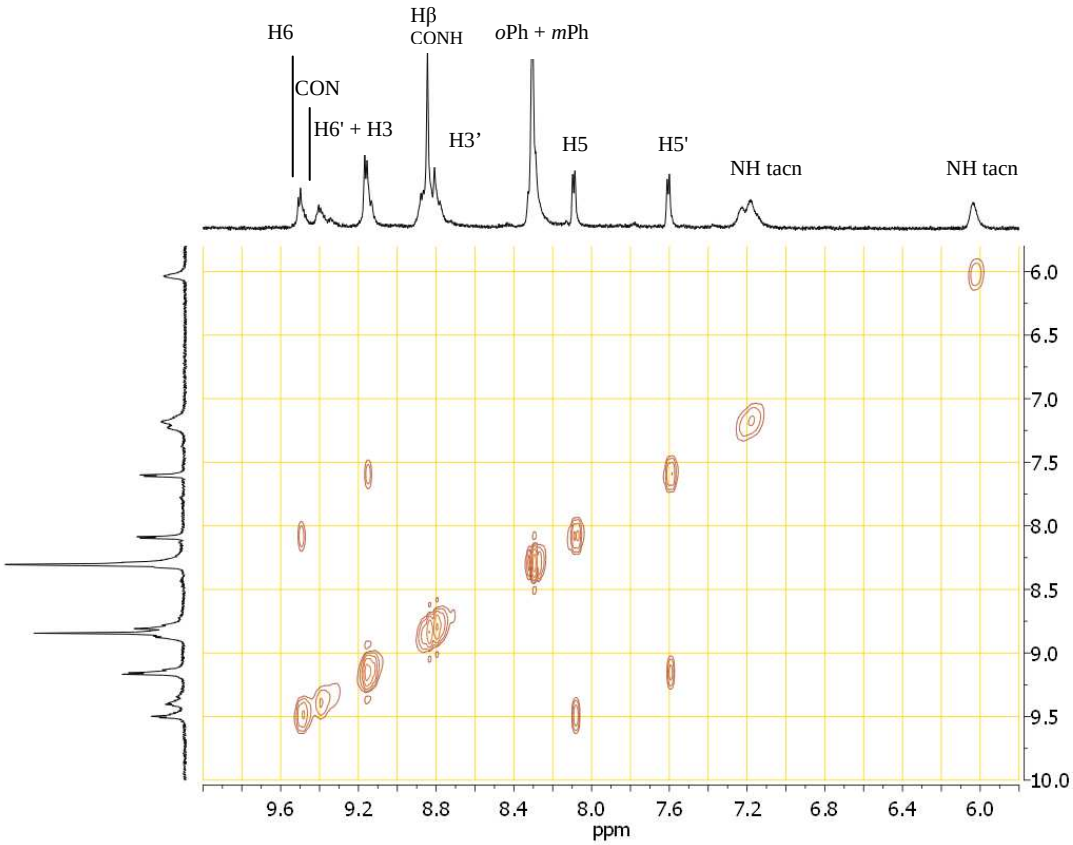

Figure37. H-H COSY NMR spectrum of **13** in dmso-d_6 in the downfield region.

The HSQC spectrum of the porphyrin **13** in dmso-d_6 in the downfield region shows only CH groups (Figure 38a). In particular, this experiment confirms the assignment of the NH of the [9]aneN3 at δ 6.06 and at 7.22 and of the CONH at δ 8.49 and 8.99 (for the absence of cross peaks). Furthermore it shows the overlap of two CH resonances at δ 8.30 (*o/m*Ph) and 9.17 (H6'and H3).

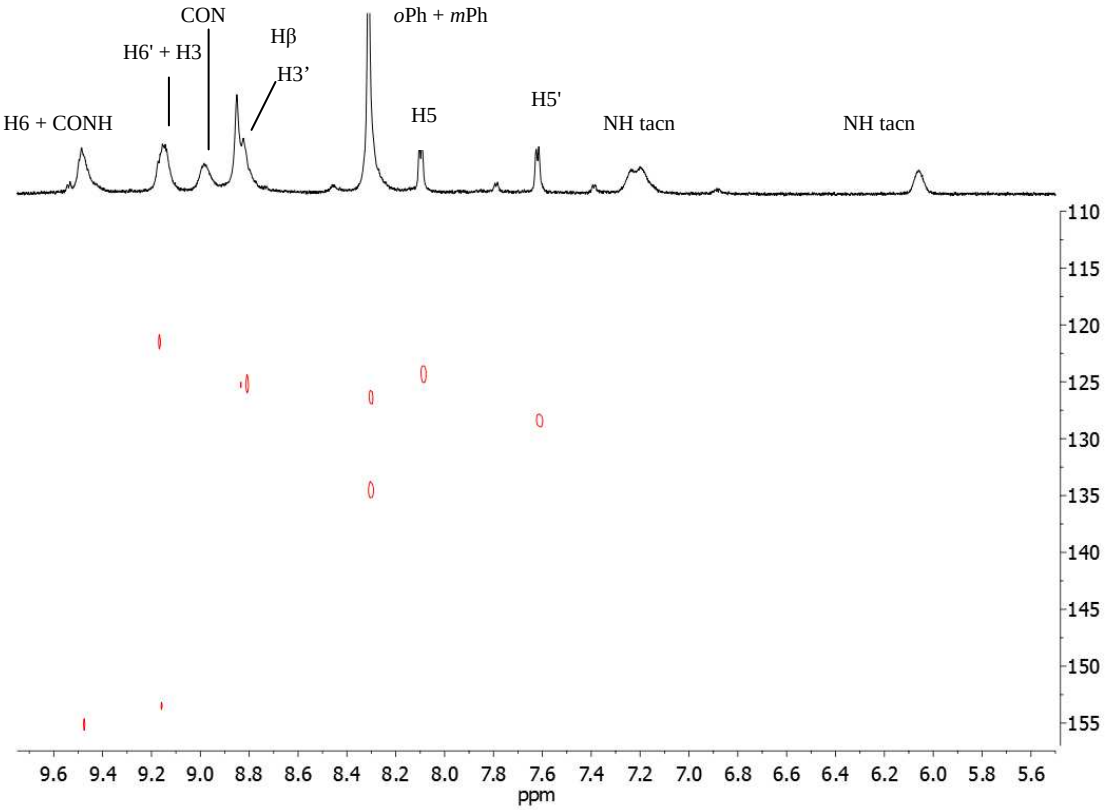

Figure 38a. HSQC spectrum of **13** in dmso-$d_6$in the downfield region. Read peaks: CH/CH_3 groups.

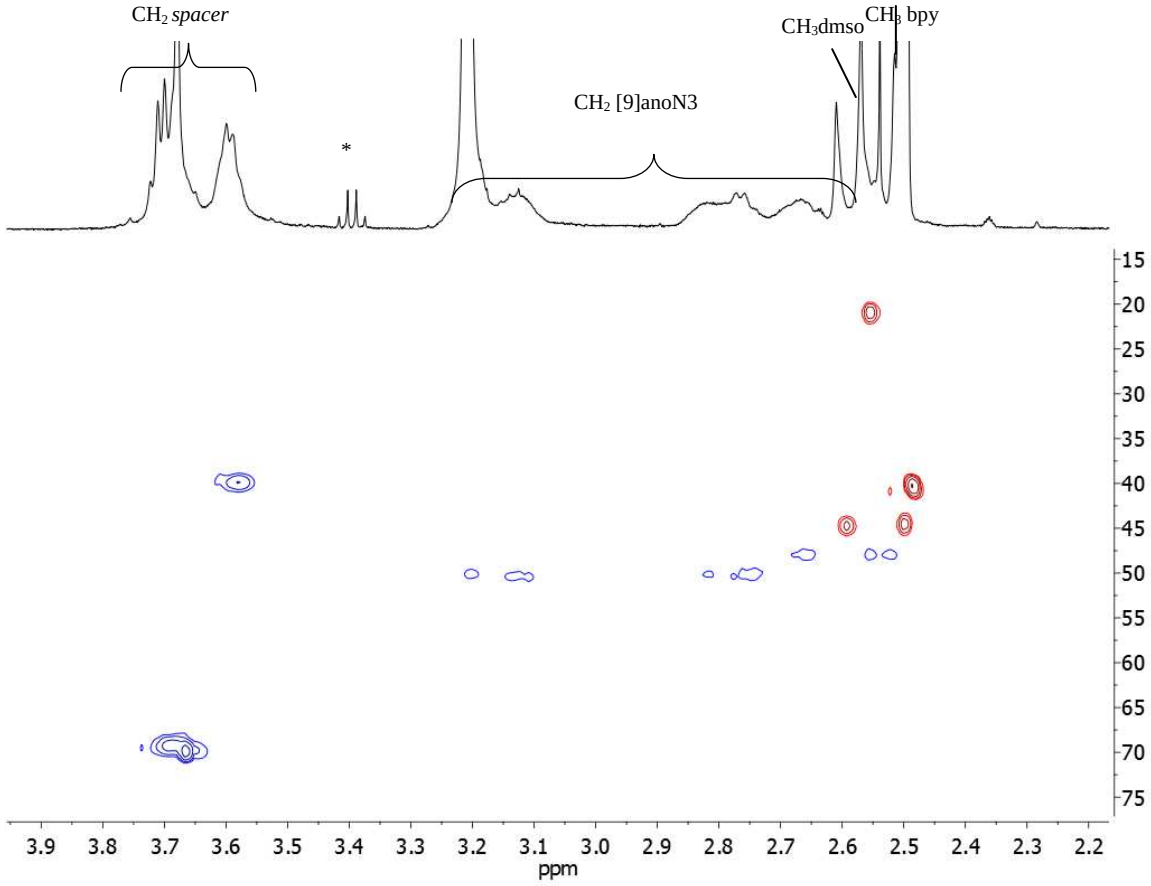

Figura 38b. HSQC spectrum of **18** in dmso-$d_6$in the upfield region. Blue peaks: CH_2 groups; read peaks: CH/CH_3 groups. *:impurity.

In the upfield region the HSQC shows the blue cross-peaks of CH_2 group of the spacer. The red cross peak of the CH_3 bypiridil at δ 2.56 correlates with a carbon that resonates at about δ 20.

The protons of the methyl groups of the ruthenium-bonded dmso correlate with carbon atoms that resonates at about δ 45. One of the two diastereotopic methyl groups resonates at δ 2.61, the other overlaps with the resonance of the solvent.

Compound **13**, besides being soluble in organic solvents such as methanol, is also well soluble in aqueous solution and in PBS at pH=7.4.

2.2.5. Conclusions

In this part we have described different synthetic approaches to the preparation of porphyrin conjugates with Ru(II) coordination compounds. We have varied the number and charge of the peripheral Ru fragments, and described conjugates whose total charge ranges from +4 to +8. The connection can occur through a single N(pyridyl)–Ru bond or through a chelating bpy unit. The Ru compounds can either contain one labile ligand or be coordinatively saturated and substitutionally inert.

Meso-pyridylporphyrins (PyPs), beside being synthetically more affordable, allow to tune the geometry of the conjugates. We have shown that when 3'PyPs, instead of 4'PyPs, are used, the peripheral metal fragments typically lay both above and below the plane of the chromophore, thus giving access to diverse shapes and geometries.

In the first serie of porphyrins with peripheral bpy units at *meso*positions described in this work, bpy_4-PPs, the linker is relatively short and rigid.

Due to the mild solubility of these compounds, we developed two novel “extended-arms”versatile porphyrins, namely TetbpyPP and TedabpyPP, with a multistep approach and reasonable overall yield. These porphyrins are particularly suited for the strong coordination of peripheral metal fragments.

In general we demonstrated that all the porphyrins can effectively bind four half-sandwich Ru(II) coordination compounds to give the cationic conjugates in excellent yields.

2.5. Determination of Singlet oxygen Quantum Yield (Φ_Δ)

The singlet oxygen quantum yield (Φ_Δ) is a key property of a photosensitising agent.

Since the most common mechanism of action of the PDT photosensitizers involves the production of singlet oxygen upon photo-excitation (Type II mechanism), Φ_Δ was measured for the conjugates previously described Most PDT photosensitizers clinically used typically have $\Phi_\Delta$values of ca. 0.5.[117]

The singlet oxygen generation by the Ru(II)-porphyrin conjugates was measured using 9,10-dimethylanthracene (DMA) as a substrate. This compound reacts with $^1O_2$ and is converted to the non-fluorescent 9,10-endoperoxide with 100% efficiency (no physical quenching). [118]

The amount of photogenerated $^1O_2$ was calculated by measuring the residual DMA concentration as a function of the irradiation time.[119]

In a typical experiment, 3 ml of an ethanol solution containing 1,5 ml of 20 µM DMA and 1,5 ml of a porphyrin solution of absorbance A = 0.4 were placed in a quartz cuvette of 1 cm optical path and gently stirred during exposure to the Teclas lamp (100 mW/cm^2) at a temperature of 20 ±2 °C.

The results obtained using compound **2** as a substrate are reported here as an example. The spectophotofluorimetric analysis to determine the DMA content was performed at 5-s intervals up to a total irradiation time of 25 min. The unirradiated and the irradiated DMA solutions were excited at 360 nm and the fluorescence emission was observed in the 380 – 550 nm wavelength range (Figure 39). The DMA photooxidation follows the first order kinetic: thus, the rate constant of the photoprocess was obtained from the slope of semilog plot (Figure 40) and has been converted into quantum yield of singlet oxygen generation by comparison with the rate constant for DMA photooxidation by hematoporphyrin (Hp) (Φ_Δ 0.65 in ethanol).[120]

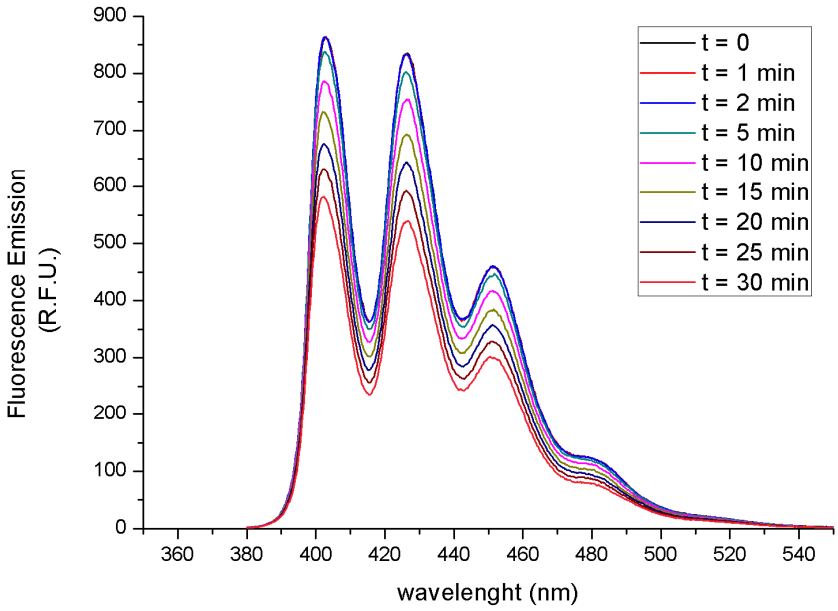

Figure 39. Photobleaching of an ethanol solution of DMA by **2** upon irradiation with a Teclas lamp (590–700 nm) at 100 mW/cm^2.

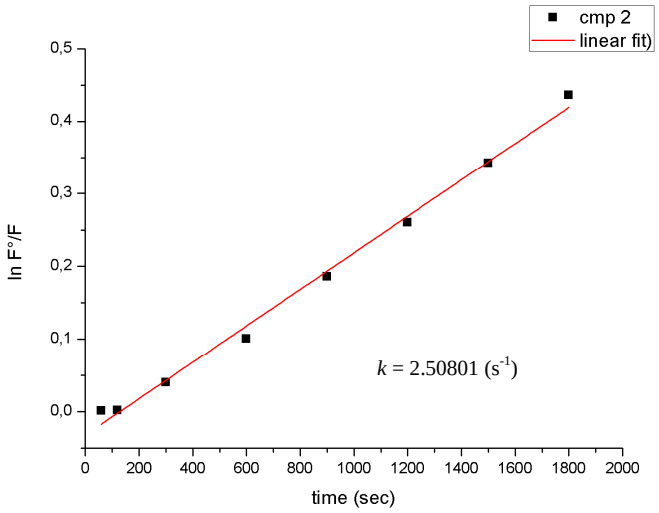

Figure 40. Photooxidation of 10 µM DMA in ethanol solution sensitized by **2**. *k* is the first-order rate *vs* constant for the photoprocess as deduced from the slope of the semilog plot.

Exposure of the porphyrins to the clinically useful red light (590-700 nm) for up 30 min using the experimental condition specified before caused a negligible decrease in the intensity of the visible absorption bands. This process, generally defined as photobleaching, is usually related to irreversible destruction of the tetrapyrrolic macrocycle.

All the compounds appeared to photosensitize the oxidation of the DMA according to first-order kinetics; a behavior typically observed for most photodynamically active photosensitizers.

For each porphyrin, the photokinetic experiments were performed in ethanol. The results are showed in Table 2.

photosensitizer	$k\times 10^{-4}s^{-1}$ **in ethanol**	Φ_Δ **in ethanol**
Hp	2.5716	0.65[a]
4'TPyP (**1**)	1.95290	0.49
[4'TPyP{Ru([9]aneS3)(en)}$_4$][CF_3SO_3]$_8$(**2**)	2.50801	0.63
[4'TPyP{Ru([9]aneS3)(bpy)}$_4$][CF_3SO_3]$_4$ (**3**)	3.31698	0.84
3'TPyP(**4**)	1.71403	0.43
[3'TPyP{Ru([9]aneS3)(en)}$_4$][PF_6]$_8$(**6**)	1.68385	0.43
[3'TPyP{Ru([9]aneS3)(bpy)}$_4$][PF_6]$_8$(**5**)	3.48938	0.88
Bpy_4-PP (**7**)	1.50587	0.38
[Bpy_4-PP{Ru([9]aneS3)(dmso-*S*)}$_4$][CF_3SO_3]$_8$(**8**)	1.39556	0.37
TedabpyPP(**10**)	1.5846	0.40
[TedabpyPP{Ru([9]aneS3)Cl}$_4$]Cl_4(**11**)	1.40215	0.35
[TedabpyPP{Ru([9]aneN3)(dmso-*S*)}$_4$](Cl)$_8$(**13)**	1.0330	0.26

Table 2. Quantum yield of production of singlet molecular oxygen (Φ_Δ**)** and order rate *vs* constant for the photoprocess in ethanol upon irradiation with a Teclas lamp (590–700 nm) at 100 mW/cm^2.
[a]: from reference 120

The investigated Ru-porphyrin conjugates have from moderate (Φ_Δ = 0.35 and 0.26 for **11** and **13**, respectively) to good (Φ_Δ =0.84and 0.88 for **3** and **5**, respectively) singlet oxygen quantum yield. In general Ru(II)-porphyrins conjugates through single coordination bond show Φ_Δ values higher than conjugates through two coordination bonds. Ru(II)-porphyrins conjugates through two coordination bonds have moderate singlet oxygen quantum yields (Φ_Δ = 0.37 and 0.35 for **8** and **11**, respectively). These Φ_Δ values are not significantly different from those of the corresponding parent porphyrins (0.38, 0.40 for the precursors of **7** and **10**, respectively).

2.6. Cell culture studies

Out of the above-mentioned porphyrin-Ru conjugates, we selected the four cationic compounds described in Figure 41, representative of both types of connections, for biological tests.

Compounds **2** and **3** bear coordinatively saturated Ru compounds, whereas **8** and **11** have half-sandwich Ru fragments with a relatively labile dmso or Cl ligands and are therefore, in principle, more prone to coordination to biological targets. All conjugates are either soluble in water or in dmso; those conjugates that are not well soluble in aqueous solution usually become moderately soluble in phosphate buffer at physiological pH or upon addition of small amounts of dmso.[109]

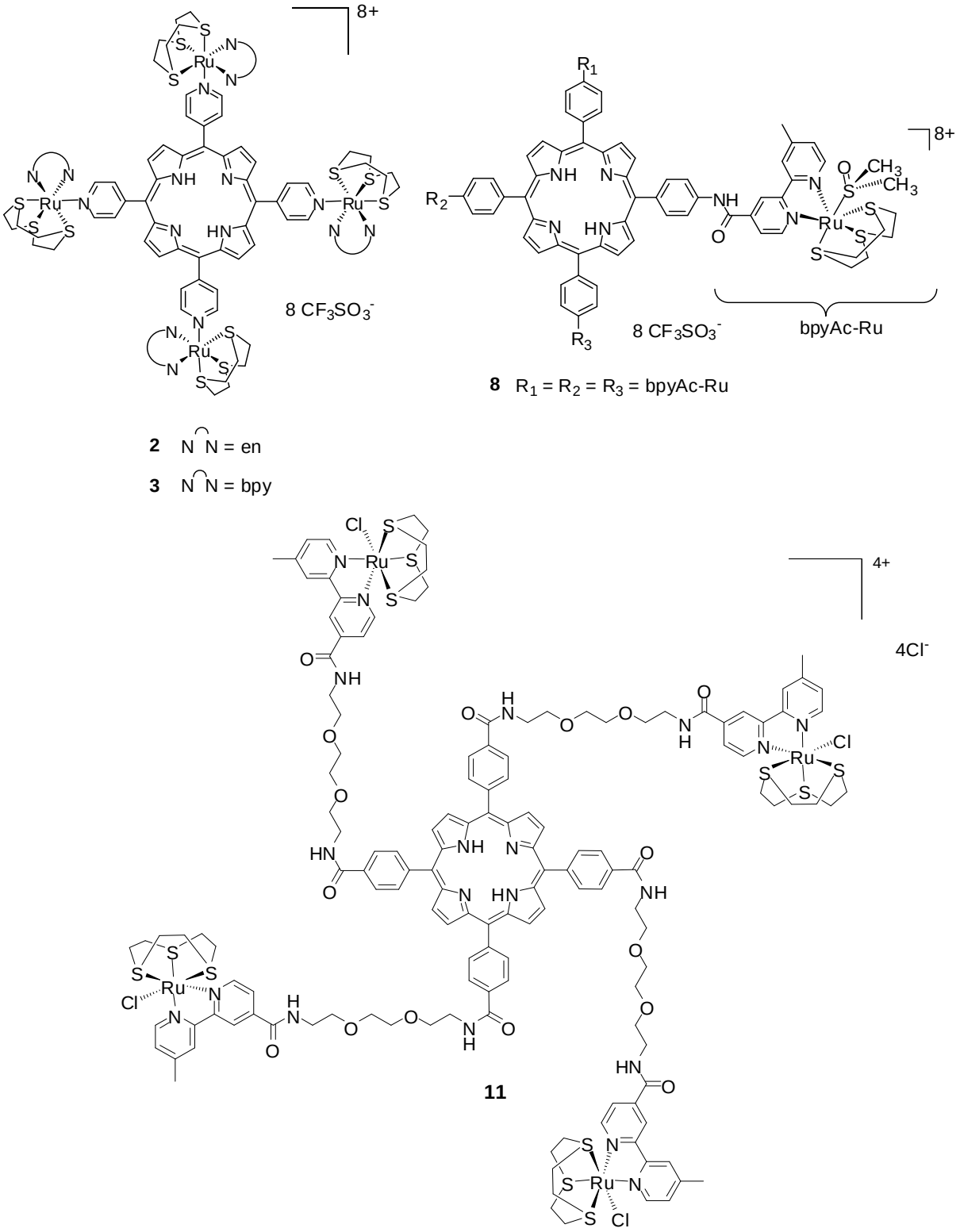

Figure 41. Schematic structures of ruthenium-porphyrin conjugates **2**, **3**, **8** and**11**.

2.6.1. Cytotoxicity

The cytotoxicity of conjugates **2**, **3**, **8** and **11**– in the dark –was evaluated by Dr. Alberta Bergamo in the human breast cancer cells MDA-MB-231 and in the non tumorigenic epithelial cells HBL-100, after an exposure of 72 h. The IC_{50} values are reported in Table 3 and are compared with those obtained by treating cells with two half-sandwich Ru(II) complexes that closely mimic the peripheral fragments on the conjugates: [Ru([9]aneS_3)(bpy)Cl][CF_3SO_3] (**14**) and [Ru([9]aneS_3)(en)Cl][CF_3SO_3] (**15**) (Figure 42).

Table 3. IC_{50} values of porphyrins **2**,**3**,**8** and **11,**and complexes**14** and **15**on MDA-MB-231 and HBL-100 cells after 72 h. (in the Dark)[a]

	IC_{50} [μM]	
	MDA-MB-231	**HBL-100**
2	4 ± 1	2 ± 1
3	5 ÷ 5	4 ÷ 5
8	4 ÷ 6	10 ÷10
11	12 ± 2	26 ± 2
[Ru([9]aneS_3)(bpy)Cl][CF_3SO_3] (**14**)	> 300*	n.d.
[Ru([9]aneS_3)(en)Cl][CF_3SO_3] (**15**)	146 ÷ 177*	175**

[a]MDA-MB-231 cells grown in multi-well plates are treated with compounds **2**- **11** at 0.1 μM ÷ 30 μM for 72 h, then cell cytotoxicity was detected by MTT. IC_{50} are the mean ± S.D. calculated from values obtained in three separated experiments (compounds **2**, **11**) or the values obtained in two separate experiments (compounds **3**, **8**). Statistics: unpaired t test.*from ref. 88. **from ref. 87

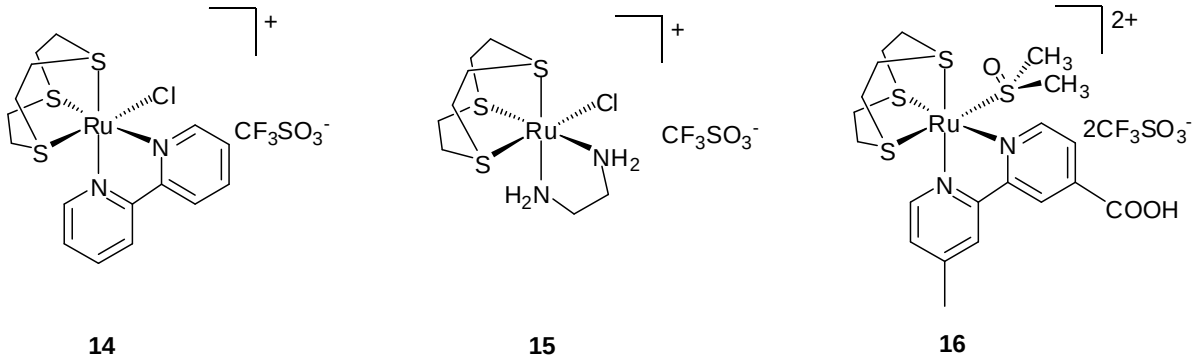

14 **15** **16**

Figure 42. Schematic structures of [Ru([9]aneS_3)(bpy)Cl][CF_3SO_3] (**14**), [Ru([9]aneS_3)(en)Cl][CF_3SO_3] (**15**) and [Ru([9]aneS_3)(bpyAc)(dmso-*S*)][CF_3SO_3]$_2$(**16**).

While the reference Ru complexes are either mildly (**15**) or not cytotoxic at all (**14**), the Ru-porphyrin conjugates **2**, **3** and **8** show IC_{50} values in the low micromolar range (2 ÷ 10 μM),

i.e. up to two orders of magnitude lower than those measured for **14**. Compound **11** is slightly less active in reducing cell proliferation as it shows, in both cell lines, IC_{50} values statistically higher than those of the other conjugates. Taken together, these results show that, even when the cell growth inhibition per Ru fragment is considered, conjugates remain remarkably more cytotoxic compared to the reference Ru complexes. In addition, their cytotoxic activity seems to be scarcely dependent on the type of porphyrin-Ru connection on the total positive charge of the adduct, and on the solubility in water (only **2** and **11** are well soluble). These observations suggest that the increase of cytotoxic potency of the porphyrin conjugates with respect to the Ru complexes might derive from an improved uptake in cancer cells.[121] In addition, the cell growth inhibition, which is apparently independent on the presence of substitutionally-labile ligands on the ruthenium fragments (compare **2** and **3** *vs* **8** and**11**), probably does not involve direct coordination of the conjugates to biological targets. The finding of cytotoxic activity in substitutionally inert metal complexes, which apparently contradicts the paradigms established for anticancer Pt compounds, is becomingly an increasingly common feature in modern inorganic anticancer research.[122]

Whereas for **2** and **3** the IC_{50} values are substantially independent of the cell line being treated, compounds **8** and **11** are ca. two times more active against the highly invasive tumour MDA-MB-231 cells than against the non tumorigenic HBL-100 cells, with IC_{50} values of approximately 5 μM and 10 μM for compound **8** (p = 0.0283 for MDA-MB-231 *vs* HBL-100), and of 12 μM and 26 μM for compound **11** (p = 0.0009 for MDA-MB-231 *vs* HBL-100), respectively. Despite what might be a first-sight impression, the half-sandwich Ru fragments of compounds **8** and **11** are remarkably similar: the investigation performed on the reference complexes $[Ru([9]aneS_3)(bpy)Cl][CF_3SO_3]$ (**14**) and $[Ru([9]aneS_3)(bpyAc)(dmso)][CF_3SO_3]_2$ (**16**) showed both dmso and Cl are relatively labile ligands that are released in aqueous solution.[67] Thus both **8** and **11**, under in vivo conditions, are likely to generate the same peripheral $[Ru([9]aneS_3)(bpy\text{-}PP)(H_2O)]^{2+}$fragments. Thus, the main structural difference of **11** compared to **8** are the flexible hydrophilic spacers between the chromophore and the peripheral Ru fragments. Apparently, this feature makes **11** less cytotoxic but preserves its capability to distinguish between the non tumorigenic HBL-100 and the highly invasive MDA-MB-231 cell line showing selectivity against this latter. This finding suggests that compounds **8** and **11** might have a specific interaction with a target differently expressed by the two cell lines.

2.6.2. Phototoxicity

Conjugates **2**, **8** and **11** were selected for performing a detailed investigation of their cytotoxic activity against MDA-MB-231 human breast cancer cells under irradiation with visible red light (phototoxicity). These compounds, besides being soluble in dmso, are also well (**2** and **11**), or at least appreciably (**8**), soluble in water, and represent three types of porphyrins with increasing structural complexity and both types of porphyrin-Ru connections. The cells cultures were exposed for 24 h at concentrations of the conjugates ranging from 0.1 μM to 10 μM, then were irradiated at 590-700 nm with a fluence rate of 25 mW/cm^2 and light doses from 1 to 10 J/cm^2. The exposure of control cells to these total doses does not induce an inhibition of cell proliferation as reported in Figure 43.

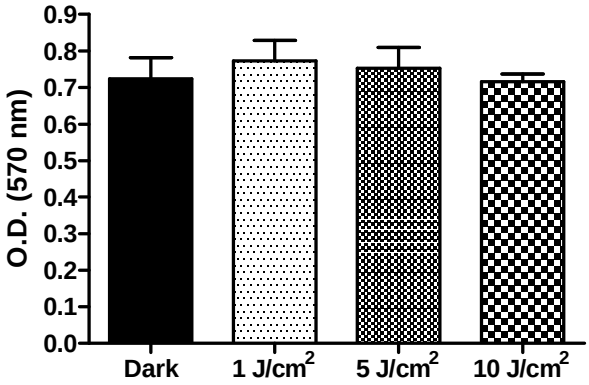

Figure 43. Cell viability of control cells exposed or not to different total light doses. MDA-MB-231 human breast cancer cells were irradiated or not (Dark), at a fluence rate of 25 mW/cm^2 and total light doses ranging from 1 J/cm^2 to 10 J/cm^2. Cell cytotoxicity was determined 24 h after the end of irradiation by MTT test. Bars represent the mean ± S.D. of optical density values obtained in a representative experiment performed in quadruplicate.

Cell cytotoxicity was determined using the MTT test 24 h after the end of the irradiation. Cells treated with the same concentrations of the test compounds, but kept in the dark, were used as controls for photo-cytotoxicity, whereas cells not exposed to drugs neither to light were used as controls for cytotoxicity. The optimal total light dose was determined in a preliminary series of experiments using **11** as representative ruthenium-porphyrin conjugate (Figure 44). By irradiating the tumour cells at increasing total light doses from 1 to 30 J/cm^2, the dose-response curve shifts to the left and the IC_{50} value correspondingly decreases. Light doses greater than 10 J/cm^2 were discarded as induced to excessive toxicity.

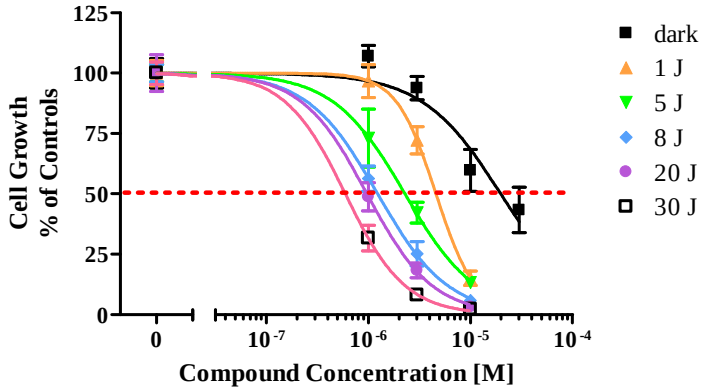

Figure 44. Light dose-effect curves for **11** as representative ruthenium-porphyrin conjugate. MDA-MB-231 human breast cancer cells were exposed to 1 μM to 10 μM for 24 h, then cells were irradiated at a fluence rate of 25 mW/cm^2 and total light doses ranging from 1 J/cm^2 to 30 J/cm^2. Cell cytotoxicity was determined 24 h after the end of irradiation by MTT test. The dotted line corresponds to 50% inhibition of cell proliferation.

The phototoxicity of compounds **2**, **8** and **11** against MDA-MB-231 cells at increasing total light doses is shown in Table 4. IC_{50} values are compared to those calculated from cell cultures similarly treated with the Ru-porphyrin conjugates but kept in the dark. For example, compound **2** has an $IC_{50}$of 3.34 μM in the dark, that becomes 1.73 μM, 0.29 μM ($p< 0.05$ *vs* dark) and 0.13 μM ($p< 0.05$ *vs* dark) when cells are exposed to 1 J/cm^2, 5 J/cm^2 and 10 J/cm^2, respectively. Similar results were observed for compound **11**, whose IC_{50} drops from 2.09 μM (dark) to 0.10 μM (10 J/cm^2, $p < 0.01$ *vs* dark). Under these experimental conditions, compound **8** is slightly less active than the others when cells are kept in the dark (IC_{50} = 24.62 μM) but, after light exposure its IC_{50} value decreases by one order of magnitude, similarly to the other two compounds: 1.71 μM at 10 J/cm^2 ($p < 0.001$ *vs* dark, and $p < 0.05$ *vs* 1 J/cm^2).

Table 4. IC_{50} values of compounds **2**, **8** and **11** in MDA-MB-231 cells treated for 24 h and then exposed to increasing doses of visible light (590-700 nm).[a]

	IC_{50} [μM]			
	Dark	**1 J/cm^2**	**5 J/cm^2**	**10 J/cm^2**
2	3.34 ±1.87	1.73 ± 1.10	0.29 ± 0.02	0.13 ± 0.04
8	24.62 ± 6.38	10.64 ± 1.61	3.93 ± 1.24	1.71 ± 0.64
11	2.09 ± 0.78	0.56 ± 0.12	0.24 ± 0.10	0.10 ± 0.04

[a] MDA-MB-231 cells grown in multi-well plates were treated with compounds **2**, **8** and **11** at 0.1 μM ÷ 10 μM for 24 h, then cells were irradiated with visible light (590-700 nm) at 25 mW/cm^{2}fluence rate and total light doses of either 1 J/cm^2, 5 J/cm^2 or 10 J/cm^2. Cell cytotoxicity was detected by MTT test 24 h after irradiation. Statistics: ANOVA Analysis of variance and Tukey-Kramer post test.

It should be noted that the experimental conditions used in these experiments for determining the cytotoxicity in the dark (*i.e.* 24 h of cell challenge with each compound followed by further 24 h in a drug free medium and evaluation by the MTT test) are different from those

described above (*i.e.* 72 h continuous drug treatment followed by the MTT test). The two schedules do not affect the IC_{50} of **2** but yield moderately different values for **8** and **11**: **8** is ca. 5 times more active after a continuative 72 h exposure, whereas the opposite result – *i.e.* a ca. 5-fold decrease of the cytotoxic activity – is found for compound **11** when cell treatment is prolonged from 24 h to 72 h.

Most interestingly, compounds **2**, **8** and **11** are all good candidates for being used in PDT because they are effective at mild light doses (10 J/cm^2), and show IC_{50} values one order of magnitude lower than those calculated in the dark in the same experimental conditions. Compounds **2** and **11** are the most potent and most promising since they already cause a significant reduction of tumour cells growth at a treatment dose as low as 1 J/cm^2.

2.6.3. Intracellular localization

The intracellular localization in MDA-MB-231 cells of compounds **2**, **8** and **11** was determined after 16 h of exposure using fluorescence microscopy; the results for compound **11** are reported in Figure 45. The porphyrin-associated fluorescence revealed that **11** accumulates in the cytoplasm of the breast cancer cells (Figure 45B), yielding red emission spots, but not in the nucleus as demonstrated by the overlay with the blue fluorescence of DAPI (Figure 45C), a compound that selectively stains the nucleus (Figure 45A). Compound **11** apparently accumulates in not yet identified granular structures of the cytoplasm. Similar results were obtained with compounds **2** and **8** (data not shown). DAPI staining, several hours after treatment, did not show morphological changes at nuclear level typical of apoptosis. On the basis of this observation the most likely mechanism of cell death seems to be necrosis, consistent with literature data showing that both death mechanisms are possible in PDT, depending on the characteristics of the photosensitising agent [123], on the cell lines used [124]and on the treatment schedule used[125].

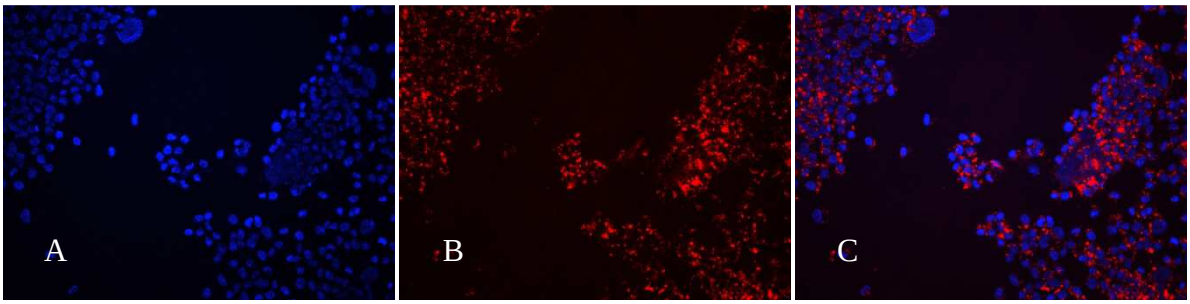

Figure 45. Evaluation of the intracellular localization of **11** in MDA-MB-231 human breast cancer cells by fluorescence microscopy. MDA-MB-231 cells were grown on histological glass slides and exposed to **11** (10 μM) for 16 h in the dark. Cells were fixed in 4% buffered formol, stained with DAPI and examined (magnification 200×). (A) DAPI (excitation at 365 nm), (B) compound **11** (excitation at 535 nm), (C) overlay of excitation at 365 nm for DAPI staining of cell nuclei (blue) and excitation at 535 nm, indicating accumulation of **11** (red spots) in the cytoplasm of the cells.

2.6.4. Ruthenium cell uptake

The uptake of compound **8** by MDA-MB-231 and HBL-100 cells was measured by atomic absorption spectroscopy after treatment for 1 h, 2 h, 4 h and 24 h. Two concentrations (4.5 μM and 10 μM) were used for each cell line, that represent the IC_{50} values calculated for this compound in MDA-MB-231 and HBL-100 cells after a 72 h exposure, respectively. Figure 46 shows the μg of ruthenium/10^6 cells as a function of the time of treatment: in both cell lines the ruthenium associated to cells increases proportionally to the duration of the treatment reaching approximately the same maximum value of 0.1 μg/10^6 cells in both cell lines (after 24 h at the concentration of 10 μM), although the accumulation kinetic seems slower in the human breast cancer cells in comparison to the non tumorigenic cells.

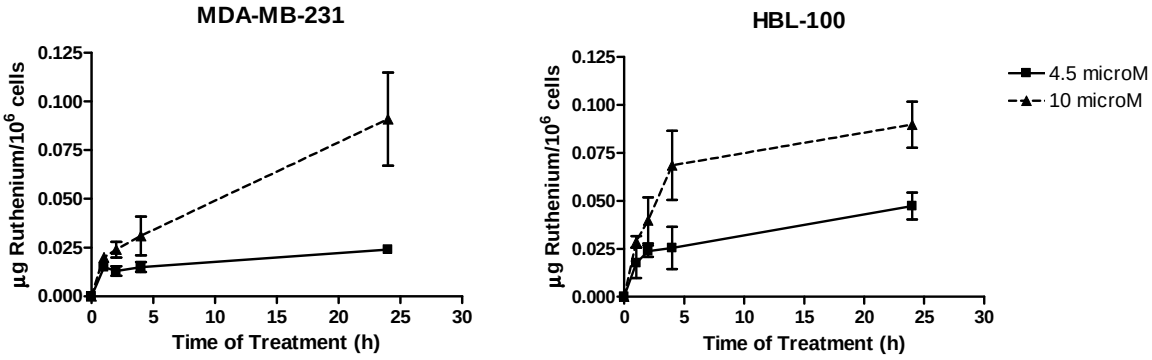

Figure 46. Ruthenium uptake in MDA-MB-231 and HBL-100 cells treated with compound **8**. Cells grown in multi-well plates were treated with compound **8** at 4.5 μM or 10 μM for 1, 2, 4 or 24 h. At the end of the treatment ruthenium content was measured with atomic absorption spectroscopy.

Thus, the large positive charge of the conjugate does not seem to inhibit its cellular uptake. Indeed, it has been demonstrated that highly charged metal complexes are capable of crossing cell membranes even better than neutral or low-positively charged complexes [126].

2.6.5. Conclusions

Compound **11**, together with the three other cationic Ru-porphyrin conjugates **2**, **3**, **8** were investigated for in vitro cell growth inhibition toward MDA-MB-231 human breast cancer cells and HBL-100 human non tumorigenic epithelial cells. In the dark, all compounds showed IC_{50} values in the low micromolar range, *i.e.* at least 2 orders of magnitude lower than the corresponding Ru complexes.

Their cytotoxic activity is scarcely dependent on the type of porphyrin and of Ru fragment. In other words, conjugation of the Ru(II) half-sandwich compounds to the porphyrin led to a remarkable increase of cytotoxicity, possibly due to improved uptake (see above).

Three compounds were selected for investigating their phototoxic effects on MDA-MB-231 human breast cancer cells upon illumination. Conjugates **2**, **8**, and **11** became ca. 10 times more cytotoxic after irradiation with visible light (590-700 nm) and proved to have from moderate to good singlet oxygen quantum yields. According to fluorescence microscopy experiments, they accumulate in the cytoplasm of the breast cancer cells but do not penetrate significantly into the nucleus. The most potent compounds **2** and **11** were active at nanomolar concentration and very low light dose (1 J/cm^2), making them promising sensitizers for the PDT of tumors

2.7. Experimental Section

Mono and bidimensional (H-H COSY) ^{1}H NMR spectra were recorded at 400 or 500 MHz, respectively, on a JEOL Eclipse 400FT or on a Varian 500 spectrometer. All spectra were run at ambient temperature. ^{1}H chemical shifts in D_2O were referenced to the internal standard 2,2-dimethyl-2,2-silapentane-5-sulfonate (DSS) at $\delta = 0.00$. In other solvents chemical shifts were referenced to the peak of residual non-deuterated solvent ($\delta = 7.26$ for $CDCl_3$, 5.32 for CD_2Cl_2, 3.31 for CD_3OD, 2.50 for dmso-d_6). UV-vis spectra were obtained at T = 25 °C on a Jasco V-500 UV-vis spectrophotometer equipped with a Peltier temperature controller, using 1.0 cm path-length quartz cuvettes (3.0 mL). Electrospray mass spectra were recorded in the positive ion mode on a Bruker Esquire ESI-MS instrument. Fluorescence spectra were recorded on a F-4550 Hitachi spectrofluorimeter.

Column chromatography was performed on silica gel 60 Å (Merck, 230-400 mesh ASTM), eluting with chloroform/ethanol mixtures as specified below.

All chemicals were purchased from Sigma-Aldrich and used without further purification unless otherwise specified.

The porphyrin-Ru conjugates precipitate with variable amounts of crystallization solvent, that depends on the batch. For this reason elemental analysis of such conjugates did not afford reliable and reproducible results and the values are not reported here (typically, some of the elemental analysis values, especially for C, differ from calculated values by > 0.5%). Nevertheless, the proposed formulas are all consistent with the ^{1}H NMR and ESI spectra.

Conjugates with 4'TpyP

[4'TPyP{Ru([9]aneS3)(en)}$_4$][CF_3SO_3]$_8$ (2).

A 46.5 mg amount of [Ru([9]aneS3)(en)Cl](CF_3SO_3) (0.14 mmol) dissolved in 2 ml of MeOH was added to a suspension of 4'TPyP (20 mg, 0.032 mmol) in 15 ml of $CHCl_3$. After addition of $AgCF_3SO_3$ (35.7 mg, 0.14 mmol), the reaction mixture was heated to reflux for 4 h. The reaction was monitored by TLC analysis (silica gel, CH_2Cl_2/EtOH 90:10). The dark suspension was concentrated in vacuo to ca. 10 ml and a few drops of diethyl ether were added. A purple solid formed upon standing, which was removed by filtration and vacuum dried. The solid was redissolved in 10 ml of MeOH and centrifuged to eliminate AgCl. The solution was evaporated to dryness under reduced pressure to obtain the title compound. Yield: 59 mg (92%).

^{1}H NMR(D_2O, δ, see Scheme 2for numberingscheme): 2.6 – 3.1 (m, 64H, CH_2 [9]aneS3 + en), 4.17 (m, 8H, NH_2), 5.09 (m, 8H, NH_2), 8.52 (d, 8H, J = 5.67, H3,5), 9.11 (v br s, 8H, βH), 9.36 (d, 8H, J = 5.71, H2,6). δ_H (CD_3OD, 25 °C, see Scheme 2 for numbering scheme): 2.5 – 3.1 (m, 64H, [9]aneS3 + en), 4.38 (br m, 8H , NH_2), 5.32 (m, 8H , NH_2),8.42 (d, 8H, J = 6.48, H3,5), 9.04 (v br, 8H, βH), 9.33 (d, 8H, J = 6.34, H2,6). δ_H (CD_3OD, -15 °C): 2.5 – 3.1 (m, 64H, [9]aneS3 + en), 4.46 (m, 8H , NH_2), 5.43 (m, 8H , NH_2), 8.42 (d, 8H, J = 6.21, H3,5), 8.97 (s, 4H, βH), 9.30 (s, 4H, βH), 9.34 (d, 8H, J = 6.18, H2,6). UV-vis(CH_3OH)λ_{max},nm (relative intensity, %): 419 (100), 513 (7.7), 549 (4.0), 589 (2.8), 646 (1.8).

[4'TPyP{Ru([9]aneS3)(bpy)}$_4$][CF_3SO_3]$_8$ (3).

A 89.5 mg amount of [Ru([9]aneS3)(bpy)(dmso-*S*)][CF_3SO_3]$_2$ (0.11 mmol) dissolved in 2 ml of methanol was added to a suspension of 4'TPyP (15.5 mg, 0.025 mmol) in 15 ml of $CHCl_3$. The mixture was heated to reflux for 8 h, until disappearance of the spot of unreacted porphyrin according to TLC analysis (silica gel, $CHCl_3$/EtOH 90:10). Dropwise addition of diethyl ether to the solution induced the precipitation of a purple solid, that was removed by filtration and washed with diethyl ether and dried under vacuum at r.t. Yield: 70 mg (78%).

^{1}H NMR (CD_3NO_2 , δ): -3.35 (s, 2H, NH), 3.5 – 2.7 (m, 48H, CH_2 [9]aneS3), 7.92 (t, 8H, H5,5'), 8.13 (d, 8H, H3,5), 8.33 (t, 2H, H4,4'), 8.63 (m, 16H, βH + H2,6), 9.22 (d, 2H, H3,3'), 9.48 (d, 2H, H6,6'). UV-vis(CH_3NO_2)λ_{max}, nm (relative intensity, %): 425 (100), 518 (8.8), 553 (5.4), 590 (4.2), 646 (2.8).

Table 5. Crystallographic data and details of structure refinements for compounds **3**.

	4·4(CH_3NO_2)	**10**
Empirical formula	$C_{116}H_{118}F_{24}N_{20}O_{32}Ru_4S_{20}$	$C_{22}H_{28}F_6N_2O_9RuS_6$
Formula weight	3805.78	871.89
Crystal system	Monoclinic	Monoclinic
Space group	*P* 2_1/c	*P* 2_1/c
a (Å)	23.157(5)	10.026(3)
b (Å)	16.581(4)	23.075(4)
c (Å)	20.833(5)	14.057(3)
β (°)	97.01(3)	96.40(2)
Volume (Å^3)	7939(3)	3231.8(13)
Z	2	4
D_{calcd} (g cm^{-3})	1.592	1.792
μ(mm^{-1})	0.890	0.958
F(000)	3844	1760
θ_{max} (°)	25.52	28.28
Reflns collected	49860	35958
Unique reflections	4833	7081
R_{int}	0.0404	0.0532
Observed $I > 2\sigma(I)$	3965	4120
Parameters	733	418
Goodness of fit	1.117	0.870
$R1$ ($I > 2\sigma(I)$) [a]	0.0844	0.0427
$wR2$ [a]	0.2515	0.1043
Δρ (e/Å^3)	1.161[b] –0.831	0.420 –0.425

[a] $R1 = \Sigma \left| |Fo| - |Fc| \right| / \Sigma |Fo|$, $wR2 = [\Sigma w(Fo^2 - Fc^2)^2 / \Sigma w(Fo^2)^2]^{½}$
[b] residual peak close to a triflate anion.

Table 6. Selected coordination bond lengths (Å) and angles (°) for compound **3**.

Ru(1)–N(1)	2.175(12)	Ru(2)–N(3)	2.152(12)
Ru(1)–N(2)	2.165(12)	Ru(2)–N(4)	2.163(12)
Ru(1)–N(5)	2.194(11)	Ru(2)–N(6)	2.212(12)
Ru(1)–S(1)	2.376(4)	Ru(2)–S(4)	2.381(5)
Ru(1)–S(2)	2.378(5)	Ru(2)–S(5)	2.361(4)
Ru(1)–S(3)	2.376(4)	Ru(2)–S(6)	2.365(5)

N(1)–Ru(1)–N(5)	87.4(4)	N(3)–Ru(2)–N(6)	88.2(4)
N(1)–Ru(1)–S(1)	175.6(4)	N(3)–Ru(2)–S(4)	96.8(4)
N(1)–Ru(1)–S(2)	96.6(4)	N(3)–Ru(2)–S(5)	175.7(4)
N(1)–Ru(1)–S(3)	92.7(3)	N(3)–Ru(2)–S(6)	91.7(3)
N(2)–Ru(1)–N(5)	84.5(4)	N(4)–Ru(2)–N(6)	87.0(5)
N(2)–Ru(1)–S(1)	99.1(4)	N(4)–Ru(2)–S(4)	174.9(4)
N(2)–Ru(1)–S(2)	172.2(4)	N(4)–Ru(2)–S(5)	97.4(4)
N(2)–Ru(1)–S(3)	95.3(3)	N(4)–Ru(2)–S(6)	94.0(4)
N(5)–Ru(1)–S(1)	91.6(3)	N(6)–Ru(2)–S(4)	91.1(3)
N(5)–Ru(1)–S(2)	91.4(3)	N(6)–Ru(2)–S(5)	91.0(3)
N(5)–Ru(1)–S(3)	179.8(4)	N(6)–Ru(2)–S(6)	179.0(4)
S(1)–Ru(1)–S(2)	87.70(16)	S(4)–Ru(2)–S(5)	87.43(16)
S(1)–Ru(1)–S(3)	88.32(15)	S(4)–Ru(2)–S(6)	87.91(17)
S(2)–Ru(1)–S(3)	88.83(16)	S(5)–Ru(2)–S(6)	89.12(16)

Conjugates with 3'TpyP

[3'TPyP{Ru([9]aneS3)(bpy)}$_4$][PF$_6$]$_8$ (5)

A 44.0 mg amount of [Ru([9]aneS3)(bpy)Cl](PF$_6$) (0.07 mmol) was dissolved in 10 ml of MeOH. After addition of AgPF$_6$ (17.7 mg, 0.07 mmol), the reaction mixture was heated to reflux for 1 h. After removal of AgCl by filtration, the yellow solution was concentrated in vacuo to ca. 5 mL and it was added to a solution of 3'TPyP (10 mg, 0.016 mmol) in 5 ml of $CHCl_3$. The mixture was heated to reflux for 48 h, until disappearance of unreacted porphyrin according to TLC analysis (silica gel, $CHCl_3$/EtOH 90:10). Dropwise addition of diethyl ether to the solution induced the precipitation of a purple solid, that was removed by filtration, washed with diethyl ether and dried under vacuum at r.t. Yield: 48 mg (86%).

UV-vis (EtOH) λ_{max}, nm ($\varepsilon\times 10^{-3}$, $dm^3\ mol^{-1}cm^{-1}$): 418 (82), 513 (10.9), 546 (8.7), 587 (7.7), 643 (5.2).

Table7. Selected coordination bond lengths (Å) and angles (°) for compound **5**.

Ru(1)-N(1)	2.084(8)	Ru(1)-S(1)	2.316(2)
Ru(1)-N(2)	2.080(8)	Ru(1)-S(2)	2.308(2)
Ru(1)-N(3)	2.118(7)	Ru(1)-S(3)	2.299(3)

N(2)-Ru-N(1)	78.3(4)	N(1)-Ru-S(2)	97.5(3)
N(2)-Ru-N(3)	90.6(3)	N(3)-Ru-S(2)	91.6(2)
N(1)-Ru-N(3)	88.7(3)	S(3)-Ru-S(2)	87.69(9)
N(2)-Ru-S(3)	96.6(3)	N(2)-Ru-S(1)	89.9(2)
N(1)-Ru-S(3)	174.7(3)	N(1)-Ru-S(1)	93.0(2)
N(3)-Ru-S(3)	89.9(2)	N(3)-Ru-S(1)	178.3(2)
N(2)-Ru-S(2)	175.2(3)	S(3)-Ru-S(1)	88.44(9)
		S(2)-Ru-S(1)	88.01(8)

[3'TPyP{Ru([9]aneS3)(en)}$_4$][PF$_6$]$_8$(6)

To a 37.1 mg amount of [Ru([9]aneS3)(en)Cl](PF$_6$) (0.07 mmol) dissolved in 10 ml of MeOH a 17.8 mg amount of AgPF$_6$(0.07 mmol) was added and the reaction mixture was heated to reflux for 1 h. After removal of AgCl by filtration, the yellow solution was concentrated in vacuo to ca. 5 mL and it was added to a solution of 3'TPyP (10.0 mg, 0.016 mmol) in 5 ml of $CHCl_3$. The mixture was heated to reflux for 48 h, until disappearance of the unreacted

porphyrin according to TLC analysis (silica gel, $CHCl_3$/EtOH 90:10). Dropwise addition of diethyl ether to the solution induced the precipitation of a purple solid, that was removed by filtration and washed with chloroform and diethyl ether and dried under vacuum at r.t. The solidwas recrystallized from methanol/diethyl ether. Yield: 38 mg (76%).

^{1}H NMR (CD_3NO_2, δ, see Scheme 3 for numbering scheme): -2.92 (s, 2H, NH), 2.73 – 3.02 (m, 64H, CH_2 [9]aneS3 + en), 3.60 (m, 8H, NH_2), 5.09 (m, 8H, NH_2), 8.17 (t, 4H, H5), 8.94 – 9.02 (d, 12H, βH + H6), 9.37 (t, 4H, H4), 9.64 – 9.75 (m, 4H, H2).
UV-vis (EtOH) λ_{max}, nm ($\varepsilon \times 10^{-3}$, $dm^3\ mol^{-1}cm^{-1}$): 421 (221), 513 (16.4), 546 (6.8), 587 (7.3), 643 (3.9).

***meso*-tetra(bpy-phenyl)porphyrin (Bpy_4-PP) (7)**

A 42.0 mg amount of bpyAc (0.196 mmol, 4.4 equiv.) and 58.8 mg of ECDI (0.274 mmol) were dissolved in 4 ml of pyridine. The solution was stirred for 30 min, then a 30.0 mg amount of *p*$(NH_2)_4$PP (0.045 mmol) was added and stirring was continued at r.t. The reaction was monitored by TLC (silica gel, $CHCl_3$/EtOH 90:10). After 3h, water (20 ml) was added to the reaction mixture. The purple precipitate was removed by filtration, washed with water (80 ml) and vacuum dried at r.t. Yield: 60 mg (91%).

^{1}H NMR ($CDCl_3$, δ see Scheme 4 for numberingscheme): -2.76 (br s, 2H, NH), 2.52 (s, 12H, CH_3), 7.26 (d, 4H, H5' overlapped with the resonance of residual $CHCl_3$), 8.03 (dd, 4H, *J*= 0.7, 4.1 Hz, H5), 8.13 (d, 8H, *J* = 8.3 Hz, *m*bg), 8.28 (m, 8H, *J* = 8.2 Hz,*o*bg), 8.38 (s, 4H, H3'), 8.55 (s, 4H, H3), 8.64 (d, 4H, *J* = 5.0, H6'), 8.95 (m, 12H, βH + H6). UV-vis($CHCl_3$)λ_{max}, nm: 424, 518, 556, 594, 651. ESI-MS: *m/z* 1481.5 [M+Na^+].

[Bpy_4-PP{Ru([9]aneS3)(dmso-S)}$_4$][CF_3SO_3]$_8$ (8).

A 20.0 mg amount of Bpy_4-PP (0.014 mmol) dissolved in 10 ml of $CHCl_3$ was added to a solution of [Ru([9]aneS3)$(dmso)_3$][CF_3SO_3]$_2$ (47.5 mg, 0.058 mmol) dissolved in 45 ml of acetone. The resulting solution was heated to reflux for 2 h, during which time a purple precipitate formed. The solution was concentrated under vacuum to ca. 15 ml. The solid was removed by filtration, washed with diethyl ether and dried under vacuum. Yield: 46 mg (81%).

^{1}H NMR (CD_3NO_2, δ, see Scheme 5 for numberingscheme): -2.72 (br s, 2H, NH), 2.75 (s, 12H, CH_3), 2.81 (s, 12H, dmso-*S*), 2.89 (s, 12H, dmso-*S*), 2.65 – 3.50 (m, 12H, CH_2 [9]aneS3), 7.76 (d, 4H, *J* = 5.4 Hz, H5'), 8.35 (m, 20H, H5 + *m*bg + *o*bg), 8.75 (s, 4H, H3'), 8.98 (d, 4H, *J* = 5.8 Hz, H6'), 9.08 (m, 8H, βH), 9.13 (s, 4H, H3), 9.33 (d, 4H, *J* = 5.6 Hz, H6), 9.92 (br s, 4H, CONH). UV-vis(dmso)λ_{max}, nm (relative intensity, %): 424 (100), 519 (5.9), 557 (4.8), 593 (2.1), 651 (2.6).

Conjugates with TetBpyPP and with TedabpyPP

4-formyl benzoate

HCl (g) was bubbled for 30 min in a solution of 4-formylbenzoic acid (5 g, 0.33 mmol) dissolved in 250 ml of methanol and cooled in an ice bath. The mixture was heated to reflux for 30 min and evaporated to dryness under reduced pressure to obtain a white solid that was recrystallized from petroleum ether to obtain the title compound. Yield 4.17 g (77%). M_p = 60 °C (lit. 60 °C).

^{1}H NMR ($CDCl_3$, δ): 3.97 (s, 3H, CH_3), 7.96 (d, H3,5, *J* = 8.3 Hz), 8.20 (d, H2,6, *J* = 8.2 Hz), 10.11 (s, CHO).

***meso*-4'-tetracarboxymethylphenylporphyrin (4'-TCMePP)**

A 2.30 g amount of methyl 4-formyl benzoate (14 mmol) in propionic acid (50 ml) was heated at 120 °C. Freshly distilled pyrrole (1.0 ml, 14 mmol) was added and the mixture was refluxed for 1.5 h, then stored at –18 °C for 12 h. The purple precipitate was removed by filtration, thoroughly washedwith cold methanol and dried *in vacuo* at room temperature. Yield 0.63 g (21%).

^{1}H NMR ($CDCl_3$, δ): -2.81 (br s, 2H, NH), 4.12 (s, 12H, CH_3), 8.30 (d, 8H, *o*Ph, *J* = 8.1 Hz), 8.45 (d, 8H, *m*Ph, *J* = 8.1 Hz), 8.82 (s, 8H, Hβ). UV-vis (CH_2Cl_2, 25°C) λ_{max}, nm (relative intensity, %): 420 (100), 515 (4.0), 550 (2.0), 590 (1.4), 646 (1.0). Selected IR (KBr, cm^{-1}): 3313 (NH),1723 (s, C=O),1276 e 1020 (C-O).

***meso*-4'-tetracarboxyphenylporphyrin (4'-TCPP)**

A 12 ml amount of a 40% KOH aqueous solution was added to a 200 mg amount of 4'-TCMePP (0.236 mmol) dissolved in 200 ml of a 2:1 THF/MeOH mixture. The reaction mixture was stirred at 40 °C for 1 h, acidified with conc. HCl (pH 5) and extracted with THF/CH_2Cl_2 1:1 (4 × 50 ml). The organic fraction was evaporated under reduced pressure affording 174 mg of the desired purple product. Yield: 93%.

^{1}H NMR (dmso-d_6, δ): - 2.94 (s, 2H, NH), 8.40 (m, 16H, *m*Ph + *o*Ph), 8.87 (s, 8H, βH), 13.32 (s, 4H, COOH). UV-vis (EtOH) λ_{max}, nm (relative intensity, %) 416 (100), 513 (4.2), 548 (2.1), 590 (1.3), 646 (0.9).

TedaNHBocPP

A 146 mg amount of EDCI (0.76 mmol) and a 103 mg amount of HOBt (0.76 mmol) were added to a solution of 4'-TCPP (100 mg, 0.126 mmol) dissolved in 4 ml of anhydrous DMF. To this solution, after stirring for 30 min, a 138 mg amount of *N*-Boc-2,2′-(ethylenedioxy)diethylamine (0.56 mmol) [168] and a 68 mg amount of dimethylaminopyridine (DMAP) (0.56 mmol) dissolved in 1 ml of anhydrous DMF were added. The reaction mixture was shielded from light and stirred at room temperature for 24 h, then the solvent was removed on a rotary evaporator to yield a dark semi-solid. A 1:1 THF/CH_2Cl_2 mixture (100 ml) was added and the organic layer was washed with water (40 ml × 3) and dried over anhydrous Na_2SO_4. The organic fraction was evaporated to dryness under vacuum and the resulting solid was dissolved in 3 ml of CH_2Cl_2 and purified by column chromatography (4 × 20 cm) using CH_2Cl_2/EtOH (90:10) as eluent. The work-up afforded 153 mg of the product as a purple solid (yield 72%).

^{1}H NMR ($CDCl_3$, δ): -2.83 (br s, 2H, NH), 1.38 (s, 36H, CH_3 Boc), 3.35 (m, 8H, CH_2*spacer*), 3.61 (t, 8H, CH_2*spacer*), 3.73 (m, 16H, CH_2*spacer*), 3.84 (m, 16H, CH_2*spacer*), 5.04 (br s, 4H, NHCO), 8.24 (dd, 16H, 8H *m*Ph + 8H *o*Ph), 8.81 (s, 8H, βH).

TetNHBocPP

A procedure similar to that described above was used, with the following parameters: 170 mg of 4'-TCPP (0.215 mmol) in 10 ml of anhydrous DMF, 247.3 mg of EDCI (1.29 mmol) and 174 mg of HOBt (1.29 mmol). To this solution a 275 mg amount of *N*-Boc-ethylenediamine [127] (1.72 mmol) was added and the reaction mixture stirred for 2.5 h at r.t. Yield 176 mg (60%).

^{1}H NMR ($CDCl_3$, δ): -2.84 (br s, 2H, NH), 1.48 (s, 36H, CH_3 Boc), 3.56 (m, 8H, *CH_2*NHCO), 3.74 (m, 8H, *CH_2*NHBoc), 5.09 (m, 4H, NHBoc), 7.57 (m, 8H, *CH_2*NHCO) 8.24 (dd, 16H, 8H mPh + 8H oPh, *J* = 8.22, 19.53 Hz), 8.79 (s, 8H, βH).

TedaNH$_2$PP·4CF$_3$COOH

A 6 ml amount of trifluoroacetic acid (TFA) was added to a solution of TedaNHBocPP (153 mg, 0.096 mmol) dissolved in 9 ml of anhydrous CH_2Cl_2. The mixture was shielded from light and stirred at room temperature for 2 h, after which the solvent was completely removed on a rotary evaporator to give a dark green semi-solid of the title porphyrin as triflate salt. A small amount (20 mg ca.) was neutralized with triethylamine (2 drops), dissolved in methanol (2 ml), precipitated with diethyl ether, filtered and thoroughly washed with diethyl ether for characterization. The remaining product was used in the following step without further purification.

^{1}H NMR (free base) (CD_3OD, δ): 3.17 (t, 8H, *CH*$_2$NH$_2$), 3.80 (m, 40H, CH$_2$*spacer*), 8.32 (dd, 16H, *m*Ph + *o*Ph), 8.90 (br s, 8H, βH). UV-vis (MeOH) λ_{max}, nm (ε × 10^{-3}, $dm^3mol^{-1}cm^{-1}$) : 415 (479), 513 (20), 546 (11), 587 (7.1), 645 (5.9). ESI-MS *m/z*: 1312.7 (MH^+), 1334.6($M+Na^+$), 1350.6 ($M+K^+$).

TetNH$_2$PP·4CF$_3$COOH

The same procedure as above was used, with the following parameters: 189 mg of TetNHBocPP (0.14 mmol) in 10 ml of anhydrous dichloromethane and 5 ml of TFA.

^{1}H NMR (free base) (dmso-*d*$_6$, δ): -2.93 (s, 2H, NH), 3.13 (d, 8H, *CH*$_2$NH$_2$), 3.63 (d, 8H, NH*CH*$_2$), 8.35 (dd, 16H, *m*Ph + *o*Ph), 8.84 (m, 8H, βH), 9.11 (m, 4H, NHCO). ESI-MS (*m/z)*: 959.4 (MH^+), 981.4 ($M+Na^+$),

TedabpyPP (10)

A 115 mg amount of bpyAc (0.54 mmol), a 155 mg amount of EDCI (0.81 mmol), and a 109 mg amount of HOBt (0.81 mmol) were dissolved in 5 ml of anhydrous DMF. After stirring for 30 min at room temperature, a solution of TedaNH$_2$PP (0.090 mmol) and 110 mg of DMAP (0.90 mmol) in 5 ml of anhydrous DMF was added. The reaction mixture was stirred for 24 h in the dark. At reaction completion (TLC: aluminium oxide, CH_2Cl_2/EtOH 90:10) the solvent was evaporated under vacuum and the resulting solid was triturated with diethyl

ether, filtered, thoroughly washed with diethyl ether and dried in vacuum. Yield: 180 mg (96%).

^{1}H-NMR (CD_2Cl_2, δ): -3.00 (s, 2H, NH), 2.21 (s, 12H, CH_3bpy), 3.68-3.83 (m, 48H, CH_2 *spacer*), 6.96 (d, 4H, *J* = 4.72 Hz, H5'), 7.21 (t, 4H, NHCO bpy), 7.31(t, 4H, NHCO), 7.66 (dd, 4H, *J* = 1.64, 4.96 Hz, H5), 8.10 (s, 4H, H3'), 8.10 (d, 8H, *J* = 7.95 Hz, *o*Ph), 8.18 (d, 8H, *J* = 7.95 Hz, *m*Ph), 8.35 (d, 4H, *J* = 4.96 Hz, H6'), 8.62 (d, 4H, *J* = 4.96 Hz, H6), 8.65 (s, 4H, H3), 8.74 (s, 8H, βH). ESI-MS *m/z*: 2096.7 (MH^+)2118.6 ($M+Na^+$), 2134.5 ($M+K^+$). UV-vis (MeOH) λ_{max}, nm (relative intensity, %): 418 (100), 514 (4.7), 549 (2.4), 590 (1.5), 646 (1.1).

TetbpyPP (9)

The same synthetic procedure as above was used, with the following parameters: 191 mg of bpyAc (0.89 mmol), 218 mg of EDCI (1.14 mmol) and 159 mg of HOBt (1.17 mmol) in 13 ml of anhydrous DMF. TetNH_2PP (0.14 mmol), 154 mg of DMAP (1.26 mmol) in 7 ml of anhydrous DMF. Yield: 181 mg (74%).

^{1}H-NMR (dmso-d_6, δ): -2.94 (br s, 2H, NH), 2.40 (s, 12H, CH_3), 3.64 (m, 16H, CH_2), 7.28 (d, 4H, H5'), 7.87 (d, 4H, H5), 8.26 (s, 4H, H3'), 8.31 (m, 16H, *o*Ph + *m*Ph), 8.57 (d, 4H, H6'), 8.84 (m, 16H, βH+H6+H3), 9.00 (t, 4H, CONH), 9.16 (t, 4H, CONH). ESI-MS *m/z*: 1744.7 (MH^+), 1766.7 ($M+Na^+$), 1782.6 ($M+K^+$). UV-vis (MeOH + 5% dmso) λ_{max}, nm ($\varepsilon\times10^{-3}$, dm^3 $mol^{-1}cm^{-1}$): 416 (237), 512 (13), 547 (7.1), 589 (5.1), 645 (3.8).

[TedabpyPP{Ru([9]aneS3)Cl}$_4$][Cl]$_4$ (11)

A 50 mg amount of TedabpyPP (0.024 mmoli) was dissolved in a mixture of MeOH (6 ml) and CH_2Cl_2 (2.5 ml). To this solution a 41 mg amount of [Ru([9]aneS3)(dmso)Cl_2] (0.095 mmol) dissolved in 16 ml of hot MeOH was added. The mixture was refluxed for 24 h and its colour turned deep red. After reaction completion (TLC: aluminium oxide, CH_2Cl_2/EtOH 90:10) the solvent was evaporated under vacuum and the residue redissolved in a few drops of methanol. Dropwise addition of diethyl ether to the purple-brown solution induced the precipitation of a purple solid, that was removed by filtration and washed repeatedly with diethyl ether and dried under vacuum at r.t. Yield: 79 mg (92%).

^{1}H NMR (dmso-d_6, δ): -2.93 (s, 2H, NH), 2.40 – 2.85 (m, 48H, CH_2 [9]aneS3), 2.53 (s, 12H, CH_3 bpy), 3.55 – 3.70 (m, 48H, CH_2 *spacer*) 7.50 (d, 4H, *J* = 5.03 Hz, H5'), 7.95 (d, 4H, *J* = 5.12 Hz, H5), 8.30 (s, 16H, *o*Ph + *m*Ph) 8.65 (s, 4H, H3'), 8.82 (d, 4H, *J* = 5.75 Hz, H6'), 8.84 (s, 8H, βH), 8.93 (t, 4H, CONH), 9.01 (s, 4H, H3), 9.11 (d, 4H, *J* = 5.74 Hz, H6), 9.27 (t, 4H, CONH).ESI-MS *m/z*: 841.5 (MH^+). UV-vis (MeOH) λ_{max}, nm (relative intensity, %): 417 (100), 513 (5.5), 549(2.9), 590 (1.5), 645 (1.0).

[TetbpyPP{Ru([9]aneS3)Cl]$_4$}][Cl]$_4$ (12)

The same synthetic procedure as above was used, with the following parameters: 25 mg of TetbpyPP (0.014 mmol) in 25 ml of MeOH. 27 mg of [Ru([9]aneS3)(dmso)Cl_2] (0.063 mmol). Yield: 39 mg (92%).

^{1}H NMR (dmso-d_6, δ): -2.94 (br s, 2H, NH), 2.5 – 2.9 (m, 48H, CH_2 [9]aneS3), 7.49 (d, H5'), 8.03 (d, H5), 8.34 (dd, 16H, *o*Ph + mPh) 8.78 (s, H3'). 8.84 (m, 16H, βH + H6'), 9.17 (m, 12H, CONH + H3), 9.52 (m, 4H, CONH).UV-vis (MeOH) λ_{max}, nm (relative intensity, %): 417 (100), 513 (8.1), 548 (3.9), 589 (2.6), 645 (1.8).

[TedabpyPP{Ru([9]aneN3)(dmso-S)]$_4$}][Cl]$_4$ (13)

A 30.0 mg amount of TedabpyPP (0.014 mmol) was dissolved in a mixture of MeOH (10 ml) and CH_2Cl_2 (3 ml). To this solution a 39.3 mg amount of [Ru([9]aneN3)(dmso)$_2$Cl] (0.086 mmol) dissolved in 7 ml of hot MeOH was added. The mixture was refluxed for 48 h and its colour turned deep red. After reaction completion (TLC: aluminium oxide, CH_2Cl_2/EtOH 90:10) the solvent was evaporated under vacuum and the residue dissolved in a few drops of methanol. Dropwise addition of diethyl ether to the purple-brown solution induced the precipitation of a purple solid, that was removed by filtration and washed repeatedly with diethyl ether, dicloromethane and dried under vacuum at r.t. Yield: 36.8 mg (79%).

^{1}H NMR (dmso-d_6, δ) T = 25 °C: -2.94 (s, 2H, NH), 2.56 (s, 12H, CH_3 bpy), 2.61 (s, 12H, CH_3 dmso), , 2.62 – 3.23 (m, 48H, CH_2 [9]anoN3), 3.53 – 3.75 (m, 48H, CH_2 *spacer*), 6.06 (s, 4H, NH tacn), 7.22 (m, 8H, NHtacn), 7.62 (d, 4H, *J* = 5.05 Hz, H5'), 8.10 (d, 4H, *J* = 4.95

Hz, H5), 8.31 (m, 16H, *o*Ph + *m*Ph) 8.85 (m, 12H, βH + H3'), 8.99 (m, 4H, CONH), 9.16 (d, 8H, H6' + H3), 9.49 (m, 8H, H6 + CONH).

^{1}H NMR (dmso-d_6, δ) T = 50 °C: -2.87 (s, 2H, NH), 2.57 (s, 12H, CH_3bpy), 2.61 (s, 12H, CH_3 dmso), 2.60 – 2.90 (m, 48H, CH_2 [9]anoS3), 3.53 – 3.75 (m, 48H, CH_2 *spacer*), 6.04 (s, 4H, NH tacn), 7.19 (m, 8H, NH tacn), 7.61 (d, 4H, *J* = 5.05 Hz, H5'), 8.09 (d, 4H, *J* = 4.95 Hz, H5), 8.30 (m, 16H, *o*Ph + *m*Ph) 8.81 (s, 4H, H3'), 8.85 (m, 12H, βH + CONH), 9.16 (m, 8H, H6' + H3), 9.41 (m, 4H, CONH), 9.50 (d, 4H, H6).

UV-vis (MeOH) λ_{max}, nm (relative intensity, %): 416 (100), 513 (6.2), 547 (3.7), 588 (2.3), 645 (1.4).

Tumour cell lines for in vitro tests

The MDA-MB-231 – highly invasive – human breast cancer cell line was kindly supplied by Dr. P. Spessotto (Cro, Aviano, Italy), and maintained in Dulbecco's modified Eagle's medium (EuroClone®, Devon, UK) supplemented with 10% fetal bovine serum (FBS, Gibco, Invitrogen™, Paisley, Scotland, UK), 2 mM L-glutamine (EuroClone®, Devon, UK), 1% non-essential aminoacids, and 100 IU/ml penicillin and 100 μg/ml streptomycin (EuroClone®, Devon, UK).

The HBL-100 human non-tumorigenic epithelial cell line was kindly supplied by Dr. G. Decorti (Department of Biomedical Sciences, University of Trieste, Italy), and maintained in McCoy's 5A medium supplemented with 10% FBS, 2 mM L-glutamine, and 100 IU/ml penicillin and 100 μg/ml streptomycin.

All cell lines were kept in a CO_2 incubator with 5% CO_2 and 100% relative humidity at 37 °C. Cells from a confluent monolayer were removed from flasks by a trypsin-EDTA solution. Cell viability was determined by the trypan blue dye exclusion test. For experimental purposes cells were sown in multiwall culture clusters.

Determination of cell cytotoxicity

Cell growth inhibition was determined by the MTT viability test [29]. Cellssown on 96-well plates were incubated 24 h later with concentrations from 0.1 μM to 30 μM of the appropriate compound, prepared by dissolving it in a medium containing 5% of serum, for 72 h. Solutions of the conjugates **2 – 11** were prepared by diluting a freshly prepared stock solution (10^{-2} M) of each compound in dimethylsulfoxide (dmso) (Sigma, St. Louis, MO, USA). Maximum dmso concentration in the cell incubation medium was ≤ 0.3% v/v. Cell toxicity analysis was performed at the end of the incubation time. Briefly, MTT (3-(4,5-dimethylthiazol-2-yl)-2,5-diphenyltetrazolium bromide) dissolved in PBS (5 mg ml^{-1}) was added (10 μl per 100 μl of medium) to all wells and the plates were then incubated at 37°C with 5% CO_2 and 100% relative humidity for 4 h. After this time, the medium was discarded and 200 μl of dmso were added to each well according to the method of Alley et al. [128]. Optical density was measured at 570 nm on a SpectraCount Packard (Meriden, CT) instrument. IC_{50} values were calculated from dose-effect curves with GraphPad Prism version 4.03 for Windows (GraphPad Software, San Diego, CA, USA)

Determination of cell phototoxicity

Cells grown in 96-well cell culture plates were incubated 24 h later with concentrations from 0.1 μM to 10 μM of compounds **2**,**8** and **11**, prepared by dissolving them in a medium containing 5% of serum, for 24 h. Stock dmso solutions of each conjugate were prepared as described above. Maximum dmso concentration in the cell incubation medium was ≤ 0.1% v/v. Thereafter the media containing compounds were replaced with drug-free medium containing 5% of serum and cells were irradiated at 590-700 nm at a fluence rate of 25 mW/cm^2 and light doses ranging from 1 J/cm^2 to 10 J/cm^2. This wavelength interval was isolated from the emission of a halogen lamp (Teclas, Lugano, Switzerland) by the insertion of broadband optical filters. A plate similarly treated but not exposed to light was used as reference for the dark cytotoxicity in the same experimental conditions. Experiments were conducted in quadruplicate and repeated trice. Analysis of cell phototoxicity using the MTT assay as described above was performed after a further incubation of 24 h after irradiation and compared to the values of control cells without light irradiation.

Determination of the quantum yield for singlet oxygen generation

The quantum yield (Φ_Δ) of singlet oxygen generated by compounds **2**,**8** and **11** upon photoexcitationwas measured using 9,10-dimethylanthracene (DMA) as substrate [31]. Typically, 1.5 ml of a 20 μM ethanol solution of DMA and 1.5 ml solution of the porphyrin (0.4 A at Soret band maximum, ≈ 10^{-6} M) in ethanol were placed in a quartz cuvette of 1 cm optical path and irradiated with 590–700 nm light for different periods of time at 20 ± 2 °C under gentle magnetic stirring. The fluence-rate was 100 mW/cm^2. The DMA fluorescence emission was recorded in the 380–550 nm wavelength range with excitation at 360 nm. The first-order rate constant of the photo-oxidation of DMA by $^1O_2$ was obtained by plotting $\ln F_0/F$ as a function of the irradiation time t, where F_0 and F represent the fluorescence intensity at time 0 and at time t, respectively. The rate constant was then converted into $^1O_2$ quantum yield by comparison with the rate constant for DMA photo-oxidation sensitized by haematoporphyrin (Hp), for which Φ_Δ was shown to be 0.65 [120]

Microscopy experiments

MDA-MB-231 cells were grown on histological slides in complete medium until 75% confluence was reached and exposed to compounds **2**, **8** and **11** (10 μM) for 16 h in the dark. At the end of the treatment, after discarding the medium containing the compound and washing, cells were fixed for 10 min in buffered formol, and nuclei were stained with 4',6-diamino-2-phenylindolyl hydrochloride (DAPI, Molecular Probes, Invitrogen, Italy) according to the manufacturer's instructions. Then slides were mounted with 20% PBS-glicerol and analyzed under a fluorescence microscope (Leica, DM 2000, Italy) with filters set at 365 ± 5 nm excitation light (BP 340/380, FT 400, LP 425) for DAPI, and 535 ± 25 nm excitation light (BP 515-560, FT 580, LP 590) for porphyrins.

Determination of ruthenium cell uptake

Ruthenium cell uptake was determined by atomic absorption spectroscopy (AAS) on samples processed with a modification of the procedure by Tamura and Arai. [129] MDA-MB-231 and HBL-100 cells were seeded in complete medium containing 5% of serum in a 6-well plate. When cells reached 75% confluence they were incubated with 4.5 μM or 10 μM of compound **8** for 1, 2, 4 or 24 h at 37 °C. At the end of the treatment the wells were washed three times with PBS, the cells collected by a trypsin/EDTA solution, counted with the trypan blue exclusion test and the intracellular concentration of ruthenium was determined. The cells were dried in Nalgene® cryogenic vials (a first drying step was performed overnight at 80 °C and a second step at 105 °C until the samples reached a constant weight). The dried cells were decomposed by the addition of an aliquot of tetramethylammonium hydroxide (25% in water) (Aldrich) and of milliQ water at a ratio of 1:1 directly in each vial at room temperature under shaking. Final volumes were adjusted to 1 ml with milliQ water. The concentration of ruthenium in treated cells was measured by flameless atomic absorption spectroscopy using a Zeeman graphite tube atomizer, model SpectrAA-300, equipped with a specific ruthenium emission lamp (hollow cathode lamp P/N 56-101447-00, Varian, Mulgrave, Victoria, Australia). Quantification of ruthenium was carried out in 10 μl samples at 349.9 nm with an atomizing temperature of 2500°C, using argon as carrier gas at a flow rate of 3.0 l/min. Before each analysis, a five-point calibration curve was obtained to check the range of linearity using ruthenium custom-grade standard 998 mg/ml (InorganicVentures, Lakewood, N.J.).

Statistical analysis

Data obtained in the experiments were subjected to Statistical Analysis of Variance (ANOVA) and Tukey-Kramer post-test, or to Unpaired t-test performed using GraphPadInStat version 3.06 for Windows (GraphPad Software, San Diego, CA, USA).

3. ^{99m}Tc/Re-Porphyrins conjugates

3.1. Approaches towards the synthesis of target specific radiopharmaceuticals

^{99m}Tc is the 'workhorse' of diagnostic nuclear medicine and it is used in some chemical form in the majority of diagnostic scans conducted each year in hospitals worldwide.[130]

Several oxidation states are available for Tc, with remarkably different chemical features. In recent years the organometallic Tc(I) fragment *fac*-$[^{99m}Tc(CO)_3]^+$ has attracted considerable interest in the design of novel ^{99m}Tc radiopharmaceuticals.[131] This core offers a number of attractive features: *i*. The synthetic precursor *fac*-$[^{99m}Tc(CO)_3(H_2O)_3]^+$ can be readily obtained in aqueous solution from the pertechnetate salt under reducing conditions as developed by Alberto et al. [132] Nowadays GMP-produced kits for preparing $[^{99m}Tc(H_2O)_3(CO)_3]^+$ are commercially available, *ii*. *fac*-$[^{99m}Tc(CO)_3(H_2O)_3]^+$ is water-soluble and the aqua ligands are readily exchanged, in particular by chelating ligands. *iii*. The *fac*-$[^{99m}Tc(CO)_3]^+$ core is chemically robust and maintains its integrity under the most forcing conditions (in addition, as the Tc(I) ion has a low spin d^6 electronic configuration, its complexes are typically inert), *iv*. the core is lipophilic and organometallic in nature, making the chelation more covalent in character, *v*. it is relatively easy to characterize the ^{99m}Tc(I) adducts using the "cold" non-radioactive (and diamagnetic) Re(I) analogue, which can be prepared on the macroscopic level and thoroughly characterized. To confirm the identity of the ^{99m}Tc-labelled compound, it is common in radiopharmaceutical chemistry to compareits retention time in the HPLC radiochromatogram with the UV-vis trace of the corresponding non-radioactive Re congener: if the two retention times are coincident, identity – and therefore – characterization of the ^{99m}Tc adduct is confirmed. *vi*. Finally, since Re has twoβ-emitting isotopes suitable for therapeutic applications,^{186}Re ($t_{1/2}$=3.8 d, E_{max}=1.07MeV) and ^{188}Re ($t_{1/2}$=0.7 d,E_{max}=2.12MeV), the possibility for combined diagnosis (^{99m}Tc) and radiotherapy (Re) emerges as an attractive concept for further exploration.

In the last decade, the research in the area of ^{99m}Tc radiopharmaceutical has been mainly focused towards developing radiotracers that preferentially localize in neoplastic tissues. In these 2nd generation radiopharmaceuticals the "vehicle" that carries the radionuclide to the diseased tissue is often a "targeting biomolecule" that must accumulate in tumor tissues with high affinity and specificity. It is this high receptor binding affinity and specificity that makes receptor imaging (often called "molecular imaging") advantageous over traditional scintigraphic imaging using simple Tc complex radiopharmaceuticals or other imaging modalities such as X-ray computed tomography (CT), ultrasound (US), and nuclear magnetic

resonance imaging (MRI).Thus, the labelling of biologically active molecules with ^{99m}Tc is a field of intense research[133,134,135,136]

Typically, the design of receptor/site-specific ^{99m}Tc compounds follows the 'conjugate' or 'pendant' method, in which a ^{99m}Tc-chelate moiety is attached to a molecule that has a high binding affinity/selectivity for tumor tissues.

Bifunctional chelates, such as that schematically illustrated in Figure 47, provide an effective strategy for binding the radioactive metal cation tothe biologically targeting molecule.[137,138,139]

The linker is important because it is able to influence the lipo- or hydrophilicity of the radiopharmaceutical and because it separates the bioactive part from the metal-complex minimizing steric effects. Usually this strategy ensures an appropriate accumulation of the radiotracer in the diseased tissues.

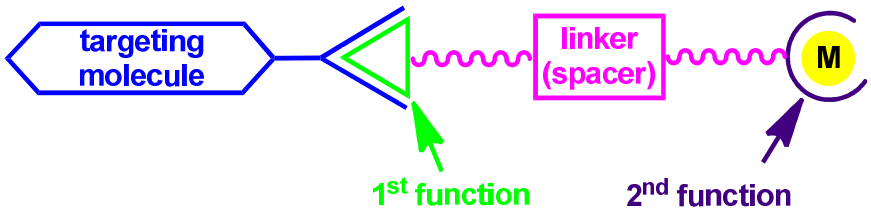

Figure47. Principle of bifunctionalchelator (BFC) and bioconjugate ready to be labelled in akit formulation.[1]

Many biomolecules, including monoclonal antibodies, antibody fragments and small peptides, have been studied for as''carriers'' for radionuclides.

Nowadays, due to the intense efforts, several molecules are under developments. Table 8 lists selected commercial ^{99m}Tc-target-specific radiopharmaceuticals and their medical applications.

Radiopharmaceutical	Trade name	Primary uses
^{99m}Tc-Apcitide	AcuTect1	Synthetic peptide for imaging DVT (deep vein thrombosis)
^{99m}Tc-Arcitumomab	Neotect1	Monoclonal antibody for colorectal cancer
^{99m}Tc-Depreotide	Zevalin	Somatostatin receptor-bearing pulmonary masses

Table 8. Selected target-specific diagnostic radiopharmaceuticals. [140]

As targeting molecule we choose water-soluble porphyrins, as these macrocycles typically show preferential uptake and retention by tumor tissues, possibly via receptor-mediated endocytosis of low density lipoproteins (LDL). This suggestion is mainly supported by the observation that lipoproteins readily incorporate porphyrins, and that tumor cells have been

found to exhibit elevated activity of LDL receptors. [8, 9, 10] Thus, porphyrins might behave as carrier ligands for the active transport of metal compounds into cancer cells.

Porphyrins can bind metal ions either inside the macrocycle (metalloporphyrins) or through accurately designed peripheral binding sites (metal-porphyrin conjugates). Both metalloporphyrins and metal-porphyrin conjugates have been investigated by us [141] and by others [142] as potential cytotoxic and photo-cytotoxic agents. For example, the in vitro anticancer activity of the gold(I)-porphyrins developed by Che[143] and co-workers is well established, and several Ru(II)-porphyrin conjugates developed in particular by some of us [142] and by Therrien [94] and co-workers possess a promising phototoxicity induced by visible light. Furthermore, provided that the metal-porphyrin conjugates are sufficiently stable, the fluorescence emission of the chromophorecan be exploited for tracking the biodistribution of the metal in the extra- and intra-cellular environment of malignant cells through fluorescence microscopy. Notably, for porphyrin compounds investigated for bio-medical purposes, water solubility is an essential requisite.

There are relatively few examples of ^{99m}Tc labelled porphyrins/porphyrins adducts, mainly concerning ^{99m}Tc(V). An earlier attempt in 1983 was made to label hematoporphyrin derivative (HpD, a complex mixture of hematoporphyrindiacetate, monoacetate, vinyl porphyrins, deuteroporphyrins and other analogs) with [^{99m}TcO$_4$]$^-$ion. The labeling mechanism was unclear and it presumably occurred at the carboxylic chain of the porphyrin.[144] Although ^{99m}Tc exhibited a high binding efficiency for HpD, the heterogeneous chemical composition of HpD caused the formation of two major labeled species. Thus it was not possible to determine the chemical nature of these species and the fraction responsible for accumulatlon in tumour tissue was never identified. Even though the ^{99m}Tc-HpD conjugate was shown to accumulate in mammary adenocarcinomas of mice, owing to the unclear composition its utility was rather limited.

Following a similar approach to obtain tumour specific imaging agents, Shetty et al. in 1996 tried to overcome those problems by a [^{99m}TcO$_4$]$^-$complexation with the water soluble porphyrins *meso*-tetrakis[3,4-bis(carboxymethyleneoxy)phenylporphyrin (T4CPP) and *meso*-5,10,15,20-tetrakis[3,4-bis(carboxymethyleneoxy)phenyl]porphyrin (T3,4BCPP) (Figure 48) in buffered saline (pH = 7). Also in this case the labelling of T4CPP and T3,4BCPP with the ^{99m}Tc(V) ion seemed to occur at the peripheral –OCH$_2$CO$_2^-$groups.[145]. The authors do not specify how many ^{99m}Tc-atom are bound to the porphyrins. They reported a mono-^{99m}Tc-T3,4BCPP (Figure 48), but they stated that three more could be potentially chelated.[146]

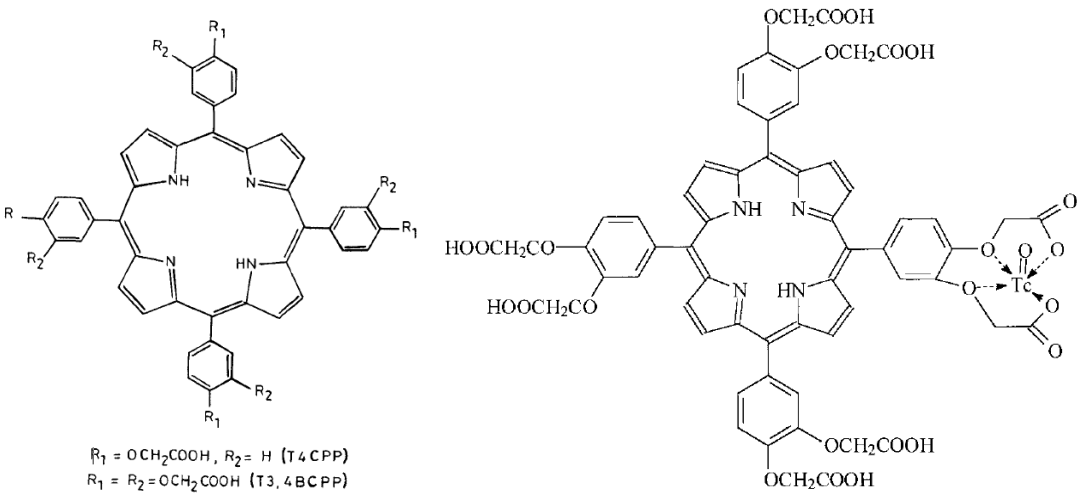

Figure 48: Schematic structure of the porphyrins T4CPP and T3,4BCPP and of ^{99m}Tc-5,10,15,20-tetrakis[3,4-bis(carboxymethyleneoxy)phenyl] porphyrin (T3,4BCPP). From ref. 145 and 146.

The labelled products remained stable for more than 4 hours at 25 °C and showed a selective accumulation in abdominal 120-sarcoma (Swiss mice) [145] and in mammary tumor (rats).[147]

Since *T/M* (tumor to muscle) ratio in nuclear medicine is a in an important parameter to evaluate the accumulation and the efficacy of an imaging agent, *T/M* ratio was evaluated for ^{99m}Tc-T3,4BCPP in mammary tumor CH3H/J mice, in rat mammary tumor and in rat C6-glioma and it was compared with those obtained with the known tumor-seeking radiopharmaceuticals ^{99m}Tc(V)-DMSA (DMSA = dimercaptosuccinic acid), ^{99m}Tc-citrate and ^{201}TlCl. [145] In the case of C6-gliomas, the ratios were 4.2 for T3,4BCPP and 2.2, 4.0 and 3.0 for the others compounds while in the case of C_3H/J mammary tumor, the ratios were 9.4, 8.8, 8.1 and 8.5, respectively.

Since an ideal agent should localize in the target tissue with a target to non-target ratio greater than 3.0, [148] those data validate the hypothesis that this porphyrin can be good candidate for tumor localizing agent. Furthermore ^{99m}Tc-T3,4BCPP appeared promising as a tumor imaging agent because it showed *T/M* ratios higher than those evaluated for the wellknown tumor-seeking radiopharmaceuticals.

The chlorin analog of T3,4BCPC (Figure 49) was also labelled with ^{99m}Tc and investigated as tumor imaging agent[149].

In vivo biodistribution studies of the labeled compound were carried out in rodent and murine tumor models in comparison with ^{99m}Tc(V)-DMSA, ^{99m}Tc-citrate and ^{201}TlCl using a gamma camera computer system.

Also in this case they found *T/M* values of 9.5 in C3H/J mammary tumor bearing rats, 6.0 in NMU-mammary tumor rats and 4.4 in C -glioma rats, in general appreciably higher than those obtained with the well known tumor-seeking radiopharmaceuticals.

Trying to improve the stability of such conjugates, more recently the same group labeled a new water-soluble cyclam acid porphyrin (CAP), 5,10,15,20-tetrakis [4-{4',8',11'-tris(carboxymethyl)-1'-(1',4',8',11'-tetraazacyclotetradecane)amidomethyleneoxy}phenyl] (Figure 49) with ^{99m}Tc, using the tetraazacyclotetradecane as tetradentate ligand for ^{99m}Tc.[150] In vivo distribution studies were performed in mammary tumour and C_6-glioma tumour-bearing rats.

Also in this case tumour to muscle (*T/M*) ratio was determined and compared with ^{99m}Tc(V)-DMSA, ^{99m}Tc-Citrate and ^{201}TlCl. In the case of mammary tumour rats the ratios were 6.93 for the porphyrins and 1.97, 5.30 and 3.29 for the others radiopharmaceuticals. In the case of C6-gliomas the ratios were 5.58 for the porphyrin, 2.18, 3.96 and 3.02 for the others compounds.

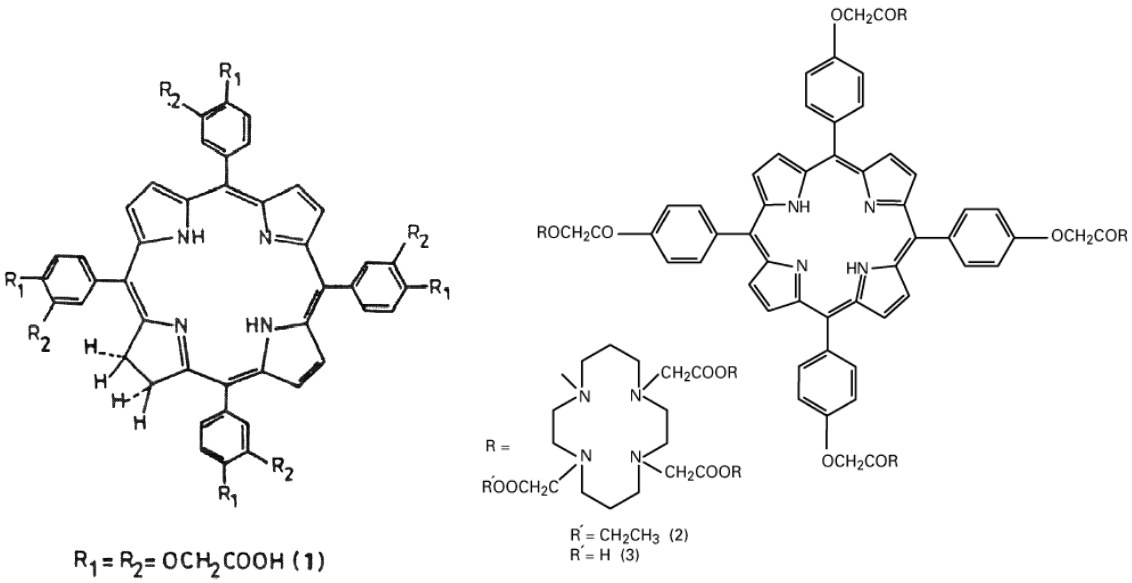

Figure 49: Schematic structureof 5,10,15,20-tetrakis[3,4bis(carboxymethyleneoxy)phenyl]chlorin (T3,4BCPC) (from ref. 148) and cyclam acid porphyrin (CAP) bound to themacrocyclic ligands 1,4,8,11-tetraazacyclotetradecane (from ref. 148).

In general those studies revealed a promising potential for detection of cancer by ^{99m}Tc-porphyrin conjugates but they also evidenced that chemical purity and stability of such conjugates can be problematic.

The exploitation of other ^{99m}Tc oxidation states, such as Tc(I), with different core geometries would allow to use new chelators and targeting strategies. Surprisingly only very few papers

describe the coordination of the $[M(I)(CO)_3]^+$(M = Tc or Re) fragment to a porphyrin.(I). In all cases the coordination seems to occur inside the porphyrinic macrocyle.

Tsutsui*et al.* reported in 1975 the unusual structures of $[Tc(I)(CO)_3]_2$-tetraphenylporphyrin (TPP) (with the long-lived ^{99}Tc isotope) and $[Re(I)(CO)_3]_2$-TPP (Figure 50), obtained by reacting TPP with either $Tc_2(CO)_{10}$ or$Re_2(CO)_{10}$in refluxing decaline.[151] Both the rhenium and technetium homodinuclear porphyrins were centro symmetric complexes having two metals bonded to the porphyrin, one above and one below the plane of the macrocycle while the porphyrins macrocycle was highly distorted.

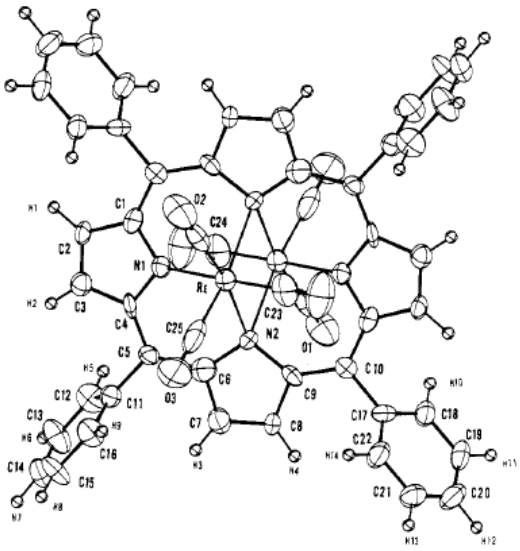

Figure 50. The structure of $[Re(I)(CO)_3]_2$-TPP. From ref. 151

More than 25 years later, in 2011, Yang at al reported the preparation of a metalloporphyrin by the reaction of $[^{99m}Tc(CO)_3(H_2O)_3]^+$ with the *meso*-tetrakis(4-sulfonatophenyl)porphyrin($TPPS_4$) (Figure51). [152]

Figure 51. Optimized 3D structure of $^{99m}Tc(CO)_3$-$TPPS_4$, From ref 152

Despite the excellent labeling yield (more than 90% at pH = 7–8) and the fairly chemical stability achieved over a range of time, pH and temperatures, the $^{99m}Tc(CO)_3$-$TPPS_4$conjugate showed very poor uptake or little retention in Hep2 tumor cells and transplanted hepatoma tissue. Thus, its potential biological application seems to be rather limited.

For the reasons detailed above and for the possibility of new developments, it is of great interest to study the coordination of long-lived $[^{99}Tc(CO)_3]^+$ to porphyrins.

We have a considerable experience in the synthesis of metal-porphyrin conjugates. Recently, we described the preparation for biomedical purposesof several new Ru-porphyrin conjugates that bear from one to four either negatively or positively charged half-sandwich Ru(II) coordination compounds at the periphery of the cromophore, at meso position.[109, 141]

Since the concentration of ^{99m}Tc formulations in the blood [153] is typically in the picomolar range, in this work we focused our attention on porphyrins capable of binding only one $[^{99m}Tc(CO)_3]^+$ fragment. Here we describe the synthesis and characterization of two new water soluble *meso*-substituted porphyrins that have in peripheral position either a diethylenetriamine unit for tridentate coordination (**18**) or a bipyridyl bidentate chelator connected to the macrocycle through a flexible and hydrophilic linker (**23**) (Figure 52). Furthermore we report the synthesis and characterization of their water-soluble conjugates that bear in peripheral position either one *fac*-$[Re(CO)_3]^+$ (**19** and **24**, respectively) or one *fac*-$[^{99m}Tc(CO)_3]^+$ fragment (**19a** and **24a**, respectively) (Figure 52), prepared in Zürich by Prof. Alberto's research group.

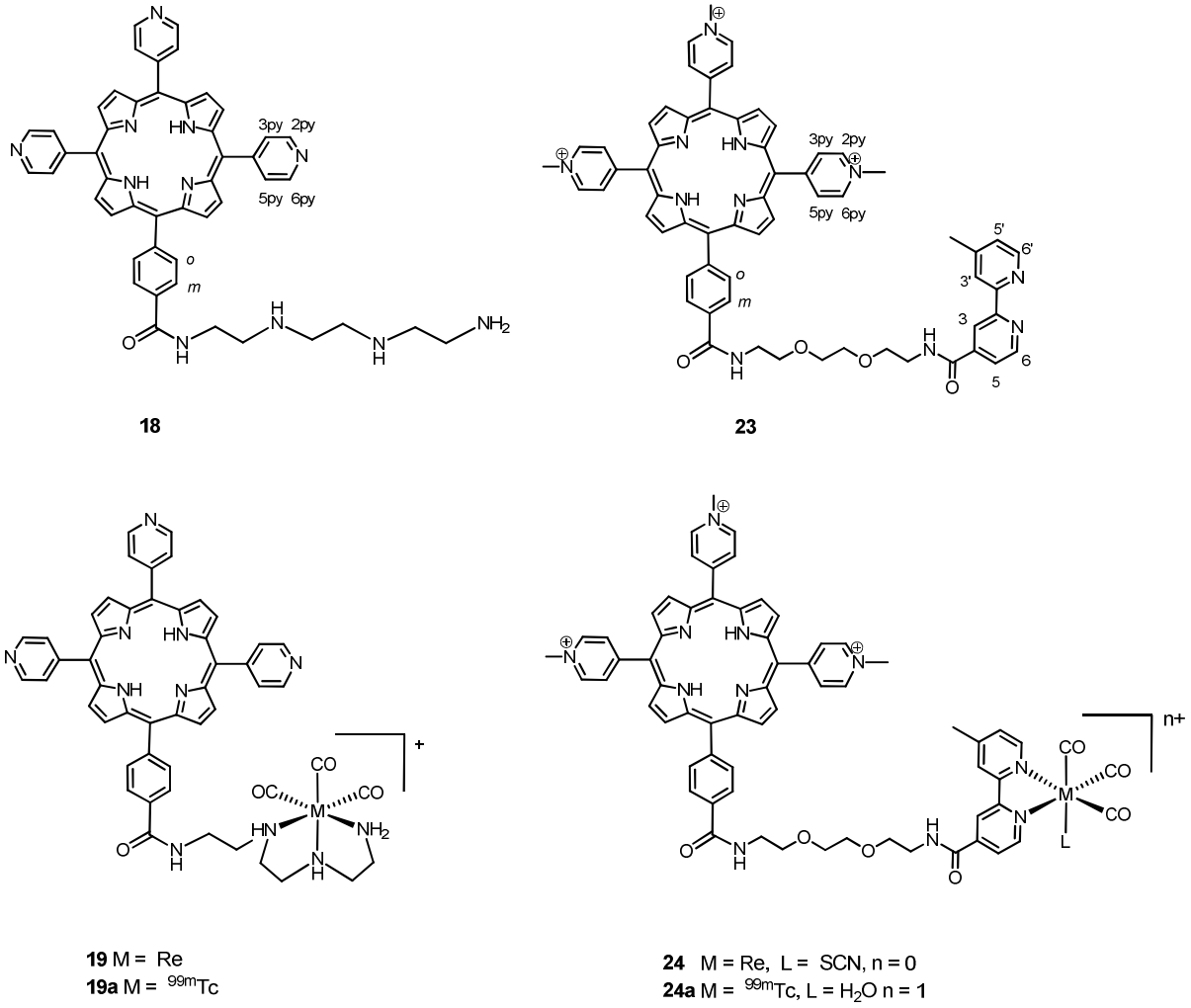

Figure 52. Schematic structures of the new porphyrins and of their $[Re(CO)_3]^+$/$[^{99m}Tc(CO)_3]^+$ conjugates.

3.2. Synthesis and Characterization

3.2.1. Water soluble porphyrins

According to our experience in porphyrin-metal conjugates, good solubility in water is difficult to achieve. Typically, it requires that the metal fragments are highly hydrophilic (e.g. they are charged and contain ligands capable of hydrogen bonding, such as NH_3 or en) and/or the porphyrin itself bears hydrophilic moieties. As our aim was to bind to the porphyrin one *fac*-$[M(CO)_3]^+$ fragment (M = Re or ^{99m}Tc), which is typically quite hydrophobic, we reasoned that – for ensuring sufficient water solubility to the conjugates – we had to rely on appropriate functionalization of the chromophore. Thus, we designed two new porphyrins with polydentate binding fragments in peripheral position via functionalization of the carboxylic group of 5,10,15-tris(4'-pyridyl)-20-(4'-carboxyphenyl)porphyrin (**15**, Scheme 9).

In one case (porphyrins **18**) a diethylenetriamine unit was attached for tridentate coordination, affording at the same time excellent water solubility. In the other (porphyrins **23**) a bipyridyl bidentate fragment was connected to the macrocycle. In this case, despite the presence of a flexible and hydrophilic linker, the aqueous solubility of the porphyrin turned out to be insufficient; good solubility was obtained by methylation of the three pyridyl N atoms, which provided three extra positive charges.

The starting material (**14**) was obtained (as the methyl ester) by condensation of 4-pyridylcarboxyaldehyde, methyl 4-formyl benzoateand pyrrole in a 3:1:4 molar ratio under Adler–Longo conditions, followed by accurate chromatographic separation of the statistic mixture of the six isomeric porphyrins (having from zero to four 4'-pyridyl rings in the *meso* positions).[115] Hydrolysis of the ester group in THF/CH_3OH under basic conditions gave porphyrin **15** that was used for the synthesis of both porphyrins **18** and **23** (Scheme 9).

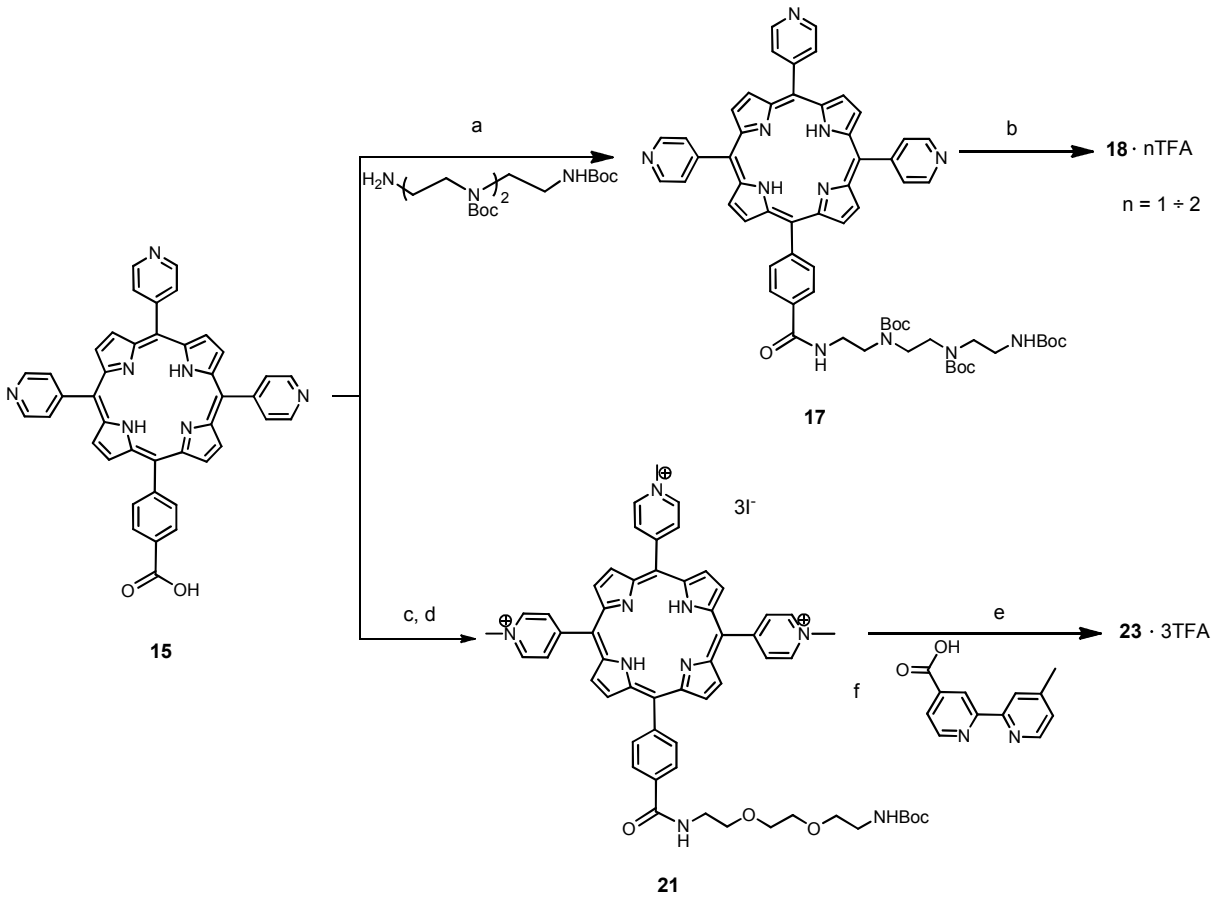

Scheme 9. Synthetic routes toporphyrins **18** and **23**.[a]
a Reactions and conditions: (a) EDCI/HOBt/DMAP, $NH_2CH_2CH_2(NBocCH_2CH_2N)_2NHBoc$, DMF, rt, 24 h(83%); (b) TFA, rt, 2 h (100%).(c) EDCI/HOBt/DMAP, $NH_2CH_2CH_2OCH_2CH_2OCH_2CH_2NHBoc$ DMF, rt, 24 h(89%); (d) CH_3I, DMF 90 °C, 2 h (97%); (e) TFA, CH_2Cl_2, rt, 2 h (100%); (f) CDMT/NMM, DMF, from 0 °C to rt, 24 h (78%).

The first step to porphyrin **18** was the coupling reaction (activated by EDCI, HOBt, DMAP in DMF under nitrogen) between the primary amine group of (2-Aminoethyl)-(2-(tert-

butoxycarbonyl-(2-tert-butoxycarbonylaminoethyl)amino)ethyl)carbamic acid tert-butyl ester (**16**) and the carboxylic acid of **15**. [154] After purification by column chromatography, the Boc-protected intermediate **17** was obtained in high yield. Its NMR characterization was unambiguous (see Figures 2 - 4); we notice that the resonances of the two equivalent pyridyl rings *trans* to one another are indistinguishable from those of the third ring. Similarly, the 8 pyrrole protons (βH) give a single unresolved multiplet (four doublets would be expected, based on the symmetry).

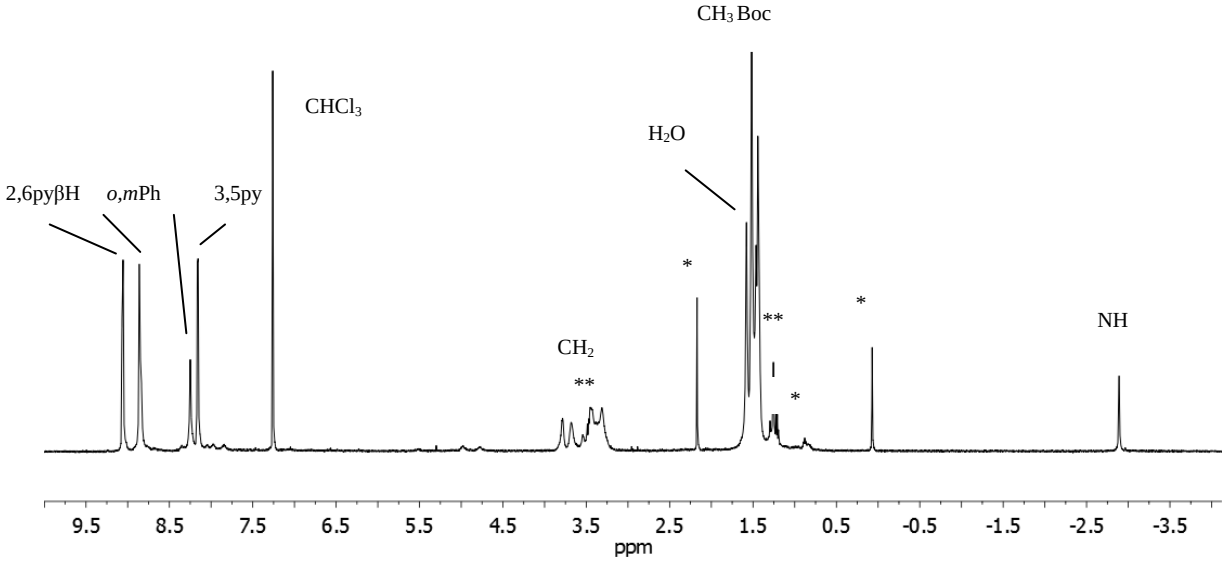

Figure 53a. [1]HNMR spectrum of **17** in $CDCl_3$ (see Figure 52 for numbering scheme). *: impurities; **: diethyl ether.

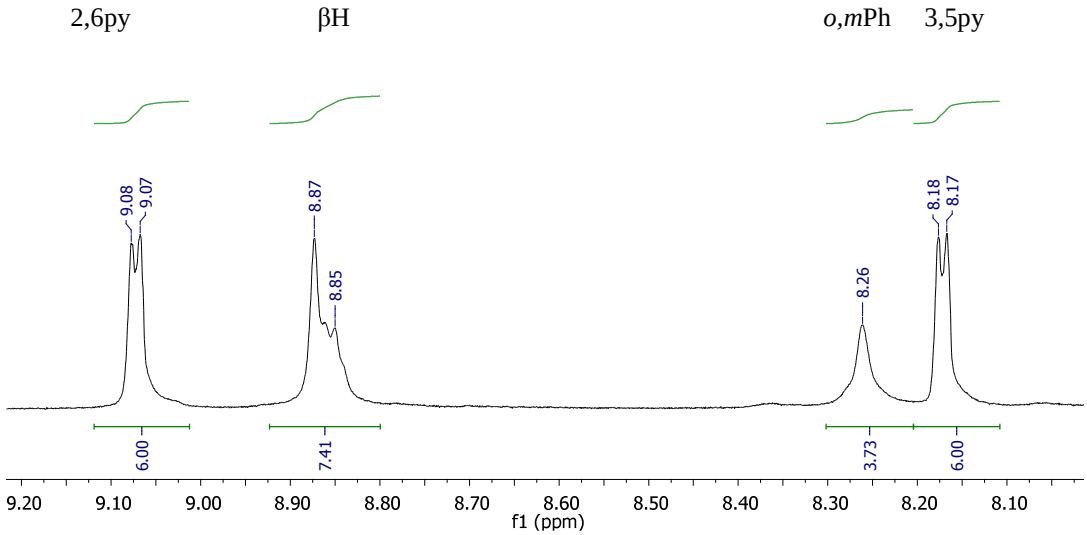

Figure 53b. [1]HNMR spectrum of **17** in $CDCl_3$downfield region (see Figure 52 for numbering scheme)

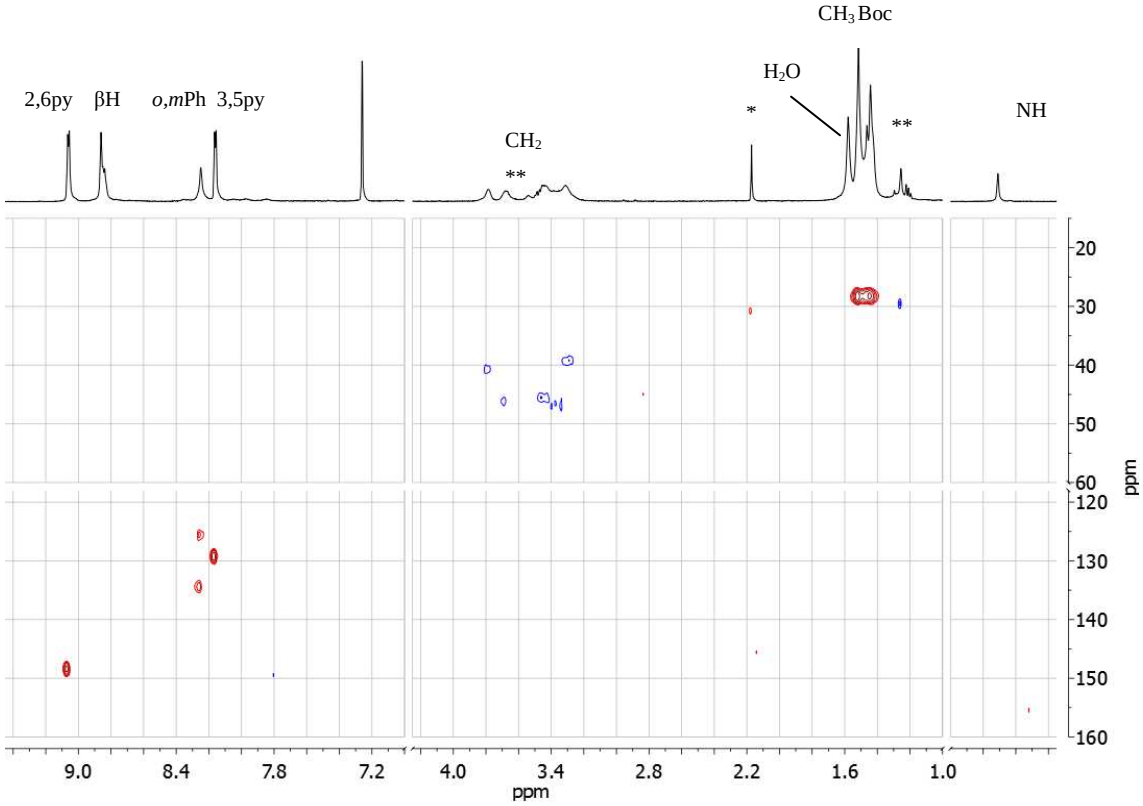

Figure 54. HSQC spectrum of **17** in $CDCl_3$.Blue peaks:CH_2 groups; read peaks:CH/CH_3 groups.(see Figure 52 for numbering scheme)*: impurities; **: diethyl ether.

Deprotection of porphyrins **17** using TFA in CH_2Cl_2, afforded **18** as TFA salt in good yield and purity (as confirmed by the ESI-MS positive spectrum, Figure 55).

We were unable to establish the charge of **18**, *i.e.* how many amino groups were – on average – protonated. The purple color of the porphyrin clearly indicates that the internal pyrrole rings are not protonated (in that case the color turns green). An NMR spectrum in CD_3OD showed that the pyridyl protons have chemical shifts that are similar to those of the precursor **17**, suggesting that the pyridyl N atoms are not protonated (protonation would be expected to induce a consistent downfield shift of the resonance of H 2,6). We expect to have 1-2 TFA molecules for each porphyrin. As the exact charge of **18** was unrelevant to its subsequent coordination to the Re/Tc fragment, and the amounts available were always small, we did not pursue its characterization further.

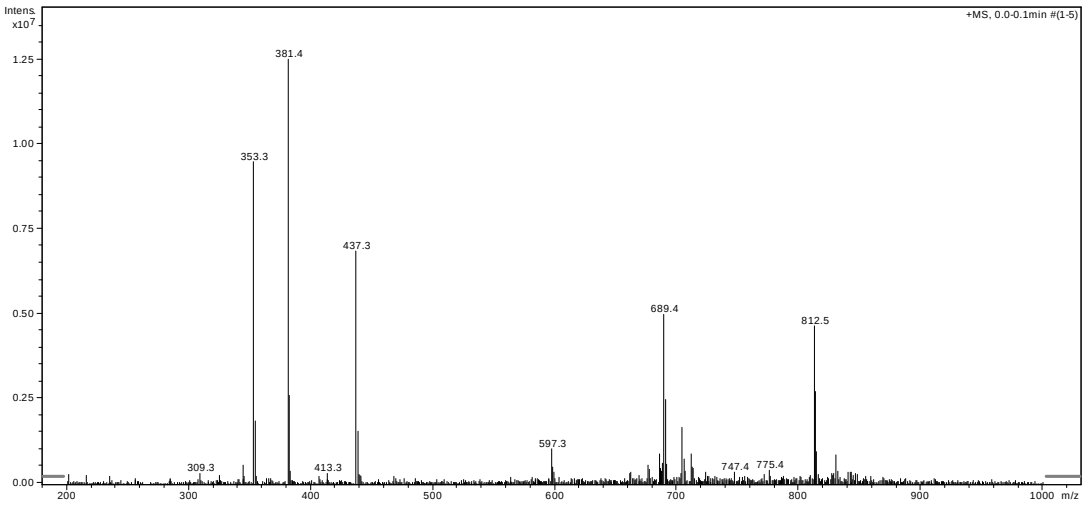

Figure 55. ESI-MS spectrum of **18**: *m/z* 812.5 ($M + Na^+$).

The procedure for obtaining the bipy-substituted porphyrins **23** involved coupling of **15**, as the hydroxybenzotriazole (HOBt) ester, with *N*-Boc-2,2'-(ethylenedioxy)-diethylamine in DMF (Scheme 9). Methylation of this intermediate with excess methyl iodide in DMF gave the tricationic porphyrins **21** (as iodide salt) in almost quantitative yield. After deprotection with an excess of TFA in CH_2Cl_2, the mono-aminoporphyrin intermediate was coupled with 4-methyl-2,2'-bipyridine-4'-carboxylic acid (bpyAc) [155] by using 2-chloro-4,6-dimethoxy-1,3,5-triazine (CDMT or Kaminski's reagent)and *N*-methylmorpholine (NMM). [156] The desidered product **23** (as trifluoroacetate salt) was conveniently purified by Soxhlet extraction.

The two porphyrins, as well as their intermediates, were characterized by mono- and bidimensional ^{1}H NMR spectroscopy and by electrospray mass spectrometry (Figures 56 - 58). Both **18** and **23**, beside being soluble in organic solvents such as methanol, are also well soluble in aqueous solution and in phosphate buffer (PBS) at pH 7.4. As mentioned above, the downfield region of the ^{1}H NMR spectrum of **18** in CD_3OD is similar to that of its precursor **17**, except that all resonances are broader. The ^{1}H NMR spectrum of porphyrins **23** in CD_3OD is similar to those already reported for other bipy-substituted phenyl porphyrins[109, 141] and is consistent with the geometry of the compound. Assignments were performed through conventional 2D correlation spectra (Figure 56). All proton resonances are sharp at 20 °C, with the exception of the βH resonance that is remarkably broad (Figure 56). In the upfield region the spectrum shows a singlet for the methyl of bpyAc at δ 1.52, and the multiplets of the aliphatic spacer (δ 3.55 –3.70). The resonances of the methyl groups on the pyridyl rings are hidden by the intense resonance of H_2O. In the downfield region, beside the two doublets for the pyridyl protons atδ 9.39 (H2,6) and 8.98 (H3,5) and the multiplet of the *o*,*m*-phenyl

protons at δ 8.24, the spectrum shows six resolved resonances, *i.e.* four doublets and two singlets, for the bpyAc protons.The H-H COSY spectrum of **23** (Figure 57) displays, beside the expected cross peaks, also two long range weak correlation peaks between the CH_3 resonance of bpyAc and those of the H3' and H5' protons that allowed the unambiguous assignment of the bpyAc resonances.

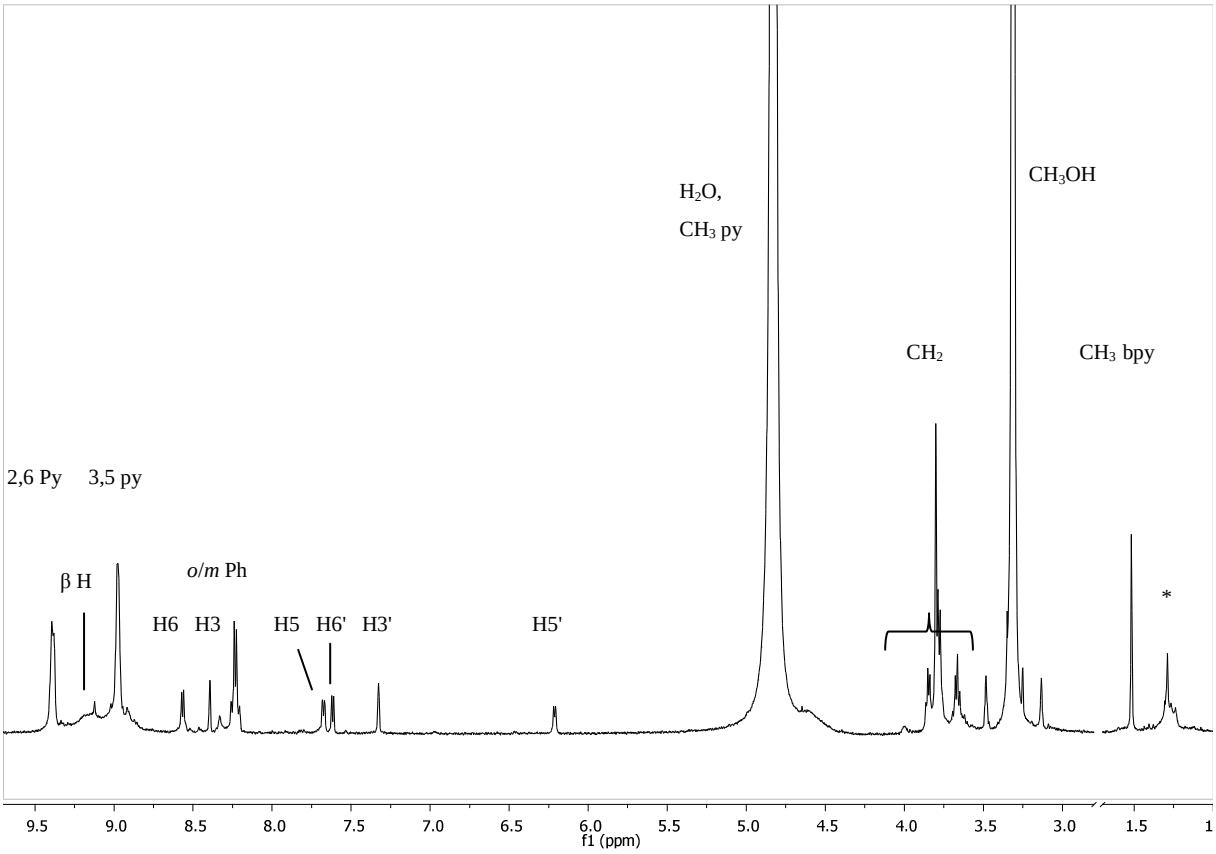

Figure 56. ^{1}HNMR spectrum of **23** in CD_3OD (see Figure 52 for numbering scheme).*: impurity.

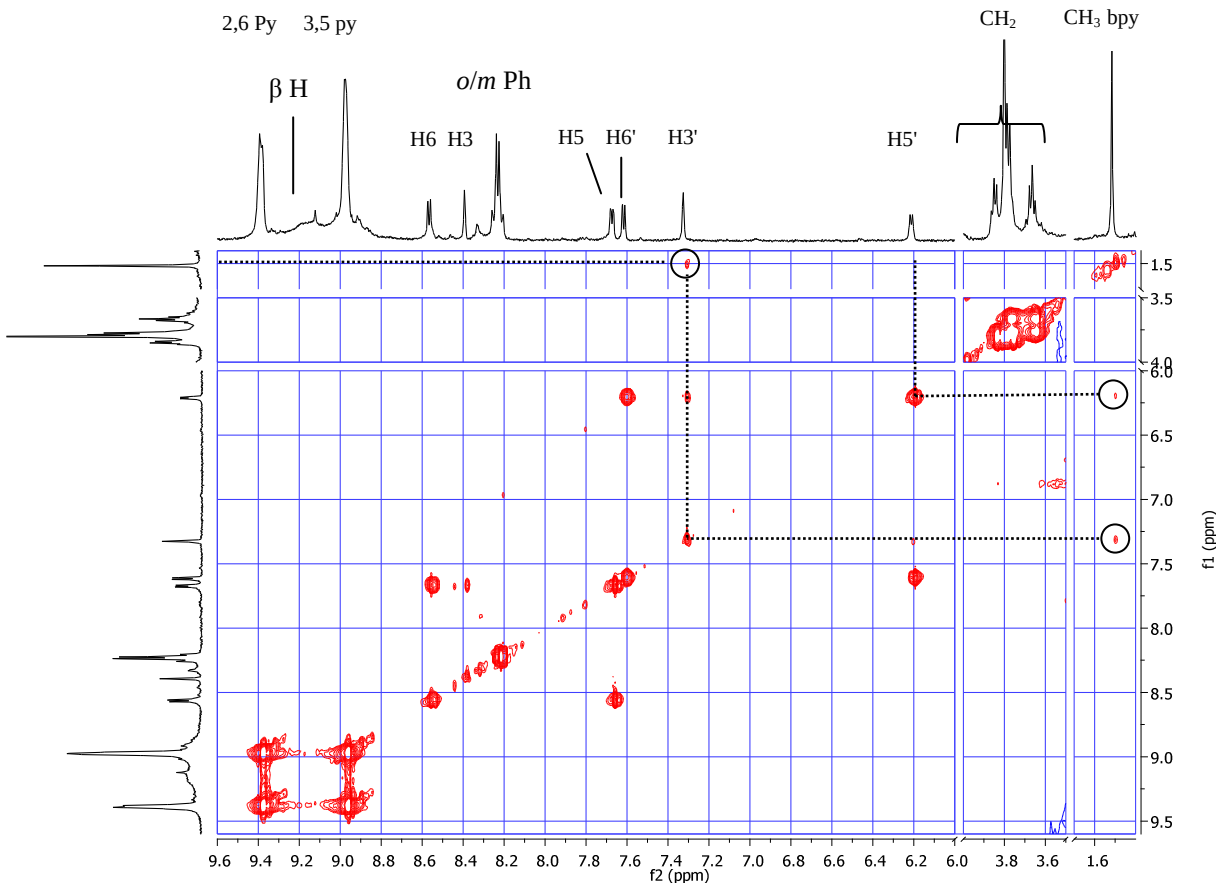

Figure 57. H-H COSY NMR spectrum of **23** in CD_3OD (see Figure 52 for numbering scheme).*: impurity.

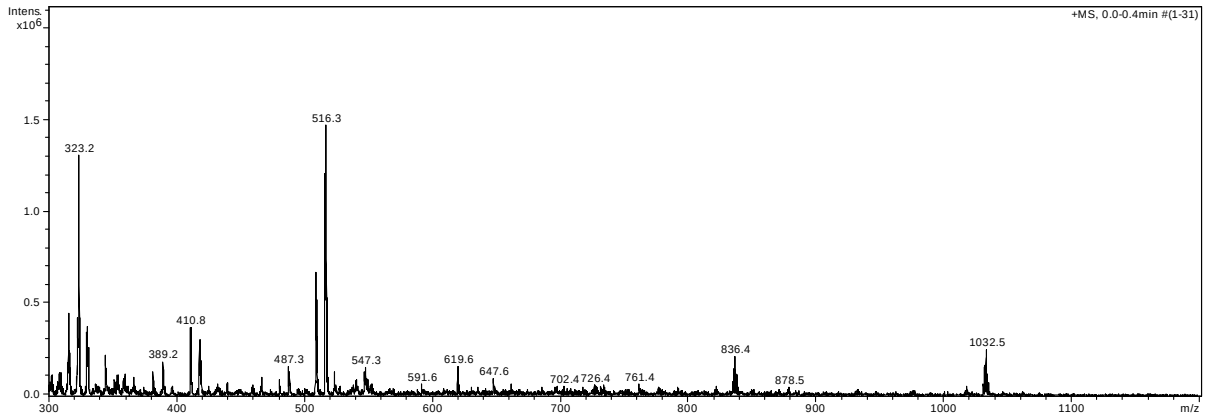

Figure 58. ESI-MS spectrum of **23**: *m/z* 1032.5 (M^+); *m/z* (*z* = 2) 516.3.

The water soluble porphyrins **18** and **23** were used as ligands for tridentate or bidentate coordination to the *fac*-$[M(CO)_3]^+$ moiety (M=Re, ^{99m}Tc) (Figure 52). As a first step, the "cold" $Re(CO)_3$ conjugates were synthesized and accurately characterized.

3.2.2. Re(I)-porphyrin conjugates

Porphyrin **18** was treated with a slight excess of $[NEt_4]_2$*fac*-$[ReBr_3(CO)_3]$ in a MeOH/PBS mixture at 70 °C, affording conjugate **19** in good yield (61%) and purity (as confirmed by the ESI-MS positive spectrum, Figure 59) after HPLC purification (Figure 60). Conjugate **19** gives a single HPLC peak, with a retention time distinctly higher than the parent porphirin **18**; according to HPLC analysis, a solution of **19** in PBS is stable at least up to 24 h. The ^{1}H NMR spectrum of **18** is not significantly different from that of **19** (Figure 61).

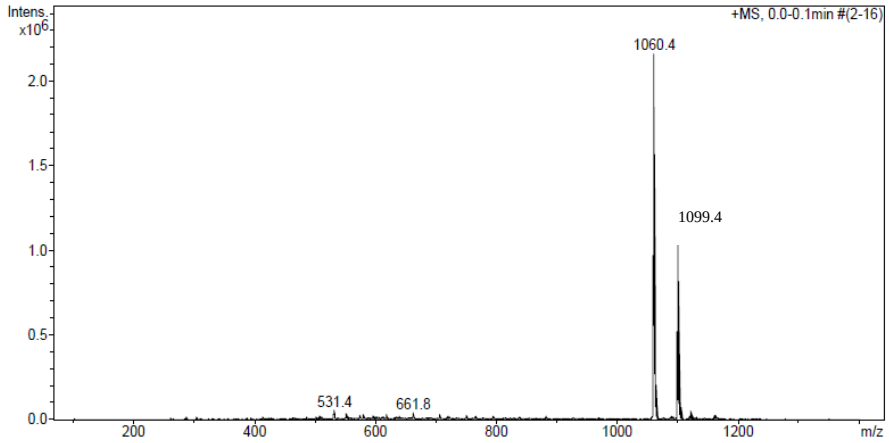

Figure 59.ESI-MSspectrum of **19**: *m/z* 1060.4 (M^+); *m/z*1099.4 (M + K^+).

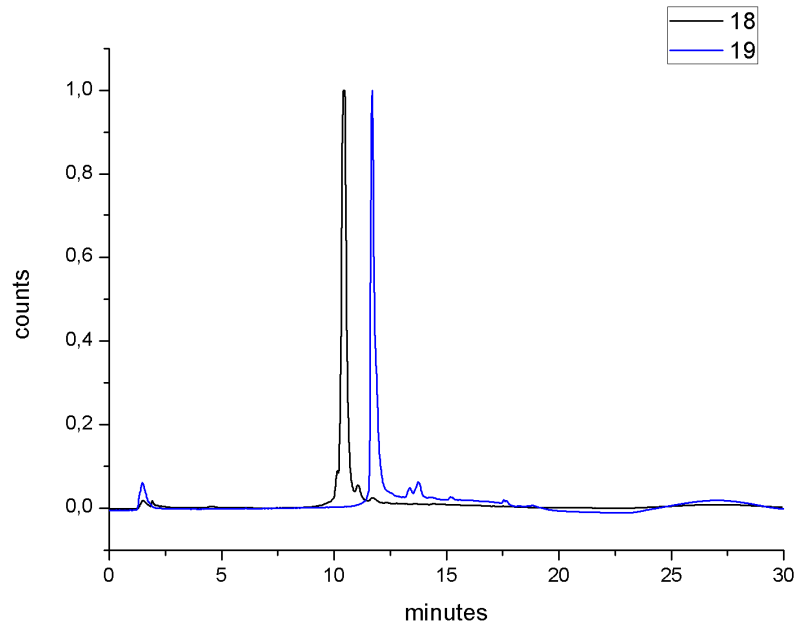

Figure 60. Comparison of HPLC traces of **18** and **19**. Gradient A, See Experimental Section.

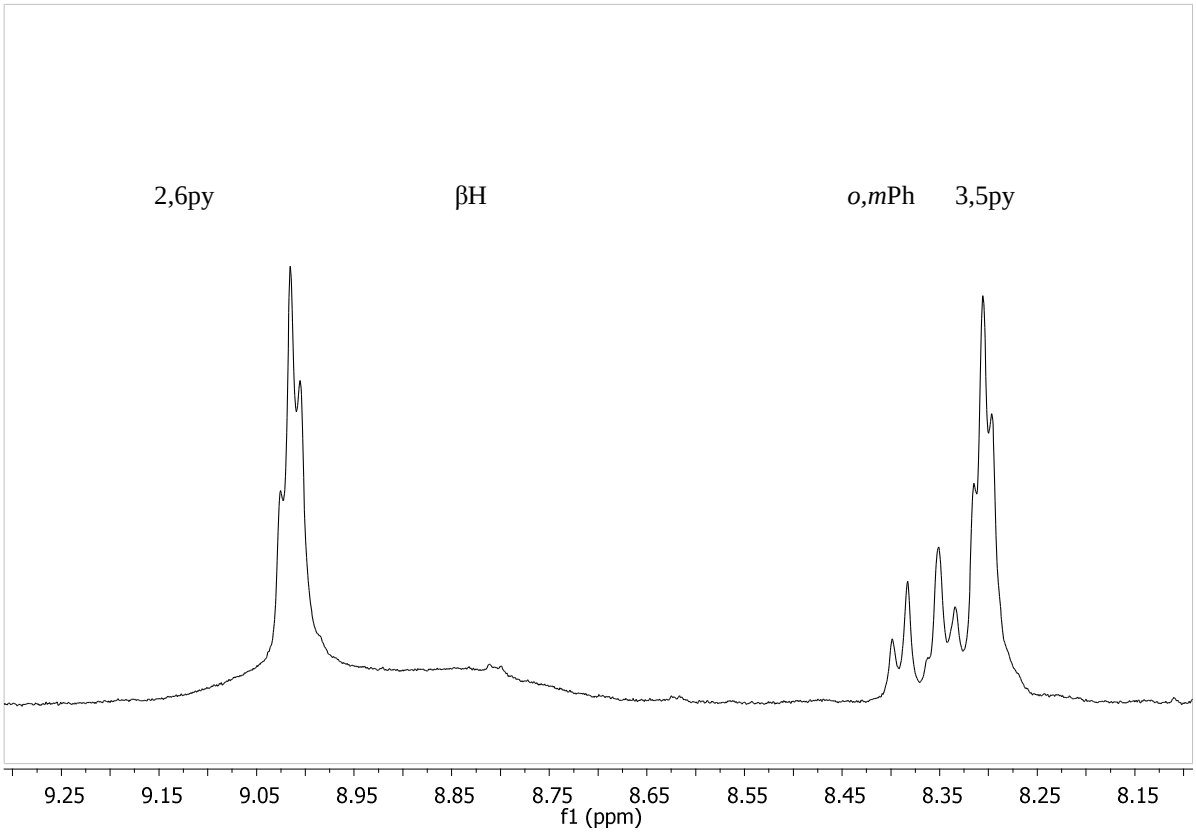

Figure 61.[1]H NMR spectrum of **19** in CD_3OD in the downfield region (see Figure 52 for numbering scheme).

Whereas porphyrin **18** bears a tridentate N-ligand capable of replacing all three (relatively) labile Br^- ligands in *fac*-$[ReBr_3(CO)_3]^{2-}$, **23** has only a bidentate chelator and its reaction with the Re(I) precursor is expected to afford *fac*-$[ReBr(CO)_3(\mathbf{23})](TFA)_3$. However, we found that, during HPLC purification, this derivative originated a complex mixture of products, presumably because the bromide ligand is still quite labile and it partially exchanges with water, methanol, and with TFA (present in the medium). A similar behaviour had been previously observed by Alberto and co-workers with another Re(I) bioconjugate: in that case, replacement of Br with I afforded a single, stable product.[157] After several attempts, we found that in our case prolonged heating of **23** with a slight excess of $[NEt_4]_2$*fac*-$[ReBr_3(CO)_3]$ and KSCN in a MeOH/PBS mixture afforded a product with a satisfactorily HPLC analysis (see below). Thus, conjugate **24** (formulated as *fac*-$[Re(CO)_3(\mathbf{23})(SCN\text{-}\kappa N)](TFA)_3$) was obtained in good yield (65%) and purity after HPLC purification. IR analysis of **23** showed (beside the CO stretching bands typical of the $Re(CO)_3$ fragment) the presence of a band at 2098 cm^{-1} attributed to the CN stretching mode of the SCN-κN ligand by analogy with the known model complex *fac*-$[Re(bpy)(CO)_3(SCN\text{-}\kappa N)]$ – whose X-ray structure was also determined.[158] Whereas the ESI-MS spectrum of **24** has a quite complicated pattern due to the 3+ charge (Figure 62), its NMR spectra were highly informative (Figure 63). As in the model complex,

coordination of the *fac*-[Re(CO)$_3$(SCN)] fragment strongly affects the six resonances of the bpy protons, that are shifted downfield by 0.5 − 1.0 ppm compared to the parentporphyrin **23**. Indeed, the NMR spectrum of **24** in CD_3OD shows, immediately after dissolution, the patterns of one major (**24a**) and one minor (**24b**) species; very slowly the initially more abundant **24a** species converts into **24b**, so that the **24a**/**24b** ratio goes from 1:5 at t = 0 to 6:1 after 3 days at ambient temperature. A similar behavior had been observed by Probst [159] for the model complex *fac*-[Re(bpy)(CO)$_3$(SCN-κN)] in dmso solution and had been attributed to the-κNto -κS isomerization of the SCN^- ligand. This linkage isomerization has been observed also with other metals (e.g. in Ru(II) complexes). [160]

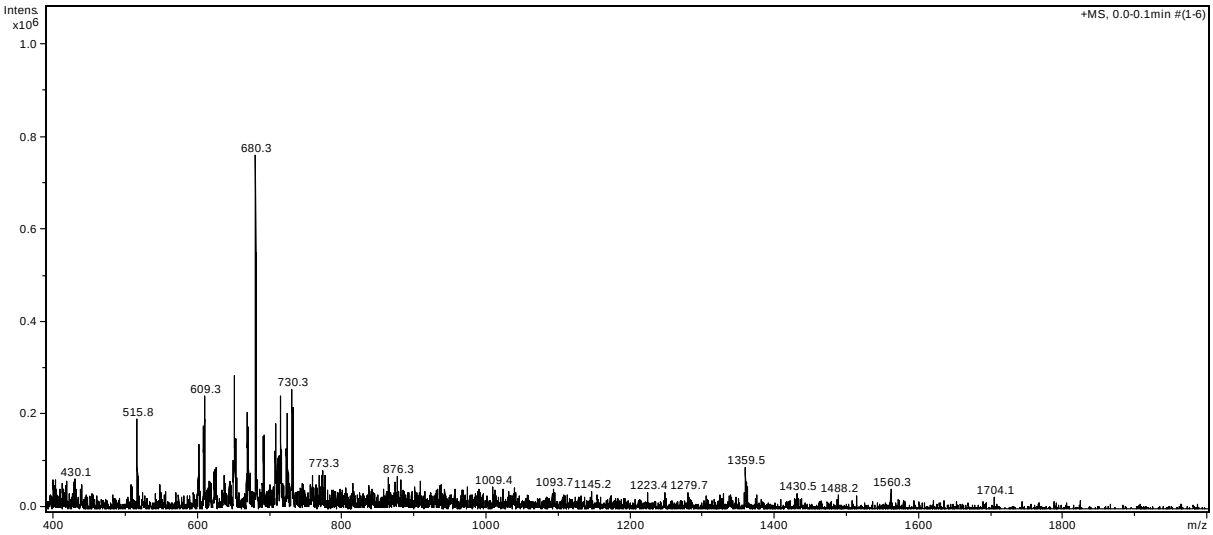

Figure 62.ESI-MS spectrum of **24**: *m/z* 1359.5 (M^+); *m/z*(z = 2) 680.5

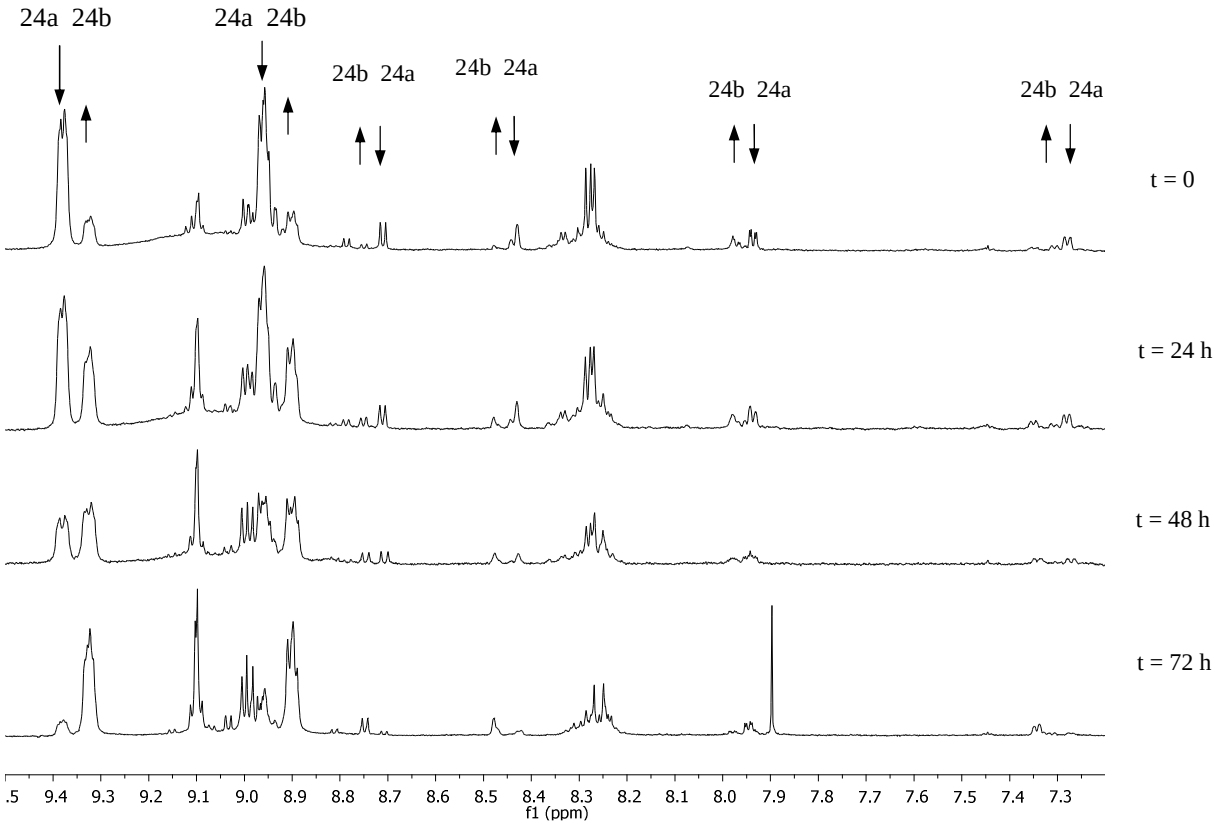

Figure 63: ^{1}H NMR spectra of **24** in CD_3OD in the aromatic region at different times: $t_1 = 0$; $t_2 = 24$ h; $t_3 = 48$ h; $t_4 = 72$ h.

The electronic absorption (Table 9) and emission spectra of conjugates **19** and **24** were not significantly different from those of the parent porphyrins **18** and **23**, respectively.

Compound	Soret	Q Band IV	Q band III	Q band II	Q band I
18	412 (100)	510 (4.8)	543 (1.6)	587 (1.5)	642 (0.6)
19	413 (100)	511 (4.8)	543 (1.6)	588 (1.4)	642 (0.7)
23	426 (100)	518 (7.2)	555 (3.7)	591 (2.8)	647 (1.0)
24	427 (100)	518 (11.7)	555 (6.9)	591 (4.6)	647 (2.0)

Table9. UV–Visible and Absorption Maxima (Relative Intensity) determined in MeOH for all compounds.

The fluorescence properties of porphyrins are useful to study their aggregation behavior in solution. In fact, porphyrins in their monomeric form usually show intense fluorescence emissions, which are partially or completely quenched upon aggregation in solution.

Whereas in PBS solution a moderate decrease of the emission intensity with time was observed for **19** (ca. 30% after 24 h, Figure 64a), a significant reduction was observed for **24** (ca. 80% after 24 h, Figure 64b), suggesting that conjugate **24** has a stronger tendence to aggregate in PBS.[161]

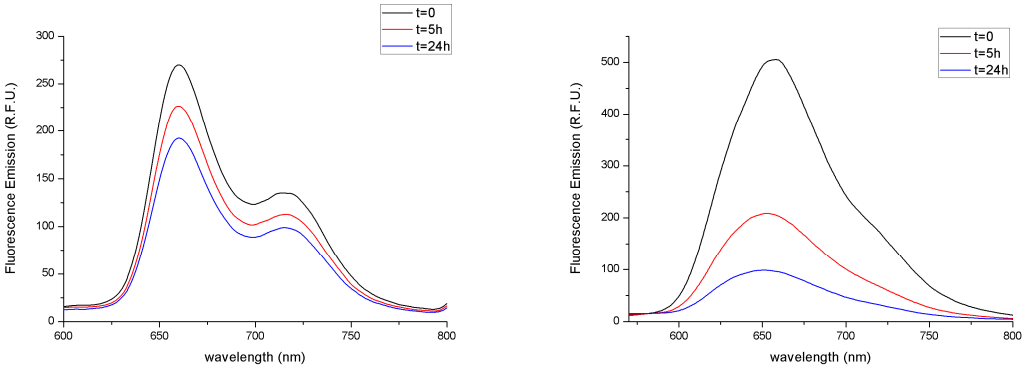

Figure 64.(a)Emission spectra of a ca. 10 µM solution of **19** in PBS at t=0 (black), t=5 h (red),and t=24 h (blue);λ_{ex} 413 nm, λ_{em}651 nm.(b)Emission spectra of a ca. 10 µM solution of **11** in PBS at t=0 (black), t=5 h (red),and t=24 h(blue); λ_{ex}427 nm, λ_{em}658 nm

3.2.3. ^{99m}Tc(I)-porphyrin conjugates

The corresponding ^{99m}Tc –porphyrinconjugates **19a** and **24a** (Figure 52) were prepared at trace level by ligand exchange reaction employing a solution of *fac*-$[^{99m}Tc(CO)_3(H_2O)_3]^+$ prepared from $[^{99m}TcO_4]^-$ according to literature procedures or with the commercially available Isolink kit (Covidien, Tyco-Mallinckrodt Med. B.V. Petten, NL).[132, 162] The concentration of *fac*-$[^{99m}Tc(CO)_3(OH_2)_3]^+$ was determined by the generator eluate and was typically in the range $10^{-6} – 10^{-7}$ M depending on the "age" of the ^{99}Mo/^{99m}Tc generator. The solution was then buffered with 0.1 M phosphate buffer to pH 7.4. The experimental conditions for obtaining the two ^{99m}Tc conjugates were optimized by testing different reaction times, concentrations and temperatures. HPLC analysis with γ-detection was performed to quantify the conversion of the ^{99m}Tc precursor. Typically, as mild as possible conditions are preferable for the preparation of ^{99m}Tc-bioconjugates as some biomolecules are not thermally stable.

We found that, when the reactions were performed at 50 °C, the peak of *fac*-$[^{99m}Tc(CO)_3(H_2O)_3]^+$ in the radiochromatograms disappeared within 30 min after the addition of the porphyrins (at a concentration of ca. 10^{-4} M for **18**, and 10^{-5} M for **23**) (Figure 65a and 66a, dashed line). In both cases the formation of a single new peak was observed (Figure 65a and 66a, solid line). According to HPLC, the labelling yield was quantitative for both porphyrins. The retention times for the parent porphyrins, the "cold" Re conjugates and the corresponding ^{99m}Tc labelled porphyrins are given in Table 10.

First of all, the comparable retention times of the corresponding $Re(CO)_3$ and $^{99m}Tc(CO)_3$conjugates confirmed the identity of the ^{99m}Tc compounds **19a** and **24a** (Figure 65b and 66b). The differences between $Re(CO)_3$ and $^{99m}Tc(CO)_3$ conjugates are explained by the separation (void volume) between the UV-vis and the radiodetector. It should be noted, however, that we formulated the Re conjugate **24** as the SCN derivative, whereas the corresponding ^{99m}Tc conjugate **24a** has either an aquo or a clorido ligand in the place of SCN^- (*i.e.fac*-$[Re(CO)_3(\mathbf{23})(SCN\text{-}\kappa N)]^{3+}$*vs*$fac$-$[^{99m}Tc(CO)_3(\mathbf{23})(H_2O)]^{4+}$ or *fac*-$[Re(CO)_3(\mathbf{23})(Cl)]^{3+}$).

(a) b)

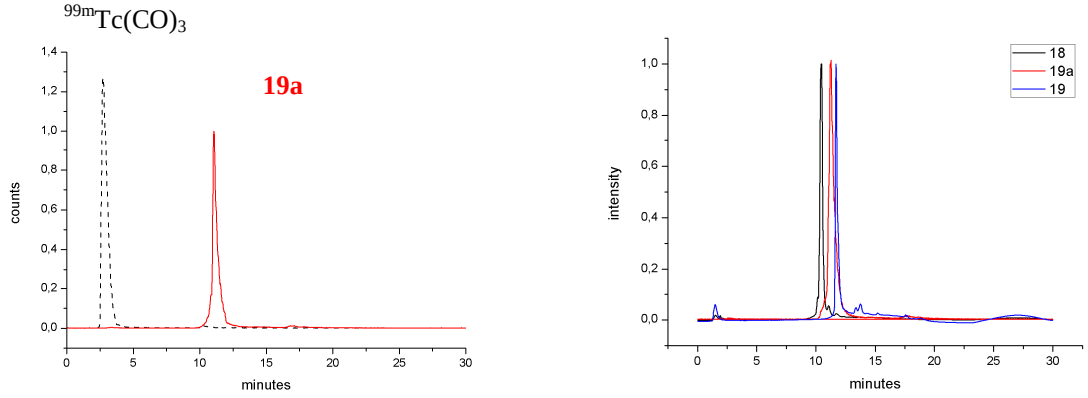

Figure 65. (a)Radioactive HPLC traces of $[^{99m}Tc(H_2O)(CO)_3]^+$ (dashed line) and of the ^{99m}Tc-porphyrin conjugate**19a** (solid line). (b) HPLC traces of porphyrin **18** (black line), of the^{99m}Tc-porphyrin conjugate **19a**(red line), and of the Re-porphyrin conjugate **19** (blue line).

(a) b)

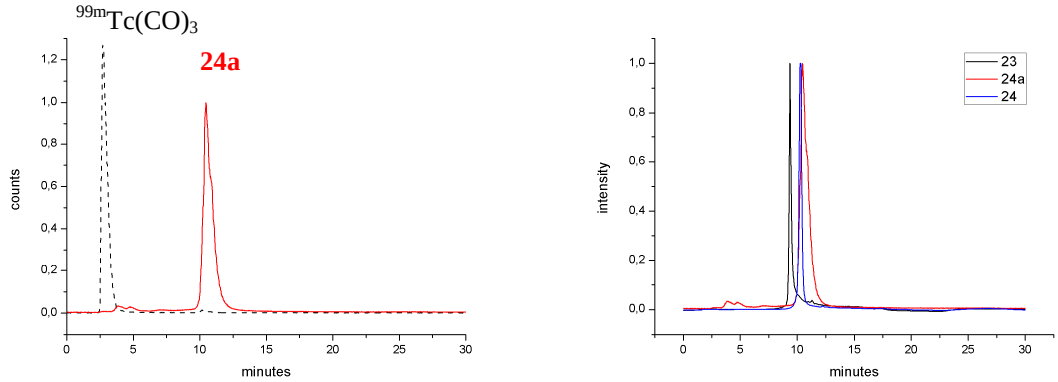

Figure 66.(a)Radioactive HPLC trace of $[^{99m}Tc(H_2O)(CO)_3]^+$ (dashed line) and of the ^{99m}Tc-porphyrin conjugate **24a** (solid line). (b) HPLC traces of porphyrin **23**(black line),of the^{99m}Tc-porphyrin conjugate **24a** (red line), and of the Re-porphyrin conjugate **24**(blue line).

Table 10. Retention times for porphyrins**18** and **23** and for their Re and ^{99m}Tc conjugates. Elution conditions: C-8 column, buffer 0,1 % TFA, Gradient A(standard TFA labelling gradient, See experimental section).

Porphyrin	Retention time (min)	Conjugate with $Re(CO)_3$	Retention time (min)	Conjugate with $^{99m}Tc(CO)_3$	Retention time (min)
18	9.72	**19**	11.70	**19a**	11.12
23	9.95	**24**	10.27	**24a**	10.46

3.2.4. Stability of Tc conjugates in aqueous solution

The stability of both technetium conjugates **19a** and **24a** was assessed by HPLC analysis under a variety of conditions. After the determination of the formation of the technetium conjugates by HPLC, ^{99m}Tc conjugates were left at ambient temperature under air and the stability was confirmed by injecting the same volume of the radioactive mixture. **19a** and **24a** were both chemically stable for a period of at least 24 h at room temperature in their preparation reaction mixture and in cell culture medium in the absence and presence of HeLa cells.

The chromatograms obtained for **19a** and **24a** from 30 min to 24h are shown in Figure 67 and 68. The slightly differences between the retention times depends from the high sensitivity of the technique used.

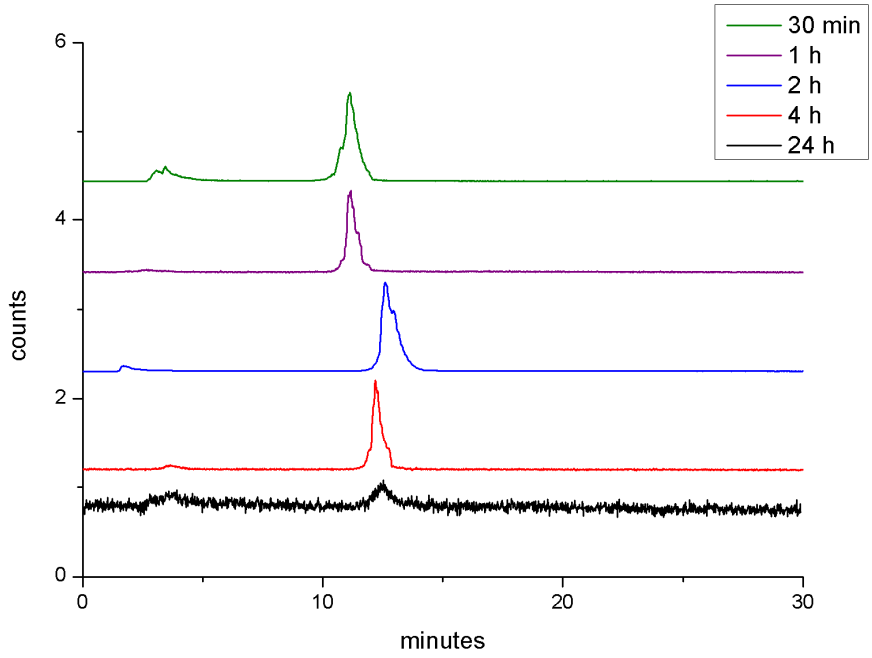

Figure 67. Radioactive HPLC traces of the^{99m}Tc-porphyrin conjugate **19a** at t=30 min (green line), 1h (purple line), 2h (blue line), and 4h (red line), 24h (black line). Elution conditions: C-8 column, buffer 0,1 % TFA, Gradient A(standard TFA labelling gradient, See experimental section).

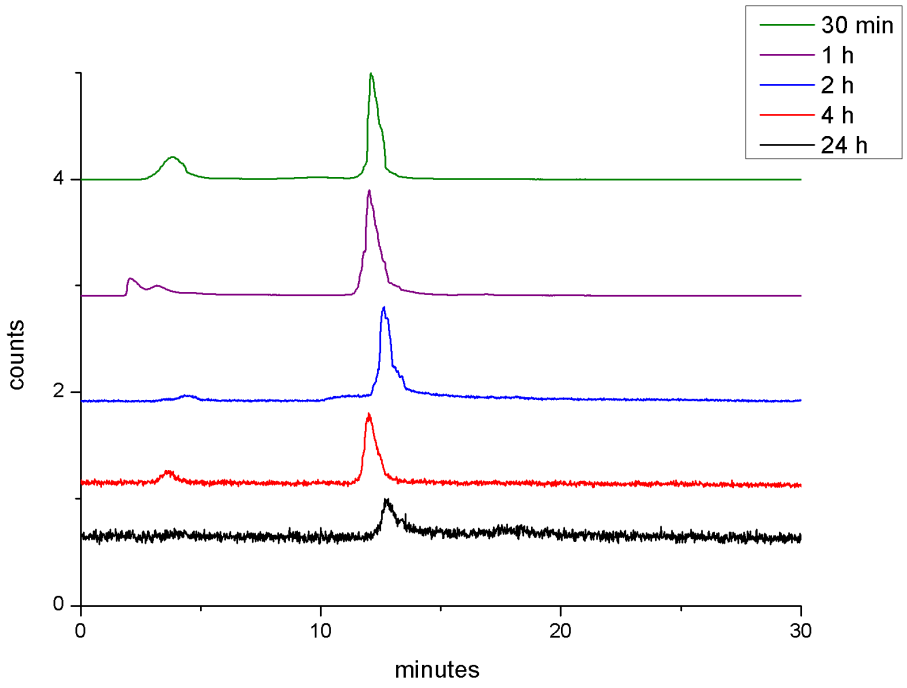

Figure 68. Radioactive HPLC traces of the ^{99m}Tc-porphyrin conjugate **24a** at t=30 min (green line), 1h (purple line), 2h (blue line), and 4h (red line), 24h (black line). Elution conditions: C-8 column, buffer 0,1 % TFA, Gradient A(standard TFA labelling gradient, See experimental section).

3.2.5. Conclusions

We synthesized and accurately characterized two water soluble porphyrins, bearing a tridentate and a bidentate chelator to evaluate the possibility of labeling with [^{99m}Tc/Re(I)$(CO)_3]^+$ fragment at the periphery of the cromophore.

By an accurate characterization of the conjugates bearing the $[Re(I)(CO)_3]^+$ fragment, we were able to demonstrate that the connection between the metal fragment and the porphyrin macrocyle occured at the periphery of the cromophore. All the conjugates were obtained with high purity level and reasonable to good yields. The total charge ranges from +1 to +3.

The same porphyrinic precursors were than labeled with $[^{99m}Tc(I)(CO)_3]^+$ fragments.

By comparison of the HPLC traces of the ^{99m}Tc conjugates (radiodetection) and the Re analogues (UV detection) we were able to confirm unambiguously the success of the labeling, the identity of such compounds and the purity of the ^{99m}Tc-conjugates.

Stability studies performed by HPLC on the ^{99m}Tc-conjugates revealed an high stability under air at room temperature, in absence or presence of cells up to 30 minutes to 24 hours.

3.3. Porphyrins and Re(I)-porphyrins as PDT agent

Since natural and synthetic porphyrins and metalloporphyrins are the most useful photosensitizers for PDT[163], we decided to evaluate the porphyrins **18** and **23** and the Re(I)-porphyrins **23** and **19** (Figure 52) as potential PS for PDT.

The uptake and in vitro cell growth inhibition of the Re(I)-porphyrins **19** and**24**and ofthe parent porphyrins **18** and **23** and was evaluated in HeLa cells.

Finally, the phototoxic effectsof the previously mentioned porphyrins on HeLa cells upon irradiation with red light (590-700 nm) have been studied.

3.3.1. Cell Uptake

The time- and concentration-dependent uptake of the water soluble porphyrins **18** and **23** and of the Re(I)-porphyrins **19** and **24** by HeLacells was investigated and the results are shown in Figure 69.

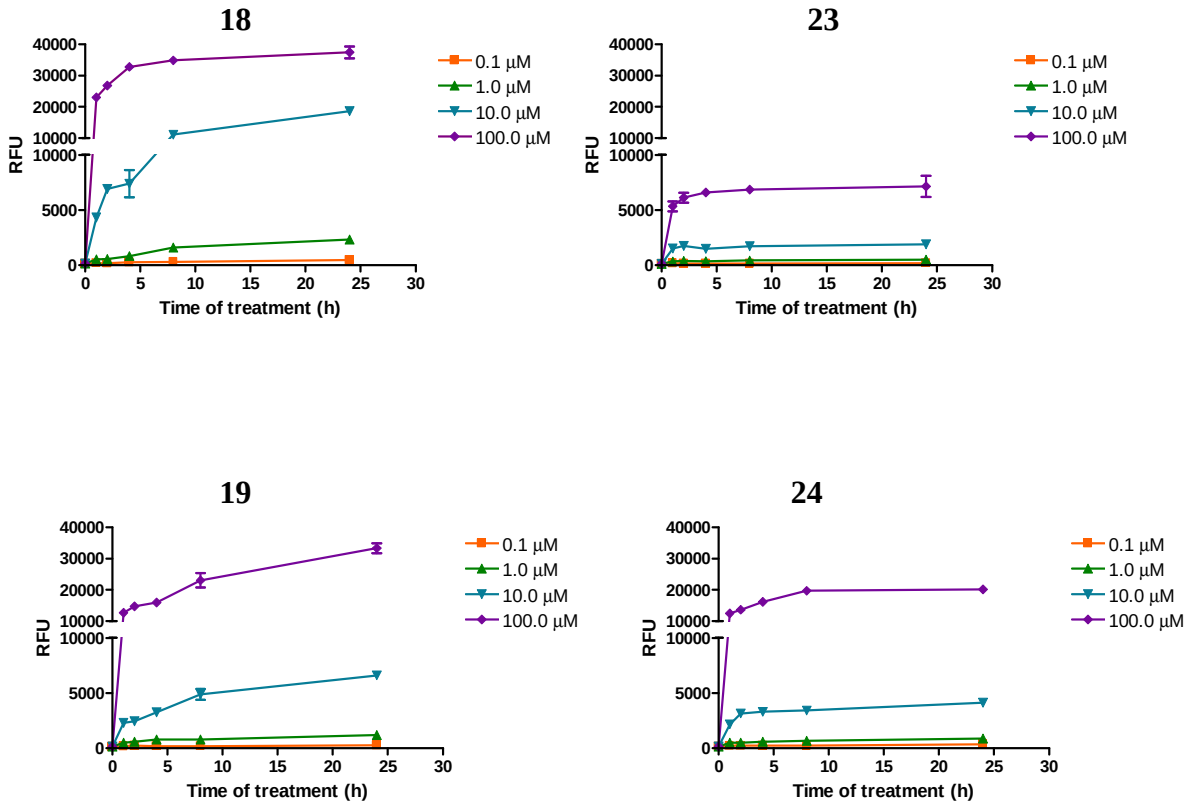

Figure 69. Time- and concentration-dependent uptake of the unlabeled porphyrins**18** and **23**, and of the Re(I)-porphyrins**19** and **24** at 0.1 µM up to 100 µM by HeLa cells. HeLa cells grown in multi-well plates were treated with compounds **18**, **23**, **19**, and **24** at 0.1 – 100 µM for 1, 2, 4, 8, or 24 h. At the end of the incubation the medium was removed, cells were washed with PBS and solubilized using 0.25% Triton X-100
Finally fluorescence emission was read at 430/670 nm (excitation/emission). Data reported in figure are the mean ± S.D. calculated from values obtained in three separate experiments.

The uptake is time- and concentration-dependent, low at 0.1 μM and 1.0 μM concentrations for all the tested compounds, also prolonging the cell exposure until 24 h. A different ability by the compounds to penetrate HeLa cells can be singled out for treatments carried out at 10.0 μM and 100.0 μM concentrations. The porphyrins **18** is readily and effectively taken up by cells, its fluorescence signal constantly increases over time at 10.0 μM, and at 100.0 μM the maximal uptake is reached already after 8 h of treatment. The porphyrins **23** shows a much lower ability to accumulate in treated cells, never reaching fluorescence levels comparable to those of **18**. At the highest concentration tested the rate of cell uptake is fast, and the maximal fluorescence is achieved after 2 h of exposure, after which it lasts practically unaltered. The uptake of Re-porphyrin **19** shows a trend similar to that of its unconjugate counterpart **18**, although its accumulation in treated cells is quantitatively slightly lower comparing the same treatment concentrations and time points. On the contrary, whether the metal fragment is bound to the unlabeled porphyrins **23** to obtain the Re-derivative **24**, the ability to enter HeLa cells is clearly increased, overall at the 100.0 μM concentration. Considering the kinetic of cell uptake, the comparison of the behavior of **19** and **24** indicates the first compound still actively taken up at 24 h, and the attainment of steady state levels after 4-8 h of treatment in the case of Re-porphyrin **4**.

3.3.2.Cytotoxicity

The organometallic porphyrin complexes were investigated in vitro as potential drug candidates for cancer therapy by evaluating the growth inhibition of human HeLa cells.
The experiments were carried out with the water-soluble compounds **19** and **24**, and with the parent water-soluble porphyrins **18** and **23**. The effects of these compounds on the cell growth were evaluated after treatment for 1 h, 2 h, 4 h and 24 h. Cell viability was determined of the MTT assay, which measures mitochondrial dehydrogenase activity. (Table 11)
Representative concentration–effect curves of all the porphyrins after 24 h of exposure are shown in Figure 70.
All tested compounds affect tumor cell growth only marginally and display IC_{50} values higher than 100 μM, the maximal concentration used in this experimental setting. Only in the case of porphyrins **18** it was possible to calculate an IC_{50} value of 74 uM. Considering, however, that such value could only be obtained using the highest concentration of compound (*i.e.*, 100 μM) for 24h, this is insufficient to define this compound as a cytotoxic agent.

Provided that Re(I) and Tc(I) form analogous conjugates with very similar physical and chemical properties that are expected to have the same pharmacokinetic behavior,[164] and considering that no cytotoxicity for the Re-conjugates was revealed at 0.01 μM even after 24h of exposure, the Tc(I) porphyrins conjugates are expected to display any toxicity.[133]

Table 11. IC_{50} values of compounds **18**, **23**,**19,** and**24** in HeLa cells treated for 1 h, 2h, 4h and 24h.

	IC_{50} [μM]			
	1h	**2h**	**4h**	**24h**
18	> 100	> 100	> 100	74.1 ± 33.6
23	> 100	> 100	> 100	> 100
19	> 100	> 100	> 100	> 100
24	> 100	> 100	> 100	> 100

HeLa cells grown in multi-well plates were treated with and with the water soluble porphyrins**18**and **23** and the Re-conjugates **19** and **24**. Cell cytotoxicity was detected by MTT test at at 0.1 – 100 μM for 1, 2, 4, 8, or 24 h. IC_{50} are the mean ± S.D. calculated from values obtained in three separate experiments.

(a) (b)

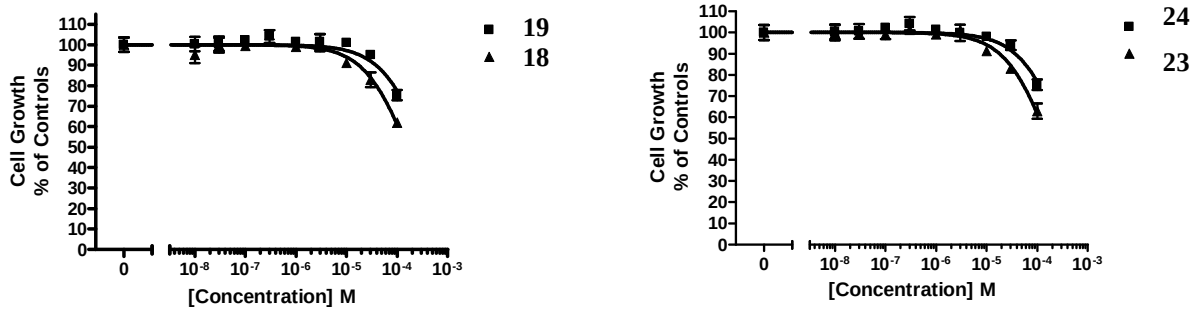

Figure 70. (a) and (b).Antiproliferative activity on HeLacells exposed for 24 h to the Re-porphyrins**19** and **24** and to the parent porphyrins**18** and **23**.

3.3.3. Phototoxicity

The porphyrins**18** and **23**, and the Re(I)-conjugates **19** and **24** have been studied to assess their cytotoxic activity against HeLa cells under irradiation with visible light (phototoxicity). To this end, cells were exposed for 24 h to compound concentrations ranging from 0.1 to 100 μM, followed by irradiation at 590-700 nm with a fluence rate of 9 mW/cm^2 and light doses from 1 to 10 J/cm^2. Cell cytotoxicity was determined using the MTT test 24 h post-irradiation. Exposure of control cells to identical light doses not induce inhibition of cell proliferation as

reported in Figure 71. Cells treated with the same concentrations of the test compounds, but kept in the dark, were used as controls for photocytotoxicity.

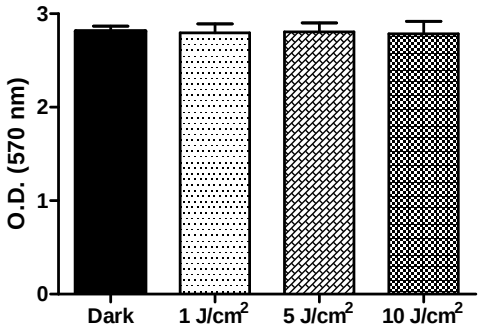

Figure 71. Effects of the exposure to light on the proliferation of untreated control cells. HeLa cells grown in multi-well plates were kept in the dark or irradiated with visible light (590 – 700 nm) at 9 mW/cm^{2}fluence rate and total light doses of 1 J/cm^2, 5 J/cm^2 or 10 J/cm^2. Cell cytotoxicity was detected by MTT test 24 h after irradiation. IC_{50} are the mean ± S.D. calculated from values obtained in four separate experiments.

All tested compounds show no cytotoxicity in HeLa cells kept in the dark, as indicated by the IC_{50} values reported in Table 12 These values are higher than 100 μM, except for the Re(I)-porphyrin conjugate **19** for which an IC_{50} value of 20 μM was calculated. All compounds become more cytotoxic after the exposure to light and the photocytotoxicity is directly proportional to the total light dose applied, as clearly showed by the dose-effect curves reported in Figure 72. The most potent compound is the unconjugated porphyrins **18** for which the IC_{50} value drops from > 100 in the dark to 2.0 μM at the lowest light dose used in our experimental setting, *i.e.* 1 J/cm^2.

The conjugation of Re(I) to porphyrins **18** slightly modifies the phototoxic features of the molecule, as confirmed by the fact the compound **19** shows IC_{50} values higher than **18**, although this difference tends to diminish with increasing light doses. On the contrary, the bonding of Re to porphyrins **23** improves the phototoxic properties of the compound in itself much less active in comparison to **18**.

Table 12. IC_{50} values of compounds **18**, **23**, **19**, and **24** in HeLa cells treated for 24 h and then exposed to increasing doses of visible light (590-700 nm).

	IC_{50} [μM]			
	dark	1 J/cm^2	5 J/cm^2	10 J/cm^2
18	> 100	2.0 ± 1.3	0.5 ± 0.1	0.2 ± 0.1
23	> 100	> 100	24.0 ± 6.5	5.8 ± 1.0
19	20.5 ± 7.2	10.9 ± 2.7	1.9 ± 1.1	0.9 ± 0.1
24	> 100	41.1 ± 13.0	4.0 ± 2.8	3.3 ± 2.3

HeLa cells grown in multi-well plates were treated with compounds **18**, **23**, **19**, and **24** at 0.1 – 100 μM for 24 h, then cells were irradiated with visible light (590 – 700 nm) at 9 mW/cm^{2}fluence rate and total light doses of either 1 J/cm^2, 5 J/cm^2 or 10 J/cm^2. Cell cytotoxicity was detected by MTT test 24 h after irradiation. IC_{50} are the mean ± S.D. calculated from values obtained in three or four separate experiments.

Comparing the results obtained in the phototoxicity experiments performed in the dark with those of the preliminary cytotoxicity determination (Table 12), compounds **18** and **19** seem to behave in an opposite way. The nonconjugate porphyrins **18** has an IC_{50} of 74 μM after a 24 h treatment (Table 11), and > 100 μM after a further 24 h wash out period, a value that is similar to that obtained in phototoxicity studies performed in the dark. It is likely that the 24 h of wash out after time that follows treatment allows cells recovering from the insult that was detectable at the end of the treatment.

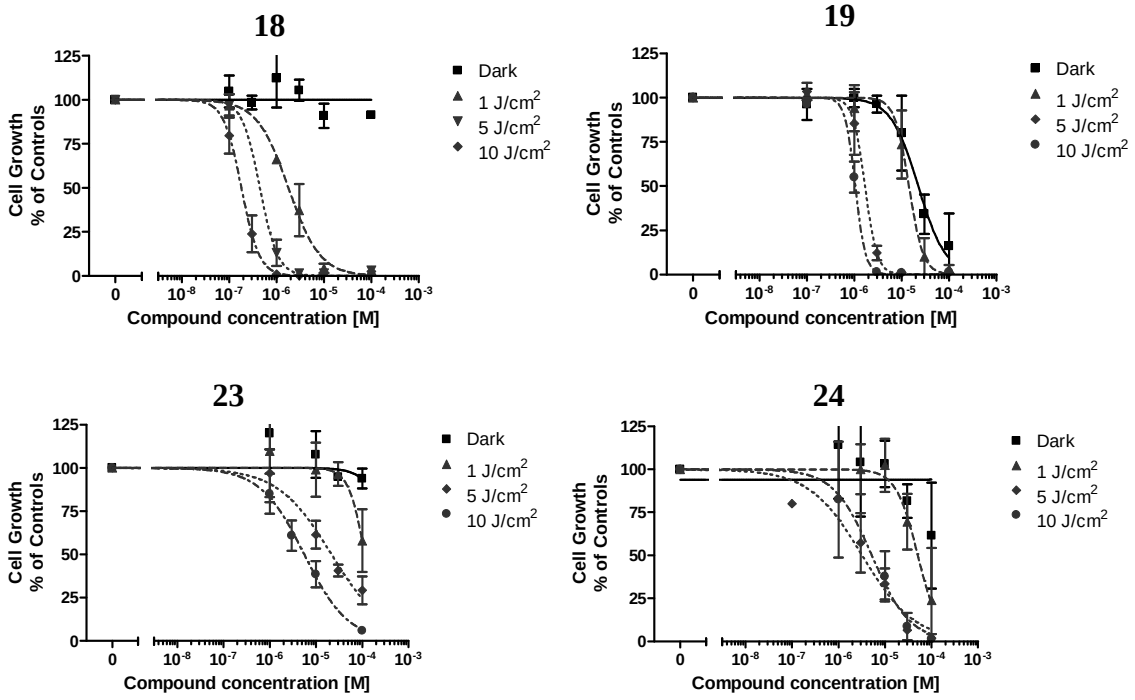

Figure 72. Light dose- and concentration-dependent effect curves of unconjugated porphyrins**18** and **23**, and of the Re(I)-conjugates **19**and **24**. HeLa human cervix cancer cells were exposed to compounds at 0.1 – 100 μM

concentrations for 24 h, then cells were irradiated at a fluence rate of 9 mW/cm^2 and total light doses ranging from 1 to 10 J/cm^2. Cell cytotoxicity was determined 24 h after the irradiation by MTT test.

An opposite consideration can be formulated for the Re(I)-porphyrin**19** for which no cytotoxicity could be detected immediately after the end of the 24 h treatment (Table 11), but which become cytotoxic after a further 24 h wash out period (Table 12). It is assumable that **19** induces cell damage that needs some time to be detected.

Compounds uptake after 24h exposure is significantly different, as reported in Figure 69, but it does not affect appreciably their cytotoxicity. On the contrary, the phototoxicity is directly related to the ability of the compounds to penetrate cells. In fact, the unconjugated porphyrins **18** and **23**, for which the greatest and the lowest uptake was measured, are respectively the most and the least phototoxic compounds. The influence of the different uptake of the compounds on the phototoxicity fades by increasing the light doses.

Trying to draw some structure-activity relationships it seems reasonable state that:

1. cytotoxicity is not affected by whatever change made on the porphyrin core (presence of diethylenetriamine or bipyridylbidentatechelator, conjugation with the Re(I)).
2. The presence of bipyridylbidentate chelator in comparison to the diethylenetriamine, as ligand on the porphyrin core or the presence of the positive charge on the pyridil ring of the porphyrin lowers the cell uptake and, consequently the phototoxicity of the compound.
3. The addition of Re on porphyrins **18** marginally affects the compound uptake and consequently weakly modify its phototoxocity.
4. On the contrary the addition of Re on porphyrins **23** improves the HeLa cell penetration giving a compound with more advantageous phototoxic features.

3.3.4. Singlet oxygen quantum yield(Φ_Δ)

Since the most common mechanism of action of the photosensitizers used in PDT (Type II mechanism) involves the production of singlet oxygen upon photoexcitation, the $^1O_2$ quantum yield (Φ_Δ) was measured for of the unconjugated porphyrins **18** and **23** and of the Re(I)-porphyrins **19** and **24** using the red light (600-700 nm) following the procedure reported before.

Here the spectophotofluorimetric data obtained using **23** as a substrate are reported.

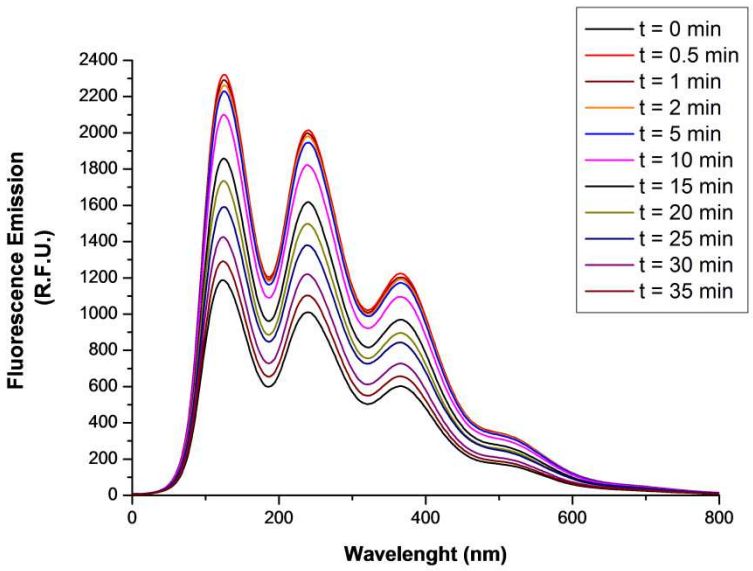

Figure 73. Photobleaching of an ethanol solution of DMA by **23** upon irradiation with a Teclas lamp (590–700 nm) at 100 mW/cm^2.

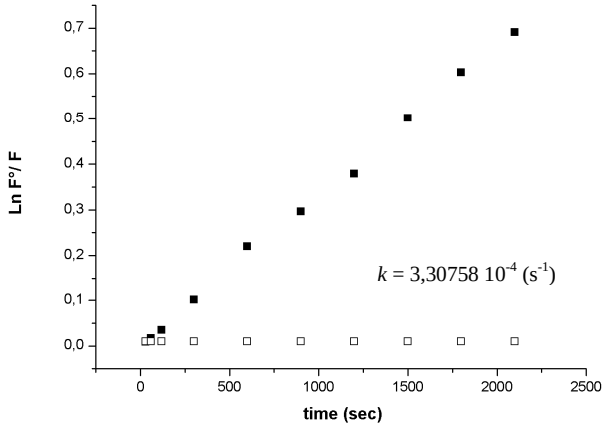

Figure 74. Photo-oxidation of 10 µM DMA in ethanol solution sensitized by **23** (■)DMA is stable in the absence of **23** (□). *k* is the first-order rate *vs* constant for the photoprocess as deduced from the slope of the semilog plot.

Compound	Φ_Δ
18	0.33
23	0.66
19	0.36
24	0.62

Table 13. Singlet oxygen quantum yield (Φ_Δ)for the photosensitizers **18**, **19**, **23** and **24**.

The investigated Re-porphyrin conjugates showed moderate (Φ_Δ = 0.36 for **19**) to good (Φ_Δ = 0.62 for **24**) singlet oxygen quantum yields. Interestingly these Φ_Δ values are not significantly different from those of the corresponding parent porphyrins (Φ_Δ = 0.33 and Φ_Δ = 0.66 for the precursors of **18** and **23** respectively) (Table 13). Those data suggest that the peripheral Re moieties do not affect by the Φ_Δ significantly.

However the phototoxicity of the investigated porphyrins does not seem to be directly related to this parameter. In fact, **18** shows the higher potency in the phototoxic assay at low light doses, despite **18** has a lower singlet oxygen quantum yield.

On the contrary, **23** displays the opposite behavior, in fact it shows the higher value of singlet oxygen quantum yield and at the same time the lower potency in the phototoxic assay at low light doses.

It is worth noting that Φ_Δ values are determined in ethanol solution and that most likely other parameters (e.g., hydrophobicity, cell uptake, ...) play a more significant role in determining the phototoxic activity of these conjugates under in vitro conditions.

3.3.5. Photostability of Compounds

The photostability of the various porphyrin derivatives is shown in Table 14. In all cases, exposure of the porphyrins to red light caused a modest decrease in the intensity of the visible absorption bands, which is indicative of a photobleaching process.[165] The data in Table 14 clearly suggest that all compounds have a high photostability under the conditions used for the PDT tests. Furthermore the absorbance decrease involved all the envelope of visible bands of the compounds indicating that the photoprocess induces a destruction of the aromatic macrocycle with no formation of new visible light-absorbing products.

The reduced extent of photodegradation exhibited by compounds **18**, **23**, and **19** and **24** would guarantee that the concentration of the photoactive principle undergoes no important changes during the required irradiation time in case of phototherapeutic applications.

	irradiation time (min)							
Cmp	0	1	2	5	10	15	20	30
18	100	100	100	99	99	99	99	98
23	100	100	100	100	99	99	99	99
19	100	100	99	99	98	98	97	93
24	100	100	100	98	97	97	97	96

Table 14. Photostability percentage of the photosensitizers after irradiation with red light (590-700 nm) for different period of time.

3.3.6. Conclusions

The water soluble porphyrins **18**, **19**, **23** and **24** previously synthesized were investigated as potential PDT agents.

Uptake studies time- and concentration-dependent on HeLa cells revealed that for Re(I)-porphyrin **19** and for its parent compound **18** the uptake at 10μM -100 μM is comparable after 24h. Interestingly, the uptake of Re(I)-porphyrin (**24**) is 4 times higher compared to its parent porphyrin **23,** suggesting a different mechanism of biological interaction under in vitro conditions.

In vitro cell growth inhibition toward HeLa cells revealed no cytotoxicity. In fact they showed IC_{50} values higher than 100 μM, the maximal concentration used in this experimental setting after 24 h of exposure.

Then the phototoxic effects on HeLa cells was evaluated upon illumination. Conjugates **18**, **19**, **23** and **24** became ca. 10 times more cytotoxic after irradiation with visible light (590-700 nm) at mild light doses (5 J/cm^2) and proved to have from moderate to good singlet oxygen quantum yields. The most potent compounds **18** and **19** were active at micromolar concentration and very low light dose (1 J/cm^2), Taken together, those results suggest that those porphyrins are promising sensitizers for the PDT of tumors.

3.4. Expermental Section

All chemicals and solvents were of reagent grade and were used without purification unless stated otherwise.

The organometallic precursor $[Re(CO)_3(Br)_2][Et_4N]_2$was prepared according to a published method. [166] The radioactive synthon $[^{99m}Tc(CO)_3(H_2O)_3]^+$ was prepared as described elsewhere [133] or using the Mallinckrodt IsoLink kit. $Na^{99m}TcO_4$ in saline solution was eluted from a $^{99}Mo/^{99m}Tc$ generator Ultra-Techne Kow from Mallinckrodt in 0.9% saline solution.

4-Methyl-2,2'-bipyridine-4'-carboxylic acid (bpyAc),[155] 4-formyl benzoate [141] and N-Boc-ethylenediamine [167] were prepared according to the published procedures.

Mono and bidimensional NMR spectra were recorded on a Varian 500 spectrometer or on a Bruker 400 and 500 spectrometers at 400/500 respectively. All spectra were run at ambient temperature. In all the solvents chemical shifts were referenced to the peak of residual nondeuterated solvent (δ =7.26 for $CDCl_3$, 3.31 for CD_3OD, 2.50 fordmso-d_6). UV-vis spectra were obtained at T = 25°C on aJasco V-500 UV-vis spectrophotometer equipped with a Peltiertemperature controller, using 1.0 cm path-length quartz cuvettes (3.0 mL). Electrospray ionisation mass spectra (ESI-MS) were recorded on a Merck Hitachi M-8000 spectrometer in the positive ion mode using methanol as the solvent. Fluorescence spectra were recorded on a Perkin-Elmer LS50B fluorescence spectrometer.

Column chromatography was performed on silica gel 60 Å (Merck, 230-400 mesh ASTM), eluting with dichloromethane/methanol mixtures as specified below.

RP-HPLC analyses were performed on a Perkin-Elmer system (LCPump, Series 200) coupled to a UV–visdetector (LC 290; Perkin-Elmer) and a γ detector (LB 507 or LB 509; Berthold, Germany) for the ^{99m}Tc compounds. Analytical separations were performed on Macherey-Nagel EC 250/3 Nucleodur C18 Gravity (7 μm particle size, 100 Å pore size, 40 × 250 mm) or Waters XTerra RP8 columns (5 μm particle size, 1 × 100 mm) with a flow rate of 0.5 $mLmin^{-1}$.

The gradients used for analyses were as follows:

Gradient A (MeOH): 0-3 min 85% A, 3.1-13 min 85-0% A, 13-20 min 0% A, 20-25 min 0-85% A 25-30 min 85% A, flow rate 0.5 $mLmin^{-1}$; Gradient B (MeOH): 0–3 min, 100% A; 3–3.1 min, 100-75% A; 3.1–9 min, 75% A;9.1-20 min, 75-0% A, 20–25 min, 0%A; 25–25.1 min 0-100% A; 25.1–30 min 100% A, flow rate 0.5 $mLmin^{-1}$. Gradient C (MeCN): 0-3 min 85% A, 3.1-13 min 85-0% A, 13-20 min 0% A, 20-25 min 0-85% A 25-30 min 85% A, flow rate 0.5 $mLmin^{-1}$.

HPLC solvents were 0.1% trifluoroacetic acid (solvent A) and MeOH HPLCgrade (solvent B).

Preparative HPLC was performed on a Varian ProStar system by using a Macherey-Nagel VP 250/40Nucleosil RP C18 HD 100 Å column and a flow rate of 40 $mLmin^{-1}$. The solvents were 0.1% trifluoroaceticacid (solvent A) and methanol or acetonitrile (solvent B).

Synthesis of Compounds.

***meso*-5-(4'-Methoxyphenyl)-10,15,20-tris(4'-pyridyl)porphyrins** or**4'TrPyMeP (14)**

In a 250 ml round-bottom flask, equipped with an efficient mechanical stirrer, were placed consecutively: propionic acid (120 mL), methyl 4-formylbenzoate (1.13 g, 6.88 mmol, 1 equiv.) and 4-pyridinecarboxaldehyde (2.03 mL, 20.65 mmol, 3equiv.). After the dissolution of the methyl 4-formylbenzoate, pyrrole (1.94 mL, 27.53mmol, 4 equiv.) was added dropwise (ca. 4 min) to the mixture. The reaction mixture was then refluxed for 2 h in the dark. The solvent was partially distilled under reduced pressure to 40 ml. After the addition of a mixture of ethylene glycol and methanol (60 mL, 1:1), it was stored at -18°C for 12 h.The purple precipitate was removed by filtration, thoroughly washed with coldmethanol, and dried *in vacuo* at room temperature.Yield 0.91g (18%).

Thin-layer chromatography of the crude product (dichloromethane/methanol 98:2) showed it to be a mixture of the six possible porphyrin isomers: 4'-TMeP (R_f = 0.95),4'-MPyTrMeP(R_f= 0.77), 4'-*trans*DPyDMeP (R_f = 0.55), 4'-*cis*DPyDMeP (R_f = 0.43), 4'-TrPyMMeP (R_f = 0.33) and 4'-TPyP (R_f = 0.13).[115]

The isomers were separated using two columns chromatography *in series*.(, dichloromethane/methanol 98:2). The fifth eluted band was identifiedby TLC as 5,10,15,20-tetrakis(4'-pyridyl)porphyrin (194 mg, 8%).

The identifications of the porphyrin was confirmed by comparing its R_f value with those of the crude mixture and by ^{1}H NMR spectroscopy.

^{1}HNMR ($CDCl_3$, δ): -2.89 (br s, 2H, NH), 4.12 (s, 3H, CH_3), 8.17 (d, 6H, *J* = 5.6 Hz, H3,5Py), 8.32 (d, 2H,*o*Ph, J=8.1 Hz), 8.45 (d, 2H,*m*Ph, J=8.1Hz), 8.86 (s, 8H, *β*H), 9.05 (d, 6H, *J* = 5.6 Hz, H2,6Py).

5-(4'-Carboxyphenyl)-10,15,20-tris(4'-pyridyl)porphyrin(4'TrPyMOHP) (15)

A 2.4 mLamount of a 40% KOH aqueous solution was added to a40 mg amount of **14** (0.051mmol) dissolved in 40mL of a 2:1 THF/CH_3OH mixture. The reaction mixture was shielded from light andstirred at 40 °C for 1 h.At reaction completion (TLC, CH_2Cl_2/MeOH 90:10), the mixture was acidified with conc. HCl (pH 5), and extracted with THF/$CH_2Cl_2$1:1 (4 ×50 mL). After the evaporation of the organic fraction, the solid was washed with petroleum ether, collected by filtration and vacuum dried. Yield: 38.4 mg, 98%.

^{1}HNMR(dmso-d_6,δ): -3.00 (s, 2H, NH), 8.27 (d, 6H, *J* = 5.6 Hz, H3,5Py), 8.37(m,4H,*m*Ph + *o*Ph), 8.90 (d, *J* = 2.4 Hz, 8H, βH), 9.05 (d, 6H, *J* = 5.6 Hz, H2,6Py).
RP-HPLC Waters XTerra RP8 (Gradient A): 13.59 min;ESI-MS *m/z*: 661.5 $(MH)^+$.TLC: R_f=0.28 (CH_2Cl_2/MeOH 90:10).

(2-Aminoethyl)-(2-(tert-butoxycarbonyl-(2-tert-butoxycarbonylaminoethyl)amino)ethyl)carbamic acid tert-butyl ester (16)

A procedure similar to that described in literature [168]was used with the following parameters: 2-acetyl-5,5-dimethyl-cyclohexane-1,3-dione (Dde) (300mg,1.65 mmol) in EtOH (5 mL) was slowly added to an ice-cooled solution of *N*,*N*'-bis-(2-aminoethyl)-ethane-1,2-diamine (482mg,491 μL, 3.29 mmol) dissolved in EtOH (5 mL). The reaction mixture was stirred overnight at rt.
At reaction completion (TLC, CH_2Cl_2/MeOH 80:20), the solvent was distilled under reduced pressure and the resulting oil was stored at -18°C for 12 h.
The crude product (2.06 g) was dissolved in EtOH (10 mL) and cooled to 0°C. Di-*tert*-butyl-pyrocarbonate($(BOC)_2O$, 3.55 g) in EtOH (10 mL) was then slowly addedto the reaction mixture, which was subsequently stirred overnight at rt. Excess of $(BOC)_2O$ was quenched with H_2O (1 mL) and the mixture was stirred at 50°C for 30 min. A 25% aqueous hydrazine solution (3.8 mL) was then added to the reaction mixture and stirring was continued for 4 hat rt.
The solvent was removed *in vacuo*. The resulting oil was purified by column chromatography using two columns chromatography *in series* (dichloromethane/methanol/NH_4OH 100:10:1) to yield a colorless oil (118mg, yield: 16% based on the amountof Dde).

^{1}H NMR ($CDCl_3$, δ): 1.42 (s, 9H, Boc); 1.46 (s, 18H, Boc), 2.23 (br s, 2H, NH_2), 2.83 (t, 2H, CH_2NH_2), 3.32 (br, 10H, CH_2), 4.88 (br s, 1H, NHCO), 5.05 (br s, 2H, NHCO).
RP-HPLC Waters XTerra RP8 (Gradient A): 11.41 min.TLC: R_f=0.19 (CH_2Cl_2/MeOH/25% NH_4OH, 100:10:1).

(17)

A 17.4 mg amount of EDCI (0.090mmol, 1.5 equiv.) and a 12.3 mg amount of HOBt (0.090mmol, 1.5 equiv.) were added to a solution under nitrogen of TrPyMOHP **15** (40mg, 0.060mmol) dissolved in 4 mLof anhydrous DMF. To this solution, after stirring for 45 min, a 40.2 mg amount of **16** (0.090mmol) and a 8.0mg amount of dimethylaminopyridine (DMAP) (0.066mmol, 1.1 equiv.) dissolved in 2 mL of anhydrous DMF were added. The reaction mixture was shielded from light and stirred at rt for 24 h. At reaction completion (TLC, CH_2Cl_2/MeOH 90:10), the solvent was distilled under reduced pressure. The resulting dark semisolid was dissolved in 3 mL of CH_2Cl_2 and purified by column chromatography using CH_2Cl_2/MeOH (90:10) as eluent. The workup afforded 62.55 mg of the product as a purple solid (yield95%).

^{1}H NMR ($CDCl_3$, δ): -2.89 (br s, 2H, NH), 1.47 (m, 27H, CH_3 Boc), 3.56 (m, 12H,CH_2), 4.78 (br s, 1H, NHCO), 4.98 (br s, 1H, NHCO), 5.51 (br s, 1H, NHCO), 8.16 (d, 6H, *J* = 5.1 Hz, H3,5Py), 8.25(s,4H, *m*Ph + *o*Ph), 8.86 (s,8H, βH), 9.06 (d, 6H, *J* = 5.1 Hz, H2,6Py).
RP-HPLC WatersXTerra RP8 (Gradient A): 12.62 min. ESI-MS *m/z*: 1090.6 $(MH)^+$.TLC: R_f=0.56 (CH_2Cl_2/MeOH 90:10).

(18)

A 300 μL amount of trifluoroaceticacid (TFA) was added to a solution of **17** (63.45 mg, 0.058mmol) dissolved in 5 mL of anhydrous CH_2Cl_2. The mixture was stirred at room temperature for 3h in the dark. At reaction completion (TLC, CH_2Cl_2/MeOH 90:10), the solvent was completely removed on a rotary evaporator to give a purple solid of the title porphyrin as trifluoroacetic salt. The product was used in the following step without further purifications.

^{1}H NMR (trifluoroacetic salt) (CD_3OD, δ):3.09 – 3.49 (m, 10H,CH_2), 3.93 (m, 2H, CH_2NH_2), 8.41 (s, 4H, *m*Ph + *o*Ph), 8.66 (m, 6H, H 3,5Py), 9.05 (b s, 8H, βH), 9.26 (m, 6H, H 2,6Py).
RP-HPLC Waters XTerra RP8 (Gradient A): 9.72 min.
ESI-MS m/z: 789.4 $(M)^+$, 812.5 $(M + Na^+)$.
TLC: R_f=0.65 (CH_2Cl_2/MeOH 90:10).UV-vis (CH_3OH) λ_{max}, nm (relative intensity): 412 (100), 510(4.8), 543 (1.6), 587 (1.5), 642 (0.6).

(19)

A 20 mg amount of **18** (0.020mmol) was dissolved in a mixture of CH_3OH (6 mL) and PBS (2 mL).To this solution a 18.2mg amount of $[NEt_4]_2[ReBr_3(CO)_3]$ (0.023mmol) dissolved in 6 mL of PBS (pH = 7.4).was added. After stirring at 70°C under nitrogen for 12h in the dark, RP-HPLC(Waters XTerra RP8, gradient A) showed the formation of the product.
The solvent was evaporated under vacuum and the residue was redissolved in 8 mL of methanol.
The crude material was purified by preparative HPLC (Nucleosil RP C18 HD 100 Å, gradient C) to afford 9 mg (61%) of compound **19** as a purple solid.

^{1}H NMR (CD_3OD, δ): 3.42 – 3.67 (m, 8H, CH_2), 3.83 – 3.90 (m, 2H, CH_2), 4.04 – 4.12 (m, 2H, CH_2), 5.60 (m, 1H, CONH), 8.31 (dd, 6H, *J* = 5.0 Hz, H 3,5Py), 8.39 (d, 2H, *J* = 7.8 Hz, *o*Ph), 8.32 (d, 2H, *J* = 7.8 Hz, *m*Ph), 8.81 (br s, 8H, βH), 9.02 (dd, 6H, *J* = 5.0 Hz, H 2,6Py).
RP-HPLC Waters XTerra RP8 (Gradient A): 11.70 min.
ESI-MS m/z: 1060.4 $(M)^+$, 1099.4 $(M + K^+)$.
UV-vis (CH_3OH) λ_{max}, nm (relative intensity): 413 (96), 511 (4.8), 543 (1.6), 588 (1.4), 642 (0.7).

(20)

A procedure similar to that described above was used, with the following parameters: 30 mg of TrPyMOHP (**15**) (0.045mmol) in 3 mL of anhydrous DMF, 13.04 mg of EDCI (0.068 mmol, 1.5 equiv.), and 9.19 mg of HOBt (0.068mmol, 1.5 equiv.). To this solution, a 16.9 mg amount of N-Boc-ethylenediamine (0.068mmol, 1.5 equiv.) and a 6.1 mg amount of dimethylaminopyridine (DMAP) (0.049 mmol, 1.1 equiv.) were added and the reaction mixture shielded from light and stirred for 12 h at rt.

The resulting solid was washed with water, dissolved in 3 mL of CH_2Cl_2 and purified by column chromatography using CH_2Cl_2/MeOH (90:10) as eluent. The workup afforded 35 mg of the product as a purple solid (yield 89%).

^{1}H NMR ($CDCl_3$, δ): -2.90 (br s, 2H, NH), 1.40 (s, 9H, CH_3Boc), 3.35 (m, 2H, CH_2 *spacer*), 3.63 (t, 2H,CH_2 *spacer*), 3.74 (m, 4H, CH_2 *spacer*), 3.85 (m, 4H, CH_2 *spacer*), 5.04(br s, 1H, NHBoc), 7.06 (br s, 1H, NHBoc), 8.16 (d, 6H, *J* = 5.6 Hz, H 3,5Py), 8.27 (dd, 4H, *m*Ph + *o*Ph), 8.86 (br s, 8H, βH), 9.06 (d, 6H, *J* = 5.6 Hz, H 2,6Py). TLC: R_f=0.75 (CH_2Cl_2/MeOH 90:10).

(21)

A 22 mg amount of 4'TrPyMetNHBocPP (**20**) (0.024mmol) was dissolved in DMF (3 mL). Subsequently CH_3I (77µL, 1.23mmol, 50 equiv.) was added to the solution and the mixture was heated under reflux for 2 h.[169]
At reaction completion (TLC: silica gel, acetic acid/MeOH/water 50:20:1), the solvent was completely removed on a rotary evaporator. The resulting solid was washed with diethyl ether, collected by filtration and vacuum dried. Yield: 30.3 mg, 97%.

^{1}H NMR(dmso-d_6, δ): -3.03 (br s, 2H, NH), 1.37 (s, 9H, CH_3Boc), 3.04 (m, 1H, CH_2 *spacer*), 3.10 (m, 2H, CH_2 *spacer*), 3.44 (t, 2H, $NHCH_2$ *spacer*), 3.59 – 3.69(m, 8H, CH_2 *spacer*), 4.71 (s, 9H, N-CH_3),6.80 (t, 1H, NHBoc), 8.35(m, 4H, *m*Ph + *o*Ph), 8.93 (t, 1H, NHBoc),9.02(m, 8H, H 3,5Py+2βH), 9,06(br s, 4H, βH), 9.15 (m, 2H, βH),9.47 (d, 6H, *J* = 5.6 Hz, H 2,6Py).
RP-HPLC Waters XTerra RP8 (Gradient A): 10.07 min. TLC R_f=0.26 (acetic acid/MeOH/water 50:20).

(22)

A 150µL amount of trifluoroacetic acid (TFA) was added to a solution of **21** (40mg, 0.031mmol) dissolved in 5 mL of anhydrous CH_2Cl_2.
After stirring at room temperature for 3 h in the dark, RP-HPLC (Waters XTerra RP8, gradient A) showed the formation of the product.
The solvent was completely removed on a rotary evaporator to give a purple solid of the title porphyrins as trifluoroacetic salt.Yield: 34.8 mg, 87%.

^{1}H NMR (acetone-d_6, δ): -2.87 (br s, 2H, NH), 3.72 (m, 2H, CH_2*spacer*), 3.73 – 3.78 (m, 2H, CH_2 *spacer*), 3.80 (m, 4H,CH_2 *spacer*), 3.94 (m, 2H, CH_2 *spacer*), 4.00 (m, 2H, CH_2 *spacer*), 5.01 (s, 9H, N-CH_3), 8.33 (d, 2H, *m*Ph + *o*Ph), 8.43 (d, 2H, *m*Ph + *o*Ph), 9.07 (m, 2H, βH), 9.15 (d, 6H, *J* = 5.3 Hz, H 3,5Py), 9.28 (m, 6H, βH), 9.67 (d, 6H, *J* = 5.6 Hz, H 2,6Py).

^{1}H NMR (CD_3OD, δ): 3.69 - 3.88 (m, 8H, CH_2 *spacer*), 3.93 (m, 2H, CH_2 *spacer*), 4.02 (m, 2H,CH_2 *spacer*), 4.98 (s , 9H, NCH_3), 8.33 (d, 2H, *m*Ph + *o*Ph), 8.41 (d, 2H, *m*Ph + *o*Ph), 9.12 (d, 6H, *J* = 5.3 Hz, H 3,5Py), 8.83 - 9.47 (m, 8H, βH), 9.63 (d, 6H, *J* = 5.6 Hz, H 2,6Py).
RP-HPLC Waters XTerra RP8 (Gradient A): 13.70 min. TLC R_f=0.16 (acetic acid/MeOH/water 50:20).

(23)

A 4.71 mg amount of bpyAc (0.022mmol, 2 equiv.) a 4.19 mg amount of CDMT (0.024mmol, 2.2 equiv.) were dissolved in DMF (3 mL). After dissolution, the mixture was cooled at 0°C and *N*-methylmorpholine (2.61 µl, 0.024mmol, 2.2 equiv.) was added.
After stirring for 4 h at 0°C, a solution of **22** (14 mg, 0.011mmol) and *N*-methylmorpholine (2.65 µl, 0.024mmol, 2.2 equiv.) in 1 mL of anhydrous DMF was added. The reaction mixture was stirred for 24 h at rt in the dark. At reaction completion (TLC, acetic acid/MeOH/water 50:20:1) DMF was removed under reduced pressure. The residue was washed with diethyl ether, placed into a thimble of a Soxhlet apparatus and continuously extracted with 300 ml of anidrous CH_2Cl_2 for 12h. The residue on the thimble was dissolved in 5 ml of isopropanol and vacuum dried to obtain the title compound. Yield: 12.83 mg (85%).

^{1}H NMR (CD_3OD, δ): 1.52(s, 3H, CH_3), 3.66 (m, 2H, CH_2 *spacer*), 3.79 – 3.82 (m, 10H, CH_2 *spacer*), 6.22 (d, *J* = 4.8,1H, H5' bpy), 7.33 (s, 1H, H3' bpy), 7.62 (d, *J* = 4.8,1H, H6' bpy), 7.67 (dd, 1H, *J* =1.50, 4.96 Hz, H5), 8.24 (m, 4H, *m*Ph + *o*Ph), 8.33(t, 1H, NHCO bpy), 8.39 (s, 4H, H3, bpy), 8.62 (d, 4H, *J* = 4.96 Hz, H6), 8.98 (d, 6H, *J* = 5.3 Hz, H 3,5Py), 8.89 - 9.28 (m, 8H, βH + NHCO), 9.39 (d, 6H, *J* = 5.6 Hz, H 2,6Py).
RP-HPLC Waters XTerra RP8 (Gradient A): 9.95 min; ESI-MS m/z: 1032.5 $(M)^+$, *m/z*: (*z*=2): 516.5.
UV-vis (CH_3OH) λ_{max}, nm ($\varepsilon\times 10^{-3}$, dm^3 $mol^{-1}cm^{-1}$): 426 (124), 518 (7.2), 555 (3.7), 591 (2.8), 647 (1.0).

(24)

A 10 mg amount of **23** (0.007mmol) was dissolved in a mixture of CH_3OH (6 mL) and PBS (2 mL).

To this solution a 7.86 mg amount of $[NEt_4]_2[ReBr_3(CO)_3]$ (0.010mmol, 1.) dissolved in 6 mL of PBS (pH = 7.4) was added. After stirring at 70°C under N_2 for 12h in the dark, RP-HPLC (Waters XTerra RP8, gradient A) showed the complete product formation. KSCN (0.011 mmol, 1.14 mg) dissolved in little H_2O, was added and the solution heated to 70 °C for 2 h to ensure complete formation of the product.

The solvent was evaporated under vacuum and the residue was redissolved in 8 mL of methanol.

The crude material was purified by preparative HPLC (Nucleosil RP C18 HD 100 Å, gradient C) to afford 8 mg (65%) of compound **24** as a purple solid.

There are two linkage isomers with a SCN- ligand, *i.e.*, thiocyanato conjugate Re-*S*-SCN which converts to the thermodynamically favored N-bound isothiocyanato conjugate Re-*N*-NCS. The spectral and analytical data of **24** prepared in the present study were consistent with those previously reported. [170]

RP-HPLC Waters XTerra RP8 (Gradient A): 10.27 min

ESI-MS *m/z*: 1359.5 $(M)^+$, *m/z*: (*z*=2): 680.3calcd for $[M]^+$ Isotopic distribution: 1361,38 (100,0%), 1362,39 (73,6%), 1359,38 (56,4%), 1360,38 (44,0%).

^{1}H NMR (t = 0, CD_3OD, δ): 2.32 (s, 3H, CH_3), 3.57 – 3.86 (m, 12H, CH_2 *spacer*),4.82 (9H, N-CH_3), 7.28 (d, *J* = 6.06, 1H, H5' bpy), 7.94 (dd, 1H, *J* =1.50, 4.96 Hz, H5), 8.30 (m, 5H, *m*Ph + *o*Ph + H3' bpy), 8.42 (d, *J* = 6.06, 1H, H6' bpy), 8.70 (d, 1H, J = 4.96 Hz, H6), 8.96 (m, 7H, *J* = 5.3 Hz, H 3,5Py +H3, bpy), 8.89 - 9.28 (m, 8H, βH), 9.39 (d, 6H, *J* = 5.6 Hz, H 2,6Py).

UV-vis (CH_3OH) λ_{max}, nm (relative intensity): 427 (100), 518 (11.7), 555 (6.9), 591 (4.6), 647 (2.0).

Labelling with ^{99m}Tc

Na[$^{99m}TcO_4$] was eluted from a ^{99}Mo/^{99m}Tc generator(Mallinckrodt, Petten, The Netherlands) using 0.9% saline.

The solution of the precursor $[^{99m}Tc(H_2O)_3(CO)_3]^+$was prepared from $[^{99m}TcO_4]^-$ (1 ml eluate) using aborocarbonate kit containing $K_2CO_2BH_3$ (4 mg, 0.029mmol), disodium tartrate dihydrate (7 mg, 0.030 mmol) and borax decahydrate (7 mg, 0.018 mmol) or with an Isolink kit®(Mallinckrodt-Tyco, Inc.), according to a previously described procedure.[132] (Solutions of the precursor $[^{99m}Tc(H_2O)_3(CO)_3]^+$were prepared from $[^{99m}TcO4]^-$ as described in the literature or by using the Isolink® kit)

After stirring for 20 min at 95°C, the mixture was cooled down, neutralised with 0.1 M HCl and the pH was adjusted to 7.4 byadding 0.1 M phosphate buffer (100–200ml).

Complete formation of $[^{99m}Tc(H_2O)_3(CO)_3]^+$ was confirmed by HPLC analysis using RP-HPLC HPLC coupled with gamma detector after cooling to r.t. (Macherey-Nagel EC 250/3 Nucleodur C18 Gravity, Gradient B). Rt for $[^{99m}Tc(H_2O)_3(CO)_3]^+$ = 5.25 min

In a nitrogen-purged glass vial, 100 µl of a PBS solution of the porphyrin (10^{-4} M for **18** and 10^{-5} for **23**), was added to 900 µl of the solution of fac-$[^{99m}Tc(CO)_3(H_2O)_3]^+$ previously prepared. The mixture was allowed to heat in the dark at 50°C for 30 min.

HPLC analysis with γ-detection was performed to verify full conversion of the $[^{99m}Tc(H_2O)_3(CO)_3]^+$(Waters XTerra RP8 , Gradient A). Rt for $[^{99m}Tc(H_2O)_3(CO)_3]^+$ = 3.53 min, R_t for **19a** = 11.12 min; R_t for **24a** = 10.46 min.

Determination of the quantum yield for singlet oxygen generation

The quantum yield (Φ_Δ) of singlet oxygen generated by compounds **18**, **19** and **23** and **24** upon photoexcitation was measured using 9,10-dimethylanthracene (DMA) as substrate.[120]

Typically, 1.5 ml of a 20 µM ethanol solution of DMA and 1.5 ml solution of the porphyrin (0.4 A at Soret band maximum, ≈ 10^{-6} M) in ethanol were placed in a quartz cuvette of 1 cm optical path and irradiated with 590–700 nm light for different periods of time at 20 ± 2 °C under gentle magnetic stirring. The fluence-rate was 100 mW/cm^2. The DMA fluorescence emission was recorded in the 380–550 nm wavelength range with excitation at 360 nm. The first-order rate constant of the photo-oxidation of DMA by $^1O_2$was obtained by plotting ln F_0/F as a function of the irradiation time t, where F_0 and F represent the fluorescence intensity at time 0 and at time t, respectively. The rate constant was then converted into $^1O_2$ quantum yield by comparison with the rate constant for DMA photo-oxidation sensitized by haematoporphyrin (Hp), for which Φ_Δ was shown to be 0.65.[120]

Photostability studies

The stability of the porphyrin to red light irradiation was determined by preparing a solution of the appropriate compound in ethanol with an absorbance of 0.4 at the maximum absoption peak. This solution was placed in a quartz cuvette with a1 cm optical path and irradiated at 25 °C for different periods of time under gentle magnetic stirring by using 590-700nm light (Techno Light 270, Karl Storzsource, 100 mW/cm^2). After each irradiation, the absorbance spectrum was recorded by a Jasco V-500 UV-vis spectrophotometer equipped with a Peltier temperature controller using 1.0 cm path-length quartz cuvettes (3.0 mL). The value of the absorbance at the maximum peak at time 0 was compared with those recorded at the various irradiation times.

Tumour cell lines for in vitro tests

The human cervix epitheloid carcinoma HeLa cell line (ATCC, CCL2, Rockville, Maryland) was maintained in Dulbecco's modified Eagle's medium (EuroClone®, Devon, UK) supplemented with 5% fetal bovine serum (FBS, Gibco, Invitrogen™, Paisley, Scotland, UK), 2 mM L-glutamine (EuroClone®, Devon, UK), and 100 IU/ml penicillin and 100 μg/ml streptomycin (EuroClone®, Devon, UK).
The cell line was kept at 37 °C in a CO_2 incubator with 5% CO_2 and 100% relative humidity. Cells from a confluent monolayer were removed from flasks by a trypsin-EDTA solution. Cell viability was determined by the trypan blue dye exclusion test. For experimental purposes cells were "grown" in multiwell culture plates.
All experiments were carried out in complete medium containing 5% FBS (CM-5%).

In Vitro Cell Uptake of Re-Porphyrins Conjugates.

HeLa cells were plated at 10000 per well in a Costar 96 well plate (Euroclone, Devon, UK) and allowed to grow for 24 h. Compound's stocks were freshly prepared in dimethylsulfoxide (Sigma, St. Louis, MO, USA) at a concentration of 10^{-2} M and then diluted into medium to final working concentrations. Cells were exposed to variable concentrations of each compound (0.1-100 uM) for 0, 1, 2, 4, 8, and 24 h. At the end of the incubation time, the medium containing treatment was removed and cells were washed with 200 μl of PBS. Cells were harvested upon addition of 100 μl of 0.25% Triton X-100 (Sigma, St. Louis, MO, USA)

in PBS. To determine the compounds uptake, fluorescence emission was read at 430/670 nm (excitation/emission) using a Tecan Infinite F 200 plate reader (Tecan Austria GmbH, Grodig, Austria). Experiments were conducted in quadruplicate and repeated tree times.

Determination of Cell Cytotoxicity.

Cell growth inhibition was determined by the MTT viability test.[171] Cells were sown at 10000 per well on 96- well plates and allowed to grow 24 h. Cells were incubated for 1 h, 2h, 4h and 24h with variable concentrations (0.1-100 μM) of the appropriate compound, obtained by serial dilutions in CM-5% of stocks freshly prepared in dimethylsulfoxide (Sigma, St. Louis, MO) at 10^{-2} M concentration. Maximum dmso concentration in the cell incubation medium was ≤ 0.3% v/v. Cell toxicity analysis was performed at the end of the incubation time. Briefly, MTT dissolved in PBS (5 mg mL^{-1}) was added (10 μL per 100 μL of medium) to all wells and the plates were then incubated at 37 °C with 5% CO_2 and 100% relative humidity for 4 h. After this time, the medium was discarded and 200 μL of dmso were added to each well according to the method of Alley et al.[128] Optical density was measured at 570 nm on a SpectraCount Packard (Meriden, CT) instrument. IC_{50} values were calculated from dose-effect curves with GraphPad Prism version 4.03 for Windows (GraphPad Software, San Diego, CA). Experiments were conducted in quadruplicate and repeated tree times.

Determination of Cell Phototoxicity.

Cells were sown at 10000 per well on 96-well plates and allowed to grow 24 h. Then, cells were incubated with concentrations from 0.1 to 100 μM of the appropriate compound, obtained by serial dilutions in CM-5% of stocks freshly prepared in dimethylsulfoxide (Sigma, St. Louis, MO) at a concentration of 10^{-2} M, for 24h. Maximum dmso concentration in the cell incubation medium was ≤ 0.3% v/v. Thereafter, the media containing compounds were replaced with drug-free medium and cells were irradiated at 590-700 nm at a fluence rate of 9 mW/cm^2 and light doses ranging from 1 to 10 J/cm^2. This wavelength interval was isolated from the emission of a halogen lamp (Techno Light 270, Karl Storz) by the insertion of broadband optical filters. Control experiments performed in the absence of any photosensitizer indicated that light doses up to 10 J/cm^2 cause no evident cell damage. A plate similarly treated, but not exposed to light was used as reference for the dark cytotoxicity in the same experimental conditions.

Analysis of cell phototoxicity using the MTT assay as described above was performed after a further incubation of 24 h after irradiation and compared to the values of control cells without light irradiation. Experiments were conducted in quadruplicate and repeated tree times.

4. Bibliography

[1]Simonneaux G., Le Maux P., *Coord. Chem. Rev*., **2002**, *228*, 43.

[2]Campbell W. M., Jolley K. W., Wagner P., Wagner K., Walsh P. J., Gordon K. C., Schmidt-Mende L., Nazeeruddin M. K., Wang Q., Grätzel M., Officer D. L., *J. Phys. Chem. C*, **2007**, *111*, 11760.

[3]BabushkinaT. A. PonomarevG. V., *Chem. Heterocycl. Compd*., **1998**, *34*, 474.

[4]Harriman A., Sauvage J.-P., *Chem. Soc. Rev.*, **1996**,25, 41.

[5]Mehdi S. H., Brisbin D. A., McBryde W. A. E., *Biochim. Biophys. Acta (BBA)*, **1976**, *444*, 407.

[6]Eguchi M., Tachibana H., Takagi S., Inoue H., *Res. Chem. Intermed*.,**2007**, *33*, 191.

[7]Weiss C., Kobayashi H., Gouterman M., *J. Mol. Spectrosc*., **1965**, *16*, 415.

[8]Reyftman J. P., Morliere P., Goldstein S., Santaus, R., *J. Photochem. Photobiol., B*,**1984,** *40*, 721.

[9]Vitols S., Garthon G., Ost A., Peterson C., *Blood*, **1984**, *63*, 1186.

[10](a) Vicente M. G. H., *Curr. Med. Chem.*, **2001**, *1*, 175. (b) Tronconi, W., Colombo A., Decesare M., Marchesini R., Woodburn K. W., Reiss J. A., Phillips D. R., Zunino F., *Cancer Lett.***1995**, *88*, 41. (c) Woodburn K. W., Phillips D. R., Bellinger G. C. A., Sadek M., Brownlee R. T. C., Reiss J. A., *Bioorg. Med. Chem. Lett.*,**1992**, *2*, 343.

[11]Mroz P., Huang Y.Y., Szokalska A., Zhiyentayev T., Janjua S., Nifli A.P., Sherwood M.E., Ruzie C., Borbas K. E., Fan D., Krayer M., Balasubramanian T., Yang E., Kee H. L., Kirmaier C., Diers J. R., Bocian D. F., Holten D., Lindsey J. S., Hamblin M. R., *FASEB. J.*, **2010**, *24*, 3160.

[12]Mroz P., Bhaumik, J., Dogutan D. K., Aly Z., Kamal, Z., Khalid L., Kee H. L., Bocian D. F., Holten D., Lindsey J. S., Hamblin M. R., *Cancer Lett.*, **2009**, *282*, 63.

[13]Mroz P., Pawlak A., Satti M., Lee H., Wharton T., Gali H., Sarna T., Hamblin M. R., *Free Radical Biol. Med*., **2007**, *43*, 711.

[14]Henderson B. W., Dougherty T. J., *J. Photochem. Photobiol.*, **1992**, *55*, 145.

[15]Vrouenraets M. B., Visser G. W., Snow G. B., van Dongen G. A., *Anticancer Res*. **2003**, *23*, 505.

[16]Mroz P., Yaroslavsky A., Kharkwal G. B., Hamblin M. R., *Cancers*, **2011**, *3*, 2516.

[17]Dougherty T. J., Gomer C. J., Henderson B. W., Jori G., Kessel D., Korbelik M., Moan J., Peng Q., *J. Natl. Cancer. Inst*., **1998**, *90*, 889.

[18]Engbreht B. W., Menon, C., Kahur A. V., Hahn S. M., Fraker, D. L., *Cancer Res.*, **1999**, *59*, 4334.

[19]Dougherty T. J., Grindey G. B., Fiel R., Weishaupt K. R., Boyle D. G., *J. Natl. Cancer Inst*., **1975**, *55*, 115.

[20](a) Dougherty T. J., *J. Clin. Laser Med. Surg.* **2002**, *20*, 3. (b) Oleinik N. L., Evans H. H., *Radiat. Res.*, **1998**, *150*, 146.

[21](a) Pass H. I., *J. Natl. Cancer Inst.* **1993**, *85*, 443. (b) Henderson B. W., Dougherty T. J., *J.Photochem. Photobiol.*, **1992**, *55*, 145.

[22]Macdonald J., Dougherty T. J., *J. Porphyrins Phthalocyanines*, **2001**, *5*, 105.

[23]Wohrle D., Hirth A., Bogdahn-Rai T., Schnurpfeil G., Shopova M., *Russ.Chem. Bull*. **1998**, 47, 807.

[24]Agostinis P., Buytaert E., Breyssens H., Hendrickx N., *Photochem. Photobiol. Sci.* **2004**, *3*, 721.

[25]Hirohara S., Obata M., Alitomo H., Sharyo K., Ando T., Yano S., Tanihara M., *Bioconjugate Chem.*, **2009,** *20*, 944.

[26]Habdasa J., Boduszek B., *J. Pept. Sci*.,**2009**, 15, 305.

[27]Swamy N., James D. A., Mohr S. C., Hanson R. N. Ray R., *Bioorg. Med. Chem*., **2002**, *10*, 3237.

[28]Otake E., Sakuma S., Torii K., Maeda A., Ohi H., Yano S., Morita A., *J. Photochem. Photobiol.,B,* **2010**, *86*, 1356.

[29]MacDonald I. J., Dougherty T. J., *J. Porphyrins Phthalocyanines*, **2001**, *5*, 105.

[30]DeRosa M. C., Crutchley R. J., *Coord. Chem. Rev*. **2002**, *233-234*, 351.

[31]Weersink R. A., Bogaards A., Gertner M., Davidson S. R. H., Zhang K., Netchev G., Trachtenberg J., Wilson B. C., *J. Photochem. Photobiol. B,* **2005**, *79*, 211.

[32](a) Nyman E. S., Hynninen P. H., *J. Photochem. Photobiol. B,* **2004**, *73*, 1. (b) Sternberg E. D., Dolphin D., Bruckner C., *Tetrahedron*, **1998**,*54*, 4151. c) Bonnett R., *Chem. Soc. Rev.*, **1995**,*24*, 19. (d) Oschner M., *J. Photochem. Photobiol. B*, **1997**,*39*, 1. e) See K. L., Forbes I. J., Betts W. H., *J.Photochem. Photobiol.*, **1984**, *39*, 631.

[33](a) Szacilowski K., Macyk W., Drzewiecka-Matuszek A., Brindell M., Stochel G., *Chem. Rev.*,**2005**, *10*5, 2647. (b) Turro N.J., Singlet oxygen and chemilluminescent organic reactions. Modern Molecular Photochemistry. University Science Books: California, 1991; 583–593.

[34] Baeumler W Light sources for photodynamic therapy and fluorescence diagnosis in dermatology. Comprehensive series in photoscience, 2001, 1st ed., vol 2. Elsevier, 83–98.

[35]Szaciowski K., Macyk W., Drzewiecka-Matuszek A., Brindell M., Stochel G., *Chem. Rev*., **2005**, *105*, 2647.

[36]Sternberg E., Dolphin D., in Photodynamic Therapy and Biomedical Lasers, P. Spinelli, M. Del Fante, R. Marchesini, Eds, ExcerptaMedica, Milan, 1992, 1011, 470.

[37]Ethirajan M., Chen Y., Joshi P., Pandey R. K., *Chem. Soc. Rev*., **2011**, *40*, 340.

[38]Ris H.B., Altermatt H.J., Nachbur B., Stewart J.C., Wang Q., Lim C.K., et al., *Int. J. Cancer*, **1993**; *53*, 141.

[39]Moan J., Berg K., *J. Photochem Photobiol., B,* **1991**, *53*, 549.

[40]Peng Q., Moan J., Nesland J.M., *J. Ultrastruct. Pathol., **1996**, 20, 109.*

[41]Almeida R. D., Manadas B. J., Carvalho A. P., Duarte C. B., *Biochim. Biophys. Acta*, **2004**, *1704*, 59.

[42](a)Magda D.*;* Wright M., Miller R. A.*;* Sessler *J.* L.*;* Sansom P. I., *J. Am. Chem. Soc.*, **1995**, *117*, 3365.
(b) Michaeli A., Feitelson J., *Photochem Photobiol*., **1994**, *59*, 284.

[43]Bonnet R., *Chem. Soc. Rev.*, **1995**, *24*, 19.

[44]Coffey M. D., Kole R.A., Kolles S. M., Chisolm G. M., *J. Clin. Invest.*, **1995**, *96*, 1866.

[45]Geiger P. G., Thomas J. P., Girotti A. W., *Arch. Biochem. BioPhys.*, **1991**, *962*, 297.

[46]Girotti A. W., *J. Photochem. Photobiol., B*, **1992**, *13*, 105.

[47](a) Ben-Hur E., Bubbleman T. M. A. R., *J. Photochem. Photobiol., B,* **1993**, *58*, 890. (b) Gibson S. L., Murant R. S., Hilf R., *Cancer Res.*, **1988**, *48*, 3360.

[48]Ferri K. F., Kroemer G., *Nat. Cell Biol.,* **2001**, *3*, 255.

[49]Kessel D., Luo Y., *J. Photochem. Photobiol., B,* **1998**, *42*, 89.

[50]Granville D. J., Carthy C. M., Jiang H., Shore G. C., Mcmanus B. M., Hunt D. W., *FEBS Lett.*, **1998**, *437*, 5.

[51]Mak N. K., Li K. M., Leung W. N., Wong R. N., Huang D. P., Lung M. L., Lau Y. K., Chang C. K., *Biochem. Pharmacol.*, **2004**, *68*, 2387.

[52]Fingar V. H., Wieman T. J., Wiehle S. A., Cerrito P. B., *Cancer Res*., **1992**, *52* , 4914.

[53](a) Fingar V. H., Wieman T. J., Haydon P. S., *J.Photochem. Photobiol.* **1997**, *66*, 513.(b) Fingar V. H., Siegel K. A., Wieman T. J., Doak K. W., *J.Photochem. Photobiol.* **1993**, *58*, 393.

[54]Moan J., Berg K., *J Photochem. Photobiol.*, **1992**, *55*, 931.

[55]Mroz P., Szokalska, A., Wu M. X., Hamblin M. R., *PLoS One*, **2010**, *5*, e15194.

[56]Mroz P., Hashmi J. T., Huang Y. Y., Lange, N., Hamblin M. R., *Exp. Rev. Clin. Immunol.*, **2011**, *7*, 75.

[57]Castano A.P., Mroz P., Hamblin M. R., *Nat. Rev. Cancer*, **2006**, *6*, 535.

[58]Korbelik M., *J. Clin. Laser Med. Surg.*, **1996**, *14*, 329.

[59](a) Lottner C., Bart K.-C., Bernhardt G., Brunner H., *J. Med. Chem.*, **2002**, *45*, 2079. (b) Lottner C., Bart K.-C., Bernhardt G., Brunner H., *J. Med. Chem.*,**2002**, *45*, 2064.

[60]Ahmed S., Davoust E., Savoie H., Boa A. N., Boyle R. W., *Tetrahedron Lett.*, **2004**, *45*, 6045.

[61](a) Lauceri R., Purello R., Shetty S. J., Vicente M. G. H., *J. Am. Chem. Soc*.,**2001**, *123*, 5835. (b) Lipscomb L. A., Zhou F. X., Presnell S. R.,. Woo R. J, Peck M. E., Plaskon R. R., Williams L. D., *Biochemistry*,**1996**, *35*, 2818; (c) Marzilli L. G., Pethö G., Lin M., Kim M. S., Dixon D. W., *J. Am. Chem. Soc*.,**1992**, *114*, 7575.

[62](a) Vicente M. G. H., Nurco D. J., Shetty S. J., Medforth C. J., Smith K. M., *Chem. Commun*.,**2001**, 483. (b) Vicente M. G. H., Shetty S. J., Wickramasinghe A., Smith K. M., *Tetrahedron Lett.*, **2000**, *41*, 7623.

[63](a) Meunier B., *Chem. Rev.*, **1992**, *92*, 1411. (b) Fiel R. J., Datta-Gupta N., Mark E. H., Howard J. C., *Cancer Res.*,**1981**, *41*, 3543.

[64](a) Song R., Witvrouw M., Schols D., Robert A., Balzarini J., De Clercq E., Bernadou J., Meunier B., *Antiviral Chem. Chemother*., **1997**, *8*, 85. (b) Dixon D. W., Schinazi R., Marzilli L. G., *Ann. N. Y. Acad. Sci*.,**1990**, *616*, 511. (c) Debnath A. K., Jiang S., Strick N., Lin K., Jaberfield P., Neurath R. A., *J. Med. Chem.*,**1994**, *37*, 1099.

[65](a) Vicente M. G. H., Nurco D. J., Shetty S. J., Medforth C. J., Smith K. M., *Chem. Commun.*,**2001**,483. (b) Vicente M. G. H., Shetty S. J., Wickramasinghe A., Smith K. M., *Tetrahedron Lett.*, **2000**,*41*, 7623.

[66]Gradl S. N., Felix J. P., Isacoff E. Y., Garcia M. L., Trauner D., *J. Am. Chem. Soc.*,**2003**, *125*, 12668.

[67]Moon S. C., Shin J.-H., Jeong B. H., Kim H. S., Yu B. S., Lee J.-S., Lee B. S., Namgoong S. K., *Bioorg. Med. Chem. Lett.*,**2000**, *10*, 1435.

[68]Sol V., Brandland P., Granet R., Kaldapa C., Verneuil B., Krausz P., *Bioorg. Med. Chem. Lett.*, **1998**, *8*, 3007.

[69]Yano S., Hirohara S., Obata M., Hagiya Y., Ogura S., Ikeda A., Kataoka H., Tanaka M., Joh T. *J. Photochem. Photobiol., C*, **2011**, 12, 46.

[70](a)Vicente M. G. H., *Curr. Med. Chem.- Anticancer Agents*, **2001**, *1*, 175. (b) Tronconi W., Colombo A., Decesare M., Marchesini R., Woodburn K. W., Reiss J. A., Phillips D. R., Zunino F., *Cancer Lett.*, **1995**, *88*, 41. (c) Woodburn K. W., Phillips D. R., Bellinger G. C. A., Sadek M., Brownlee R. T. C., Reiss J. A., *Bioorg. Med. Chem. Lett.*, **1992**, *2*, 343.

[71]Dhar S. Lippard S. J. Bioinorganic Medicinal Chemistry, Enzo Alessio, Ed., Wiley-VCH Verlag GmbH & Co. KGaA, Weinheim, Germany, 2010, 3, 79.

[72]Lebwohl D., Canetta R., *Eur. J. Cancer*, **1998**, *34*, 1522.

[73]Pineto H. M., Schornagel J. H. (Eds.), Platinum and Other Metal Coordination Compounds in Cancer Chemotherapy, Plenum Press, New York, 1996, 2, 283.

[74]Keppler B. K., Henn M., Juhl U. M., Berger M. R., Niebl R., Wagner F., *Prog. Clin. Biochem. Med*, **1989**, *10*, 41.

[75]Alessio E., Balducci G., Lutman A., Mestroni G., Calligaris M., Attia W. M., *Inorg. Chim. Acta*, **1993**, *2*, 205.

[76](a) Rademaker-Lakhai J. M., van den Bongard D., Pluim D., Beijnen J. H., Schellens J. H. M. A., *Clin. Cancer Res.*, **2004**, 10, 3717. (b) Hartinger C. G., Zorbas-Seifried S., Jakupec M. A., Kynast B., Zorbas H., Keppler B. K., *J. Inorg. Biochem.*,**2006**, 100, 891.

[77](a) Jakupec M. A., Galanski M., Arion V. B., Hartinger C. G., Keppler B. K., *Dalton Trans.*, **2008**, 183. (b) Hartinger C. G., Jakupec M. A., Zorbas-Seifried S., Groessl M., Egger A., Berger W., Zorbas H., Dyson P. J., Keppler B. K., *Chem. Biodiversity*, **2008**, *5*, 2140. (c) Hartinger C. G., Zorbas-Seifried S., Jakupec M. A., Kynast B., Zorbas H., Keppler B. K., *J. Inorg. Biochem.*, **2006**, *100*, 891. (d). Jakupec M. A Keppler B. K., *Curr. Topics Med. Chem.*, **2004**, *4*, 1575.

[78](a) Bratsos I., Jedner S., Gianferrara T., Alessio E., *Chimia*, **2007**, *61*, 105 692. (b) Alessio E., Mestroni G., Bergamo A. Sava G., *Curr. Topics Med. Chem.*, **2004**, *4*, 1525. (c) Bacac M., Hotze A. C. G., von der Schilden K., Haasnoot J. G., Pacor S., Alessio E., Sava G. Reedijk J., *J. Inorg,. Biochem.*, **2004**, *98*, 402.

[79]Alessio E., Bergamo A., Sava G., *Metal Ions Biol. Syst.* **2004**, *42*, 323.

[80](a) Douganand S. J., Sadler P. J., *Chimia*, **2007**, *61*, 704; (b) Yan Y. K., Melchart M., Habtemariam A., Sadler P. J., *Chem. Commun.*, **2005**, *125*, 4764. (c) Chen H., Parkinson J. A., Morris R. E. Sadler P. J., *J. Am. Chem. Soc.*, **2003**, *125*, 1, 173.

[81]Dyson P. J., *Chimia*, **2007**, *61*, 698. (b) Ang W. H., Dyson P. J., *Eur. J. Inorg. Chem.*, **2006**, 4003.

[82](a) Grguric-Sipka S., Stepanenko I. N., Lazic J. M., Bartel C., Jakupec M. A., Arion V. B., Keppler B. K., *Dalton Trans*., **2009**, 3334. (b) Novakova O., Nazarov A. A., Hartinger C. G., Keppler B. K., Brabec V, *Biochem. Pharmacol*., **2009**, *77*, 364.

[83](a) Das S., Sinha S., Britto R., Somasundaram K., Samuelson A. G., *J. Inorg. Biochem*., **2010**, *104*, 93. (b) Meggers E., Atilla- Gokcumen G. E., Gründler K., Frias C., Prokop A., *Dalton Trans*. **2009**, 10882.

[84]Morris R. E., Aird R. E., del Socorro Murdoch P., Chen H., Cummings J., Hughes N. D., Parsons S., Parkin A., Boyd G., Jodrell D. ISadler., P. J., *J. Med. Chem.* **2001**, *44*, 3616.

[85](a) Peacock A. F. A., Sadler P. J., Chem. Asian J., **2008**, *3*, 1890. (b) Dougan S. J., Sadler P. J., *Chimia*, **2007**, *61*, 704.

[86]Aird R. E., Cummings J., Ritchie A. A., Muir M., Morris R. E., Chen H., Sadler P. J., Jodrell D. J., *Br. J. Cancer*, **2002**, *86*, 1652– 1657.

[87]Serli, B., Zangrando E., Gianferrara T., Scolaro C., Dyson P. J., Bergamo A., Alessio E., *Eur. J. Inorg. Chem.*, **2005**, 3423.

[88]Bratsos I., Jedner S., Bergamo A., Sava G., Gianferrara T., Zangrando E., Alessio E., *J. Inorg. Biochem.*, **2008**, *102*, 1120.

[89]Bratsos I., Mitri E., Zangrando E., Bergamo A., Sava G., Alessio E., *unpublished results*.

[90](a) Song R., Kim Y., Sohn Y. S., *J. Inorg. Biochem.* **2002**, *83*, 83. (b) Song R., Kim Y. S., OckLeed C., Sohn Y. S., *Tetrahedron Lett.*, **2003**, *44*, 1537.

[91](a) Lottner C., Knuechel R., Bernhardt G., Brunner H., *Cancer Lett.*, **2004**, 203, 2, 171–180. (b) Lottner, C.; Bart, K.-C.; Bernhardt, G.; Brunner, H., *J. Med. Chem*. **2002**, *45*, 2064.

[92]Mao J. F., Zhang, Y. M., Zhu J. H., Zhang C. L., Guo Z. J., *Chem. Commun***., 2009**, 908.

[93](a) Schmitt F., Govindaswamy P., Süss-Fink G., Ang W. H., Dyson P. J., Juillerat-Jeanneret L., Therrien B., *J. Med. Chem.*,**2008**, *51*, 1811. (b) Schmitt F., Govindaswamy P., Zava O., Suss-Fink G., Juillerat-Jeanneret L., Therrien B., *J. Biol. Inorg. Chem*., **2009**, *14*, 101.

[94](a) Cunningham M, McCrate A., Nielsen M., Swavey S., *Eur. J. Inorg. Chem.*, **2009**, 1521. (b) Rani-Beeram S., Meyer K., McCrate A., Hong Y., Nielsen M., Swavey S., *Inorg. Chem.*, **2008**, *47*, 11278.

[95]Davia K., King D., Hong Y., Swavey S., *Inorg. Chem. Commun.*, **2008**, 11, 584-586.

[96](a) Iengo E., Scandola F., Alessio E., *Struct. Bond.*, **2006**, *121*, 105. (b) Scandola F., Chiorboli C., Prodi A., Iengo E. Alessio E., *Coord. Chem. Rev.*, **2006**, *250*, 1471.

[97]Hupp J. T., *Struct. Bond.*, **2006**, *121*, 145.

[98]Beletskaya I., Tyurin V. S., Tsivadze A. Yu., Guilard R., Stern C., *Chem. Rev.*, **2009**, *109*, 1659.

[99]Hwang W., Kamada T., Ahn T. K., Ko D. M., Nakamura T., Tsuda A., Osuka A., Kim D., *J. Am. Chem. Soc.*, **2004**, *126*, 16187.

[100]Anson F. C., Shi C.. Steiger B, *Acc. Chem. Res.*, **1997**, *30*, 437.

[101]Iengo E., Zangrando E., Alessio E., *Acc. Chem. Res.*, **2006**, *39*, 841.

[102]Araki K., Silva C. A., Toma H. E., Catalani L. H., Medeiros M. H. G., Di Mascio P., *J. Inorg. Biochem.*, **2000**, *78*, 269.

[103]Kon H., Tsuge K., Imamura T., Sasaki Y., Ishizaka S.. Kitamura N., *Inorg. Chem.*, **2006**, *45*, 6875.

[104]Metcalfe C., Thomas J. A., *Chem. Soc. Rev.*, **2003**, *32*, 215. (b) Erkkila K. E., Odom D. T. Barton J. K., *Chem. Rev.*, **1999**, *99*, 2777.

[105]Ravanat J. L., Cadet J., Araki K., Toma H. E., Medeiros M. H., Di Mascio P., *J.Photochem. Photobiol.*, **1998**, *68*, 698.

[106]Pauly M., Kayser I., Schmitz M., Dicato M., Del Guerzo A., Kolber I., Moucheron C., Kirsch-De Mesmaeker A., *Chem. Commun.*, **2002**, 1086.

[107]Yu H.-J., Chao H., Jiang L., Li L.-Y., Huang S.-M.. Ji L.-N, *Inorg. Chem. Commun.*, **2008**, *11*, 553.

[108]Narra M., Elliott P. Swavey and S., *Inorg. Chim. Acta*, **2006**, *359*, 2256.

[109]Gianferrara T., Bratsos I., Iengo E., Milani B., Ostric A., Spagnul C., Zangrando E., Alessio, *Dalton Trans.*, **2009**, *48*, 10742.

[110]Alessio E., Macchi M., Heath S. L., Marzilli L. G., *Inorg. Chem.*, **1997**, *36*, 5614.

[111]Casanova M., Zangrando E., Iengo E., Alessio E., Indelli M. T., Scandola F., Orlandi M., *Inorg. Chem.*, **2008**, *47*, 10407.

[112](a) Kalyanasundaram K., *Inorg. Chem.*, **1984**, *23*, 2453. (b) Adler-Longo F.R., Finarell J., Goldmach J., Assour J., Korsakof L., **1967**, *J. Org. Chem.,32*, 476.

[113](a) Gabrielsson A., Lindsay Smith J. R., Perutz R. N., *Dalton Trans.*, **2008**, 4259. (b) Gabrielsson A., Hartl F., Zhang H.,. Lindsay Smith J. R., Towrie M., Vlcek A. Jr., *J. Am. Chem. Soc.*, **2006**, *128*, 4253. (c) Gabrielsson A., Hartl F., Lindsay Smith J. R., Perutz R. N., *Chem. Commun.*, **2002**, 950.

[114]Liu X., Liu J., Pan J., Chen R., Na Y., Gao W., Sun L., *Tetrahedron*, **2006**, *62*, 3674.

[115]Gianferrara, T., Giust D., Bratsos I., Alessio E., *Tetrahedron*, **2007**, *63*, 5006.

[116]Gianferrara T., Serli B., Zangrando E., Iengo E., Alessio E., *New J. Chem.*, **2005**, *29*, 895.

[117]Ochsner, M., *J. Photochem. Photobiol., B*, **1997**, *39*, 1.

[118]Gross E., Ehrenberg B., Johnson F., *J.Photochem. Photobiol.*, **1993**, *57*, 808.

[119]Reddi E., Valduga G., Rodgers M. A. J., Jori G., *J. Photochem. Photobiol.*, **1991,** *54*, 4, 633.

[120]Fabris C., Vicente M. G. H., Hao E., Friso E., Borsetto L., Jori G., Miotto G., Collutti P., Moro D., Esposito J., Ferretti A., Rossi C. R., Nitti D., Sotti G., Soncin M., *J. Photochem. Photobiol., B*, **2007**, *89*, 131.

[121]Barrett A. J., Kennedy J. C., Jones R. A., Nadeau P., Pottier R. H., *J. Photochem. Photobiol., B,* **1990**, *6*, 309.

[122]Gianferrara T., Bratsos I., Alessio E., *Dalton Trans*. **2009**, 7588.

[123]He X. Y., Sikes R. A., Thomsen S., Chung L. W., Jacques S. L., Photochem. Photobiol. **1994**, *59*, 468.

[124]Dahle J., Steen H. B., Moan J., Photochem. Photobiol. **1999**, *70*, 363.

[125](a) Luo, Y.; Chang, C. K. Photochem. Photobiol. **1996**, *66*, 479.

[126]Klein, A. V., Hambley, T. W., *Chem. Rev.*, **2009**, *109*, 4911.

[127]Kofoed T., Hansen H. F., Orum H., Koch T., *J. Peptide Sci.*, **2001**, 7, 402.

[128]Alley M.C., Scudiero D.A., Monks A., HurseyM. L., Czerwinski M. J., Fine D. L., Abbott B. J., Mayo J. G.,Schoemaker R. H., Boyd M. R., *Cancer Res.*,**1988**, *48*, 589.

[129] Tamura H., Arai T., *Bunseki Kagaku*, **1992**, *41*, 13.

[130]Alberto R., Metal-Based Radiopharmaceuticals, in Bioinorganic Medicinal Chemistry . ed E. Alessio ed. , Wiley-VCH Verlag GmbH & Co. KGaA, Weinheim, Germany, 2011, 253-282.

[131](a)Alberto R., *J. Organomet. Chem.*, **2007**, *692*, 1179. (b) Alberto R., *J. Nucl. Radiochem. Sci.,* **2005**, *6*, 173. (c) Amann A., Descritoforo C., Ott I., Wenger M., Bader D., Alberto R., Putz G., *Nucl. Med. Biol.,* **2001**, *28*, 243. (d) Alberto R., Schlibi R., Egli A., Schubiger P. A., Abram U., Kaden T. A., *J. Am. Chem. Soc.*, **1998**, *120*, 7987.

[132]Alberto R., Ortner K., Wheatley N., Schibli R., Schubiger A. P., *J. Am. Chem. Soc.,* **2001**, *123*, 3135.

[133]Dilworth J. R., Parrott S. J., *Chem. Soc. Rev.*, **1998**, *27*, 43.

[134]Jurisson S. S., Lydon J. D., *Chem. Rev.*, **1999**, *99*, 2205.

[135]Kung H. F., Kung M. P. Choi S. R., *Semin. Nucl. Med.*, **2003**, *33*, 2.

[136]Liu S. Edwards D. S., *Chem. Rev.*, **1999**, *99*, 2235.

[137]Liu S., *Adv. Drug Delivery Rev.*, **2008**, *60*, 1347.

[138]Yeh W. M., Sherman D. G., Meares C. F., *Anal. Biochem.*, **1979**, *100*, 152.

[139]Hnatowich D. J., Mardirossian G., Rusckowski M., Fogarasi M., Virzi F., Winnard P., *J. Nucl. Med.*, **1993**, *34*, 109.

[140]Liu S., *Chem. Soc. Rev*., **2004** , *33*, 445.

[141]Gianferrara T., Bergamo A., Bratsos I., Milani B., Spagnul C., Sava G., Alessio E., *J. Med. Chem*., **2010**, *53*, 4678.

[142] Smith Gregory S., Therrien B., *Dalton Trans.*, **2011**, *40*, 10793.

[143](a) Sun R. W.-Y., Che C.-M., *Coord. Chem. Rev*., **2009**, *253*, 1682. (b) To Y. F., Sun R. W.-Y., Chen Y., Chan V. S.-F., Yu W.-Y., Tam P. K.-H., Che C.-M., Lin C.-L. S., *Int. J. Cancer.*,**2009**, *124*, 1971.

[144]Wong, D. W., *J. Label. Compd. Radiopharm.*, **1983**, 20, 351.

[145]Shetty S. J., Murugesan S., Chatterjee S., Banerjee S., Srivastava T. S., Noronha O.P.D., Samuel A. M., *J Label. Compd. Radiopharm.,* **1996**, 38, 411.

[146]Murugesan S., Shetty S. J., Srivastava T. S., Noronha O. P. D., Samuel A. M., *J. Porphyrins Phthalocyanines*, **2001**, *5*, 824.

[147]Chatterjee S. R., Murugesan S., Kamat J. P., Shetty S. J., Srivastava T. S, Noronha O. P. D., Samuel A. M., Devasagayam T. P. A., *Arch. Biochem. Biophys.*, **1997**,*339*, 242.

[148]Strauss A.W., Nunn A., Linder K., *J. Nucl. Cardiol*., **1995**, *2*, 437.

[149]Murugesan S., Shetty S. J., Srivastava T. S., Samuel A. M., Noronha O. P. D., *J. Photochem. Photobiol., B,* **2002**, *68*, 33.

[150]Murugesan S., Shetty S. J., Srivastava T. S., Noronha O. P. D., Samuel A. M., *Appl. Radiat. Isot.,***2001**,*55*, 641.

[151]Tsutsui M., Hrung C. P., Ostfeld D., Srivastava S., Cullen D. L., Meyer E. F. Jr., *J. Am. Chem. Soc.*, **1975**, *97*, 3952.

[152]Yang Y., Songa H., Songa H., Zhaob W., Pu M., *J. Porphyrins Phthalocyanines,* **2011**,*15*, 271.

[153]Hill D. M., Barnes R. K., Wong H. K. Y., Zawadzki A. W., *Appl. Radiat. Isot.*, **2000**, *53*, 415.

[154]Montalbetti C. A. G. N., Falque V., *Tetrahedron*, **2005**, *61*, 10827.

[155]D. G. McCafferty, B. M. Bishop, C. G. Wall, S. G. Hughes, S. L. Mecklenberg, T. J. Meyer and B. W. Erickson, *Tetrahedron*, **1995**, *51*, 1093.

[156]Kaminski, Z. J.; Paneth, P.; Rudzinski, J., *J. Org. Chem.*, **1998**, *63*,4248.

[157]Zelenka K., Borsig L., Alberto R., *Bioconjugate Chem*., **2011**, *22*, 958.

[158](a) Kurz P, Probst B., Spingler B., Alberto R., *Eur. J. Inorg. Chem.*, **2006**, 2966. (b) Takeda H., Koike K., Inoue H., Ishitani O., *J. Am. Chem. Soc*., **2008**, *130*, 2023. (c) Schneider J., Vuong K. Q., Calladine J. A., Sun X., Whitwood A. C., George M. W., Perutz R. N., *Inorg. Chem.*, **2011**, *50*, 11877.

[159]Probst B., Ph D thesis, **2010**, University of Zurich.

[160] Wang F., Habtemariam A., van der Geer E. P. L., Deeth R. J., Gould R, Parsons S., Sadler P. J., *Biol Inorg Chem* , **2009**, *14*, 1065.

[161]Ribo J. M., Crusats J., Farrera J.-A., Valero, M. L., *J. Chem. Soc., Chem. Commun*., **1994**, 681.

[162]Alberto R., Schibli R., Schubiger A. P., Abram U., Pietzsch H. J., Johannsen B., *J. Am. Chem. Soc*., **1999**, *121*, 6076.

[163]Nyman E. S., Hynninen, P. H., *J. Photochem. Photobiol., B*, **2004**, *73*, 1.

[164]Deutsch E., Libson K., Vanderheyden J.-L., Ketring A. R., Maxon H. R., *Nucl. Med. Biol*., **1986**, *13*, 465.

[165]Photosensitizing Compounds: Their Chemistry, Biology and Clinical Use; Bock, G., Harnett, S., Eds.; John Wiley: Chichester, 1989.

[166]Alberto R., Egli A., Abram U., Hegetschweiler K., Gramlich V., Schubiger A. P., *J. Chem. Soc., Dalton Trans*. **1994**, 2815.

[167]Beer P. D., Cadman J., Lloris J. M., Martınez-Manez R., Soto J., Pardo T., Marcos M. D. J., *Dalton Trans.*, **2000**, 1805.

[168]Hafliger P., Agorastos N., Spingler B., Georgiev O., Viola G., Alberto R., *ChemBioChem*, **2005**, *6*, 414.

[169] Perree-Fauvet M., Verchere-Beaur C., Tarnaud E., Anneheim- Herbelin G., Bone N., Gaudemer A., *Tetrahedron*, **1996**, *52*, 13569.

[170](a)Rodrıguez A. M. B., Gabrielsson A., Motevalli M., Matousek P., Towrie M., Syebera J., Zalis S., Vlcek A. Jr., *J. Phys. Chem. A* **2005**, *109*, 5016. (b) Probst B., Ph D thesis, **2010**, University of Zurich (c) Wang F., Habtemariam A., Van der Geer E. P. L., Deeth R. J., Gould R., Parsons S., Sadler P. J., *J. Biol. Inorg. Chem.*, **2009,** *14*, 1065.

[171]Mosman T., *J. Immunol. Methods*, **1983**, *65*, 55.